AFML-TR-77-143

EXPLORATORY DEVELOPMENT STUDIES FOR SUSTAINED LOAD SUBCRITICAL CRACK GROWTH IN TITANIUM ALLOYS

LOCKHEED-CALIFORNIA COMPANY
P. O. BOX 551
BURBANK, CALIFORNIA 91520

AUGUST 1977

TECHNICAL REPORT AFML-TR-77-143
Final Report for Period April 1976 – June 1977

AIR FORCE MATERIALS LABORATORY
AIR FORCE WRIGHT AERONAUTICAL LABORATORIES
AIR FORCE SYSTEMS COMMAND
WRIGHT-PATTERSON AIR FORCE BASE, OHIO 45433

NOTICE

When Government drawings, specifications, or other data are used for any purpose other than in connection with a definitely related Government procurement operation, the United States Government thereby incurs no responsibility nor any obligation whatsoever; and the fact that the government may have formulated, furnished, or in any way supplied the said drawings, specifications, or other data is not to be regarded by implication or otherwise as in any manner licensing the holder or any other person or corporation, or conveying any rights or permission to manufacture, use, or sell any patented invention that may in any way be related thereto.

This final report was submitted by Lockheed-California Company, P.O. Box 551, Burbank, CA, 91520 under Contract F33615-76-C-5168, to the Air Force Materials Laboratory, Wright-Patterson Air Force Base, Ohio, 45433. Dr. L. Bidwell, AFML/LLS was the laboratory project engineer.

This report has been reviewed and cleared for open publication and/or public release by the appropriate Office of Information (OI) in accordance with AFR 190-17 and DODD 5230.0. There is no objection to unlimited distribution of this report to the public at large, or by DDC to the National Technical Information Service.

This technical report has been reviewed and is approved for publication.

L R Bidwell

Dr. L. BIDWELL
Project Engineer
Structural Metals Branch
Metals and Ceramics Division

FOR THE COMMANDER

Nathan G Tupper

NATHAN G. TUPPER
Acting Chief
Structural Metals Branch
Metals and Ceramics Division

Copies of this report should not be returned unless return is required by security considerations, contractual obligations, or notice on a specific document.

AIR FORCE/56780/7 April 1978 — 225

UNCLASSIFIED

SECURITY CLASSIFICATION OF THIS PAGE *(When Data Entered)*

REPORT DOCUMENTATION PAGE

READ INSTRUCTIONS BEFORE COMPLETING FORM

1. REPORT NUMBER: AFML-TR-77-143
2. GOVT ACCESSION NO.
3. RECIPIENT'S CATALOG NUMBER
4. TITLE *(and Subtitle)*: EXPLORATORY DEVELOPMENT STUDIES FOR SUSTAINED LOAD SUBCRITICAL CRACK GROWTH IN TITANIUM ALLOYS.
5. TYPE OF REPORT & PERIOD COVERED: Final Technical Report. Apr 76 - Jun 77,
6. PERFORMING ORG. REPORT NUMBER: LR-28181
7. AUTHOR(s): D. E. Pettit
8. CONTRACT OR GRANT NUMBER(s): F33615-76-C-5168
9. PERFORMING ORGANIZATION NAME AND ADDRESS:
   LOCKHEED-CALIFORNIA COMPANY
   P. O. Box 551
   BURBANK, CA 91520
10. PROGRAM ELEMENT, PROJECT, TASK AREA & WORK UNIT NUMBERS: Project 7351/06/B6
11. CONTROLLING OFFICE NAME AND ADDRESS:
    Air Force Materials Laboratory (AFML/LLS)
    Air Force Wright Aeronautical Laboratories
    Wright-Patterson Air Force Base, OH 45433
12. REPORT DATE: Aug 77
13. NUMBER OF PAGES: 123
14. MONITORING AGENCY NAME & ADDRESS *(if different from Controlling Office)*: Same as 11.
15. SECURITY CLASS. *(of this report)*: UNCLASSIFIED
15a. DECLASSIFICATION/DOWNGRADING SCHEDULE: N/A
16. DISTRIBUTION STATEMENT *(of this Report)*: Approved for Public release; Distribution unlimited
17. DISTRIBUTION STATEMENT *(of the abstract entered in Block 20, if different from Report)*:
18. SUPPLEMENTARY NOTES:
19. KEY WORDS *(Continue on reverse side if necessary and identify by block number)*: Ti alloys, sustained load cracking, environmental effects, stress corrosion cracking, crystallographic texture, mechanical properties, fracture toughness, Ti-6Al-4V, Ti-6Al-6V-2Sn
20. ABSTRACT *(Continue on reverse side if necessary and identify by block number)*:

A four phase program was conducted to study the relative influence of the variables which influence the sustained load crack growth behavior of titanium alloys. In Phase I the effects of microstructure and internal hydrogen content were examined. A single 1-1/2 inch thick plate of Ti-6Al-4V was sectioned and the following five material conditions developed: solution treated and aged (206 ppm hydrogen), recrystallize annealed (245 ppm hydrogen and 72 ppm hydrogen), and beta annealed (199 ppm hydrogen and 24 ppm hydrogen). Each

next page →

DD FORM 1 JAN 73 1473 EDITION OF 1 NOV 65 IS OBSOLETE

UNCLASSIFIED

SECURITY CLASSIFICATION OF THIS PAGE *(When Data Entered)*

209 970

material was characterized metallographically and the crystallographic texture determined. Tensile and fracture toughness data were also developed for each material. Sustained load tests were then conducted in research grade dry argon, high humidity air, and 3-1/2% NaCl solution in deionized water. Phase II consisted of machining the Ti-6Al-4V(RA) material with 245 ppm hydrogen from the 1.4 inch thickness in Phase I to a thickness of 3/8 inch and repeating the tests in dry argon and high humidity air to evaluate the effect of specimen thickness. In Phase III a highly textured 3/8 inch thick plate of Ti-6Al-4V(RA) material (100 ppm hydrogen) was evaluated in the LT and TL orientation to study the effect of crystallographic texture on the sustained load cracking behavior in dry argon, high humidity air and 3-1/2% NaCl. Phase IV introduced a second alloy, Ti-6Al-6V-2Sn(STOA) to the study. Following material characterization, sustained load tests were again conducted in dry argon, high humidity air and 3-1/2% NaCl solution. The results of these tests are presented and discussed in terms of the effects of the variables on the sustained load cracking characteristics of titanium alloys.

In summary, the following conclusions seem appropriate: ~~(1)~~ The internal hydrogen level of a titanium alloy may increase the sustained load cracking behavior of the material; ~~(2)~~ The extent of this degradation is dependent upon the microstructure, environment and, possibly, short range order. Other sub-microstructural features may also be involved; ~~(3)~~ Materials with an $\alpha + \beta$ microstructure seem to show a greater susceptibility to sustained load cracking and hydrogen level than do the β processed materials; ~~(4)~~ As the thickness and associated triaxial constraint decrease, the tendency to exhibit sustained load cracking in high humidity air and dry argon decrease for Ti-6Al-4V(RA) with a high hydrogen content; (5) Crystallographic texture in Ti-6Al-4V(RA) does not appear to exhibit a major influence on sustained load cracking in high humidity air or dry argon but does exhibit a major effect in 3 1/2% NaCl solution; ~~(6)~~ Great care must be exercised in assessing sustained load cracking behavior of Ti alloys since crack tip branching can result in crack arrest at a level much above that level where extensive sustained load cracking occurs. The occurrence of crack arrest is dependent on the relative $\frac{dK}{da}$ gradient of the specimen geometry as well as the material and specimen thickness; ~~(7)~~ No single model for sustained load cracking appears to predict all of the observed sustained load cracking behavior. Rather it appears to involve a combination of effects involving internal hydrogen, creep and environmental parameters which may not always be of a detrimental nature.

TABLE OF CONTENTS

TABLE OF CONTENTS (Cont'd.)

TABLE OF CONTENTS (Cont'd.)

LIST OF ILLUSTRATIONS

LIST OF ILLUSTRATIONS (Continued)

LIST OF ILLUSTRATIONS (Continued)

LIST OF ILLUSTRATIONS (Continued)

LIST OF TABLES

LIST OF TABLES (Continued)

SECTION I

INTRODUCTION

1. BACKGROUND

As the service requirements for aerospace vehicles have become more demanding, the design procedures and material specifications have of necessity become more stringent in order to assure reliable and operational performance of the structure.

Early aircraft designs were based, in the main, on ultimate and yield strength criteria. The design methodology then evolved to include fatigue design methodology (stress cycling S-N concepts), strain cycling concepts, and more recently damage tolerance and linear elastic fracture mechanics concepts. The development of each of these design methodologies has provided another tool to aid the designer in improving structural reliability.

From an engineering perspective the impact of sustained load cracking on current damage tolerant design methodology is significant. In many service applications, the load time history of a part includes long time periods under a sustained load. Normal damage tolerance analysis procedures assume crack growth from an initial size by either fatigue or stress corrosion cracking in a hostile environment (i.e., 3.5% NaCl solution, sump tank water, etc.) to a final critical crack length defined by the material fracture toughness. If sustained load cracking occurs in environments normally not considered hostile, i.e., ambient air, then the terminal crack length which could be sustained by a structure which sees periods under sustained load must be re-evaluated. For this case, sustained load cracking could occur at stress intensities substantially lower than the rapid rising load fracture toughness values. In essence, therefore, the occurrence of sustained load cracking would constitute an unaccounted for crack extension which would make the analysis unconservative.

The development of an understanding of the controlling parameters in sustained load cracking are of major importance to material specification and procurement and to design methodology. If it can be shown that the internal hydrogen in solution in the material is indeed a controlling or a major contributing parameter to the sustained load crack growth behavior of commercial titanium alloys, then several possible routes are open to the designer. First, the material could be procured with a much lower permissible hydrogen level. Second, existing material might be vacuum annealed to remove hydrogen currently in solution. Either or both of these procedures could best minimize or eliminate the sustained load cracking which is observed in typically "non-aggressive" environments. If, on the other hand, factors other than the presence of internal hydrogen are controlling the sustained load cracking behavior, then the importance of the various parameters must be defined to permit the incorporation of a rational analysis method to include sustained load crack growth in the damage tolerant design analysis. This would then result in the addition of a new criteria and a new significant parameter in the evaluation of a damage tolerant structure. The objective of the current program was to establish the relative importance of material, environmental and loading conditions that affect the sustained load subcritical crack growth behavior of titanium alloys.

SECTION II

TECHNICAL BACKGROUND

1. SUSTAINED LOAD CRACKING IN AIR AND INERT ENVIRONMENTS

Sustained load cracking in titanium alloys was initially observed in the 1950s when Burte, et al.[1] observed time delayed failure in stress rupture tests using notched titanium specimens in ambient air. Subsequent work showed a strong correlation between sustained load cracking and residual hydrogen content of the material[2, 3]. These studies conducted on smooth or mechanically machined notched specimens indicated that relatively high hydrogen levels were required to produce such premature failures; and, as a result, a maximum hydrogen content for Ti-6Al-4V and other similar titanium alloys was set at approximately 125 ppm. More recent work using fatigue precracked specimens of Ti-8Al-1Mo-1V, the Ti-6Al-4V series of alloys, Ti-4Al-3Mo-1V, Ti-7Al-2Cb-1Ta, and other titanium alloys has indicated that sustained load cracking can occur in air and in inert environments at hydrogen levels of 125 ppm and lower. These studies which formed the technical background for the current program are briefly reviewed in the following paragraphs.

In the study by Yoder, et al.[4], eight alloys of the Ti-6Al-4V family were examined under static load in an ambient air environment. Degradation in the static load carrying capability of the alloys was shown to exist in room temperature air, the degradation ranging from 11 to 35 percent of the maximum load carrying capability of the specimen as measured in a rapid load application (K_{IQ}) test. For these tests, the hydrogen levels ranged from 35 to 80 ppm, but no consistent trend in the results could be observed with hydrogen level. This was due, in part, to the differences in static strength properties of the various plates which made interpretation of the results in terms of the interstitial content or the microstructure very difficult. Anisotropic effects were noted with crack orientation, but the effect was clouded by the difference in specimen type (SEN versus PTC) used for the two orientations.

Scanning electron microscopy showed both microvoid coalescence and cleavage to occur under sustained load, the amount of cleavage decreasing as the crack extended, i.e., as the rate increased.

In a subsequent evaluation of these tests, Krafft[5] proposed a model which appears to be consistent with the data. In this model, the initial portion of the crack growth phenomena was related to stress relaxation behavior, with the latter portion of the crack extension dominated by environmental effects. In addition, the effect of the material fracture toughness, i.e., the process zone size, was predicted to be small and therefore could be neglected. Unfortunately, no stress corrosion tests were run on these same materials, so the correlation (if one should exist) between the stress corrosion behavior and the sustained load cracking behavior could not be made.

Extensive work on the effect of hydrogen on sustained load cracking has been conducted by Meyn[6-8]. In the initial work[6], the hydrogen level was varied in two Ti-6Al-4V alloys with different oxygen contents. Unfortunately, the chemistry, particularly the aluminum content, also varied between the two alloys thus making subsequent interpretation difficult. For these conditions it was found that small increases in the hydrogen level produced significant decreases in the fracture toughness. For the high oxygen level material, the sustained load cracking behavior also degraded, but the sustained load cracking behavior did not appear to be affected by hydrogen levels down to 9 ppm in the low oxygen material. In subsequent work[7], the low oxygen material was again examined in section sizes ranging from the relatively small specimens used initially to a thickness of 2 inches. Under these conditons, studied at only one hydrogen level, a decrease in threshold behavior and an increase in crack growth rates were observed with increasing thickness. A more recent study by Meyn[8] showed a decrease in the sustained load cracking resistance for the Ti-6Al-4V material for hydrogen levels up to about 50 ppm. Further increases in hydrogen content appeared to increase the rate of sustained load cracking but have no effect on the threshold value. For Ti-8Al-1Mo-1V material, tests in vacuum and in air showed no stress corrosion cracking effect. However, the

threshold appeared to be somewhat higher in air than in vacuum. No explanation of this observation was made. Ti-6Al-6V-2Sn mill annealed material also showed a substantial reduction in crack propagation resistance under sustained loading in air.

Perhaps the most extensive fracture surface examination was conducted by Meyn[8]. A mixture of transgranular cleavage (believed in the alpha phase) and microvoid coalescence was observed. The most common cleavage plane was oriented 12 to 15 degrees from $\{0001\}_\alpha$ similar to that found in stress corrosion cracking. Individual cleavage microfacets were found to be aligned within larger colonies of similar crystallographic α plates or subgrains in the larger prior β grains. It was concluded that cleavage takes place only in the α phase. No correlation between the hydrogen content and fracture appearance was found.

Similar work by Sandoz[9] on Ti-8Al-1Mo-1V containing 14 to 40 ppm hydrogen also showed sustained load cracking behavior in desiccated air. For this material, the threshold stress intensity factor was increased as the hydrogen level was reduced. Chu[10] showed that sustained load cracking in air also occurred for Ti-721, the time to failure curve being much higher than that measured for stress corrosion cracking in 3.5% NaCl solution.

Williams[11] has conducted similar work on Ti-4Al-3Mo-1V. Initial results on relatively thin 1/4 inch specimens showed indications that sustained load cracking in vacuum and in moist air resulted in a common time to failure curve. The threshold value in air and in vacuum was indicated to lie below that for 3.5% NaCl solution, a very surprising result which requires further confirmation. This study was for a very low hydrogen material containing 10 ppm of hydrogen. As a result, it was postulated that the most likely mechanism was not hydrogen embrittlement but was instead a creep behavior viewed in terms of a critical strain concept. This is somewhat similar to that proposed by Krafft. SEM examination showed "cleavage-like" facets which increased in the slow growth region with a decrease in initial stress intensities. An alignment of the facets in bands parallel to the direction of crack propagation was observed. However, the cracking did not appear to occur predominately in the α phase,

significant α-β interface separation and microporosity being found. Subsequent work by Williams[12] on the effect of thickness in the Ti-4Al-3Mo-1V material in humid air showed the extremely thin 0.13 inch thick material failure times were longer than those observed in the 3/4 and 1/4 inch thick materials, results being approximately the same for the two thicker materials. Specimen size was found to have a marked effect on the shape of the crack front. In all cases the regions of crack extension appeared to occur in those sections of the specimens which were under a triaxial or approximately plane strain condition.

The strong effect of thickness on sustained load cracking and stress corrosion cracking behavior of titanium alloys has also been demonstrated on Ti-6Al-4V RA and β material and Ti-6Al-6V-2Sn STOA material by Pettit, et al.[13]. These results for tests conducted in moist air, sump tank water and 3.5% NaCl solution showed that in thicknesses of 1/8 inch, the time to failure of the compact tension specimen was extremely long and the apparent threshold for no fracture very high, approaching that of the K_{IQ} value. Fractographic examinations of the specimens showed the typical subsurface tunneling effect which has been observed in thin mixed mode specimens. For these particular tests, the thickness was small enough that crack arrest due to the large plastic zone relative to the thickness could actually be obtained, even in a 3.5% NaCl solution. Results for the 3/8 inch material showed the normal ranking of materials by environment, i.e., the highest threshold value and slowest crack growth rates were observed in humid air, the sump tank water results were intermediate, and the 3.5% NaCl solution results showed the lowest threshold value and the highest crack growth rates. Examination of fractured specimens by SEM showed a much higher percentage of cleavage facets in specimens failed in 3.5% NaCl solution as compared to those failed in moist air.

Work by Lane et al.[14] on the sustained load cracking behavior in air and in sea water for several alloys including Ti-7Al-2Cb-1Ta in one inch thickness again showed a time dependent fracture behavior in air as well as in sea water, the sea water threshold values being considerably lower. Fracture was found

to be generally transgranular through the β grains and across the α platelets. In this study it was shown that the sea water sensitivity of the material was a function of the aluminum content, the isomorphous beta stabilizer content (columbium, molybdenum, and vanadium), heat treatment, and the cooling rate. The results were examined using the hypothesis of Crossley[15] that coherent Ti_3Al precipitates form on a submicroscopic scale in the alpha matrix and result in an embrittlement of the material. The circumstantial evidence in this study appears to support the Ti_3Al role. In the subsequent author's closure of this article it is indicated that later data indicates an effect of the combination of the hydrogen and chlorine ions in the sea water sensitivity. This stems from work which is underway at Titanium Metals Corporation of America[16] indicating evidence of the action of cations and anions in the process. A similar hypothesis was also made by Krupp[17] as to the importance of the chloride ion in the aqueous solution on the stress corrosion behavior.

While the above studies are representative of the current work which has been done in the field, and, while many questions remain unanswered, several proposed mechanisms have emerged.

The first is that of hydrogen embrittlement. This assumes that the initial hydrogen in solution in the titanium is sufficient to embrittle the material ahead of the crack such that crack extension takes place. This mechanism[18] assumes that a critical concentration of hydrogen either exists or rapidly builds up due to hydrogen migration in the triaxial stress field immediately ahead of the crack tip. This mechanism has been proposed to successfully predict the variation of threshold stress intensity with initial hydrogen content and mixed mode loading effects which have been observed. It indicates that a quite low amount of hydrogen may result in subcritical crack growth as discussed by Williams[18]. Thus a successful model incorporating hydrogen embrittlement as a mechanism would include both the effects of the initial hydrogen in solution and the possible absorption of subsequent hydrogen from the environment (depending on the oxide continuity).

Creep rupture has also been proposed as a mechanism[5]. This model assumes that sufficient plastic flow at the crack root occurs to result in progressive crack extension as creep rupture occurs in the material immediately in front of the crack. The primary difference between the hydrogen embrittlement and the creep rupture model proposed by Krafft[5] is whether the initial phase of the crack growth occurs due to stress rupture or due to an embrittlement of the material ahead of the crack. Both models imply that as the crack proceeds, the role of hydrogen or other environmental contaminant absorbed from the environment becomes more important.

Ti_3Al has also been proposed as an embrittling agent[15]. Evaluation of the assumption that Ti_3Al has a major effect on the subcritical crack growth behavior of titanium alloys is very difficult and extremely expensive due to the submicroscopic nature of the precipitate. Most of the data relating this parameter to sustained load crack growth is indirect[14].

2. EFFECT OF MORE AGGRESSIVE ENVIRONMENTS (STRESS CORROSION CRACKING)

The interaction of microstructure and monotonic loads on titanium alloys is further complicated by the introduction of an environment and hold time at load. Titanium is inherently a chemically active material which forms a thin passive film upon exposure to an environment or air. This film is very stable and adheres tightly to the surface resulting in the good corrosion resistance normally associated with smooth bar corrosion resistance. However, the susceptibility of titanium alloys containing cracks (which is of interest here) was first found in the SST materials studies and initiated extensive work on the phenomena.

In commercially pure titanium, the introduction of a crack results in little change in the corrosion resistance in aqueous environments[19]. However, as normal alloying elements are added, the alloys become more susceptible to environmental degradation when a prior crack exists. In particular, the effect of aluminum and oxygen additions have been studied by several investigators[20-26] and the general tendency of the threshold for stress corrosion

cracking, K_{Iscc}, to decrease with aluminum and oxygen additions demonstrated. Wood, et al.[27] showed that K_Q and K_{Iscc} in salt water decreased with increasing yield strength (increasing aluminum content) and for alloys of a given yield strength, K_{Iscc} was sensitive to the aluminum content whereas K_Q was not. Alloys containing 6.5 to 8 percent aluminum showed very low values of K_{Iscc} while for the alloys with 5.5 percent aluminum or less, K_Q and K_{Iscc} were almost comparable. A 6 percent aluminum content appears to be the borderline for salt water stress corrosion susceptibility.

Wood, et al[27] also showed that increasing the oxygen content increased the tensile yield strength and decreased the K_Q and K_{Iscc} values for Ti-Al-Mo-V alloys. Increasing the oxygen content of the 6 percent aluminum-base alloy (borderline susceptibility) effected a sharp decrease in K_{Iscc}.

Consistent with the occurrence of cleavage in the alpha during stress corrosion cracking is the effect of texture on K_{Iscc}. When the (0001) planes are oriented perpendicular to the stress, the stress corrosion susceptibility increased[22,34].

The effect of both the substitutional aluminum and interstitial oxygen atoms has been attributed to promoting planar slip[22,28] in the alpha. This is consistent with the findings of Sanders and Scully[29] that titanium alloys susceptible to stress corrosion cracking form coplanar dislocation arrays while nonsusceptible alloys form dislocation tangles. In general, additions of aluminum, oxygen, magnesium, tin, and cobalt promote stress corrosion[25] while the beta stabilizers molybdenum, columbium, and vanadium decrease the susceptibility[21,25].

The exact mechanisms of stress corrosion cracking in titanium alloys are the subject of much debate and several general theories are in existence, none of which are satisfactory for a range of conditions. There is general agreement that there is either an embrittlement due to one of several contaminating species which may exist (the three most generally acknowledged ones being hydrogen, oxygen, and the halides, particularly chlorine) or a dissolution

phenomena involved. In many cases more than one mechanism may be operative. While the exact mechanism is not known, i.e., hydrogen embrittlement[19,30,31] due to hydride formation in the lattice, electrochemical dissolution[21,32], chlorine or halide embrittlement[23,33], or the preferred or forced precipitation of coherent Ti_3Al on planar slip systems[23] and the associated high strain[34], several general features can be identified for aqueous environments.

In typical alpha-beta alloys, transgranular cleavage normally occurs in the alpha phase[26,30,34] on or near the (0001) planes[34] and occasionally at the alpha-beta interface[19]. The effect of the microstructural parameters that has been observed indicates that the acicular alpha microstructure has better resistance to stress corrosion cracking than larger equiaxed alpha microstructures. This is believed to be due to the smaller alpha particle size which requires additional cleavage cracks to be developed to extend the primary crack a given increment. However, the effectiveness of the acicular microstructure is also dependent on the strength and characteristics of the beta matrix material. Some results have shown that an increase in the amount of beta reduces the stress corrosion susceptibility[25,34] but other results[39] show a decrease only if the beta is randomly distributed and tends to be in laminated layers between alpha plates.

SECTION III

PROGRAM OVERVIEW

Evaluation of the many variables involved in the sustained load crack growth behavior of Titanium alloys resulted in the development of a four-phase program for evaluating the primary variables of microstructure, material, hydrogen level, test environment, stress state, texture, and alloy. Ti-6Al-4V was selected as the primary material for use in Phases I, II and III. Phase I consisted of an evaluation of the effects of hydrogen level, microstructure and environment on the sustained load cracking behavior of Ti-6Al-4V plate under plane strain loading. Phase II extended the effort to include the effects of mixed mode loading for one of the hydrogen level/microstructures evaluated in Phase I. Phase III evaluated the effect of texture in Ti-6Al-4V plate on sustained load crack growth for the same conditions of mixed mode loading studied in Phase II. Phase IV extended the study to the behavior of a second alloy, Ti-6Al-6V-2Sn.

Three basic test environments were selected for study to provide a wide range of relative aggressiveness and available contaminating species. The environments are dry argon, moist air (relative humidity > 98%), and 3-1/2% NaCl solution. The primary test method used was that of constant load test using a compact tension specimen geometry. A limited number of constant deflection WOL specimens are also included for comparison with the constant load test results. A summary of the variables examined in each phase is shown in Figure 1. The following sections present the major features of each phase.

1. PHASE I - THE EFFECT OF MICROSTRUCTURE AND INTERNAL HYDROGEN

The primary material selected for study in Phase I, II and III was Ti-6Al-4V. This alloy was selected because it is:

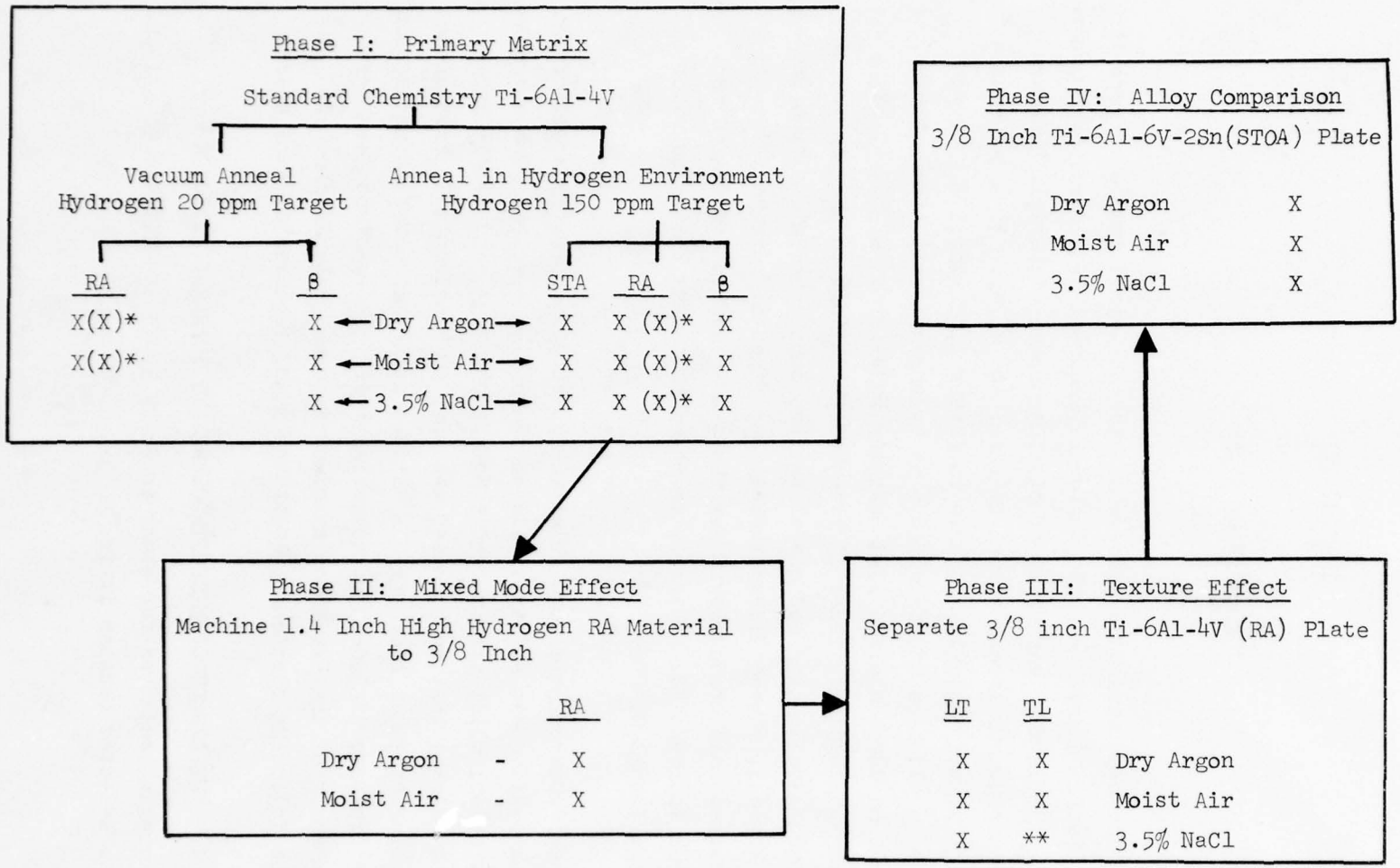

* Bolt loaded MOD WOL specimens; all other tests are constant load CT specimens.

** Specimens previously tested on another program; data available.

Figure 1. Program Test Variables by Phase

1) Widely used and of major importance
2) Used in a variety of microstructures
3) Known to be capable of developing a strong texture

The microstructural variables that can occur in Ti-6Al-4V are extensive if the shape and volume fraction of the alpha phase, etc., are considered. Three microstructural conditions were selected which were representative of 1) a wide range of microstructural conditions, 2) a wide range of stress corrosion susceptibility, and 3) microstructural conditions used in current applications. These are:

1) Solution Treated and Aged (STA): This is the highest strength Ti-6Al-4V normally used in current applications. It was also selected because internal coherency strains are high in this condition. This condition has relatively low stress corrosion resistance.

2) Recrystallized Annealed (RA): This heat treatment was selected because of its wide usage. In addition, it provides a relatively low internal strain condition with a large amount of alpha phase present in an approximately equiaxed form. This condition has reasonably good stress corrosion resistance.

3) Beta Annealed (β): This microstructure is receiving increased attention because of its good fracture toughness and apparently good stress corrosion resistance. In addition, this material provides a latticework configuration microstructure where colonies of alpha platelets separated by beta exist. This condition usually has very good stress corrosion resistance.

The hydrogen level in the material is generally considered to be one of the major parameters in the sustained load cracking of titanium alloys[6-11]. In the current program, two target hydrogen levels were selected $\approx$ 150 ppm, typical of the upper limit of current material specifications, and $\approx$ 20 ppm

typical of the lowest level that can be practically obtained by vacuum annealing large sections of titanium.

Three environments were evaluated, dry argon which represents an inert environment, moist air which introduces water vapor, hydrogen and oxygen as potential contaminating species, and 3.5% NaCl solution which provides a liquid solution environment with the possibility of dissolution as well as hydrogen, oxygen and chlorine as potential contaminating species. Since dry argon and moist air are considered the primary environments, sets of constant load specimens were tested for each microstructure. The 3.5% NaCl solution environment was considered secondary, so only two tests were conducted per microstructure to provide a comparison with selected dry argon and/or moist air results.

2. PHASE II - MIXED MODE EFFECT

Following the Phase I testing, sections of the RA, high hydrogen material were machined down to a thickness of 3/8 inch for evaluation. This material and thickness were selected for the following reasons:

1) A great deal of this material is in current use in mixed mode thicknesses.

2) The thickness is the same as that evaluated in the Phase III texture study, thus these tests evaluate the effect of thickness and provide an additional data base for comparison with the subsequent highly textured material.

3) The thickness provides mixed mode behavior, but is thick enough that complete through-the-thickness yielding should not occur.

For this examination, only dry argon and moist air were evaluated as shown in Table 1. Note that since these tests were designed to determine if the plane strain results are modified under mixed mode conditions, only triplicate specimens were used to check selected previous plane strain results.

3. PHASE III - TEXTURE EFFECT

The material selected for the texture study was the 3/8-inch thick Ti-6Al-4V (RA) material previously studied and characterized[13]. This material has been shown to possess a strong texture and some previous sustained load data in 3.5% NaCl solution and in moist air are available for this material. Tests were conducted in argon, high humidity air and 3½% NaCl solution for specimens with both the LT and TL orientation to evaluate the effect of the (0001) basal plane texture.

4. PHASE IV - ALLOY EFFECT

Due to the wide range of titanium alloy compositions and microstructures in current use, only a spot check of the applicability of the trends observed in Ti-6Al-4V was attempted. A 3/8-inch plate of Ti-6Al-6V-2Sn(STOA) was evaluated in the three test environments. This material selection provided a material with increased beta stabilizer in the form of higher vanadium level.

SECTION IV

MATERIAL PREPARATION AND CHARACTERIZATION

1. PHASE I AND PHASE II MATERIALS

A 3-ft x 3-ft x 1-1/2 inch plate of Ti-6Al-4V was purchased from Reactive Metals, Incorporated to the MIL-T-9046-H Type 3 Composition C specification. The plate received was from ingot #902509 and the average chemistry reported for the ingot is given in Table 1. The reported mill tensile properties for the as received material are presented in Table 2. All reported chemistry and mechanical properties meet or exceed those specified for MIL-T-9046-H Type 3 Composition C material.

a. Development of the Desired Hydrogen Level

The 3-ft x 3-ft x 1-1/2 inch Ti-6Al-4V plate was sectioned into two pieces, one measuring 1.5 x 36 x 24 in. and the other 1.5 x 36 x 12 inch, and the pieces subjected to a vacuum anneal at 1450°F for eight hours. Vacuum fusion hydrogen analysis showed that this operation reduced the hydrogen content from 87 ppm to 13 ppm. The 1.5 x 36 x 24 in. plate was then hydrogenated at 1650°F for nine hours using the procedure similar to that of Meyn[6]. Vacuum fusion analysis showed that this operation raised the hydrogen level from 13 ppm to 207 ppm. This is slightly higher than the 150 ppm target value, but it was decided to proceed with the 207 ppm plate since further efforts to partially vacuum anneal the plate down to 150 ppm would require added thermal cycling and an added stabilization cycle to eliminate any gradient in the hydrogen level. The plate was then machined into specimen blanks for the high hydrogen level material tests.

The remaining 1.5 x 36 x 12 inch piece of the original vacuum annealed plate was rough machined into specimen blanks for the low hydrogen level material. The specimen blanks were then given the final heat treatments.

TABLE 1

REPORTED INGOT CHEMISTRY

(Average of Top and Bottom)

Element	Percentage
C	0.03
N	0.012
Fe	0.18
Al	6.1
V	3.8
Y	< 0.005
O	0.160
H	87 ppm

TABLE 2

REPORTED AS-RECEIVED MILL PROPERTIES

Property	Orientation	Value
Ultimate Strength	L	140.8/144.1 ksi
	T	152.3/152.5 ksi
0.2% Yield Strength	L	131.0/136.5 ksi
	T	142.1/145.0 ksi
Elongation	L	13.0/13.0 percent
	T	13.0/13.0 percent
Percent Reduction in Area	L	24.0/29.0 percent
	T	24.0/30.0 percent

b. Heat Treatment of the Phase I and II Materials

Heat treatment of the low and high hydrogen Ti-6Al-4V specimen blanks was conducted by Aircraft Metal Engineering, Whittier, California in a CRESS Model C1228 electric furnace equipped with a Barber Coleman Model 271P temperature control. The furnace was baked out at 1000°F for 4 hours prior to the start of heat treating. Each load of specimen blanks was covered by a Ti-6Al-6V-2Sn sheet "tent" to minimize radiation temperature effects and to act as a getter for any hydrogen that might be present as a contaminate. The furnace (inside dimension ~ 1 cubic ft) was purged and an operating environment of 99.99% pure argon established and maintained at a flow rate of 5 cubic feet/hour during heating and at 2.5 cubic feet/hour while at temperature. Temperature of the load was monitored by thermocouple and also checked at 30 minute intervals with a Newport Model 267 digital pyrometer. Load temperature was found to be accurate to ± 15°F. The heat treatment cycles used were as follows:

Low Hydrogen Plate

- Simulated hydrogenation cycle, all specimen blanks. Same temperature cycle used on the high hydrogen plate to provide equivalent thermal histories on the high and low hydrogen specimens.
  - 1650°F for 9 hours in 99.99% pure Argon
  - Air Cool
- Recrystallize Anneal (Based on the Current B-1 Production Cycle)[35]
  - 1760°F for 4 hours
  - Fan Cool
  - 1400°F for 1 hour
  - Fan Cool
- Beta Anneal (Based on the Current F-15 Production Cycle)[35]
  - Soak at 1780°F for 45 minutes
  - 1875°F for 10 minutes
  - Fan Cool at 150°F/min. minimum

- Stabilize Anneal for 2 hours at 1400°F
- Fan Cool

High Hydrogen Plate

- Recrystallize Anneal
  - 1760°F for 4 hours
  - Fan Cool
  - 1400°F for 1 hour
  - Fan Cool
- Beta Anneal
  - Soak at 1780°F for 45 minutes
  - 1875°F for 10 minutes
  - Fan Cool
  - 1400°F for 2 hours
  - Fan Cool
- Solution Treat and Aged
  - 1750°F for 45 minutes
  - Water quench
  - 1000°F age for 8 hours
  - Air Cool

Upon completion of the heat treatment of the blanks, a block from each of the 5 heat treatment series was sent for hydrogen analysis. The initial results were obtained from a commercial analysis laboratory (hereafter referred to as #1)and are shown in Table 3. Due to the unexpected changes in the hydrogen level following heat treatment, the same hydrogen samples were sent to a second laboratory (#2) for confirmation. The hydrogen level results from the two laboratories are shown in Figure 2. Note that while significant differences in the measured hydrogen levels exist between the two laboratories, a functional relationship does appear to exist between the readings for most samples. The analysis method used at Laboratory #1 was hot extraction following the procedure in ASTM E-146 for hydrogen measurement in Zr alloys and using a LECO vacuum

TABLE 3

SUMMARY OF HYDROGEN ANALYSIS

Sample Number	Material Condition	Hydrogen Level, ppm	
		Laboratory #1	Laboratory #2
199	Vacuum annealed (All material, Plates 1 and 2)	13	25 edge 28 center
1	Plate 2 after hydrogenation cycle.	207	259
	High hydrogen material (Plate 2) after heat treatment		
A-1-H1	- recrystallize annealed	137	211 edge, 204 center
B-1-H2	- beta annealed	126	167 edge, 171 center
S-3-H3	- solution treated and aged	158	202 edge, 212 center
	Low hydrogen material (Plate 1) after simulated hydrogen cycle in argon and final heat treatment		
A-1-199	- recrystallize anneal	85	120 edge, 119 center
B-1-200	- beta anneal	69	96 edge, 103 center
	Low hydrogen material (Plate 1) after added stabilization, 1400°F for 4 hours in vacuum		
A-1-101	- recrystallize anneal	30, 33*	-
B-1-103	- beta anneal	29, 30*	-

* Second Run, same specimen

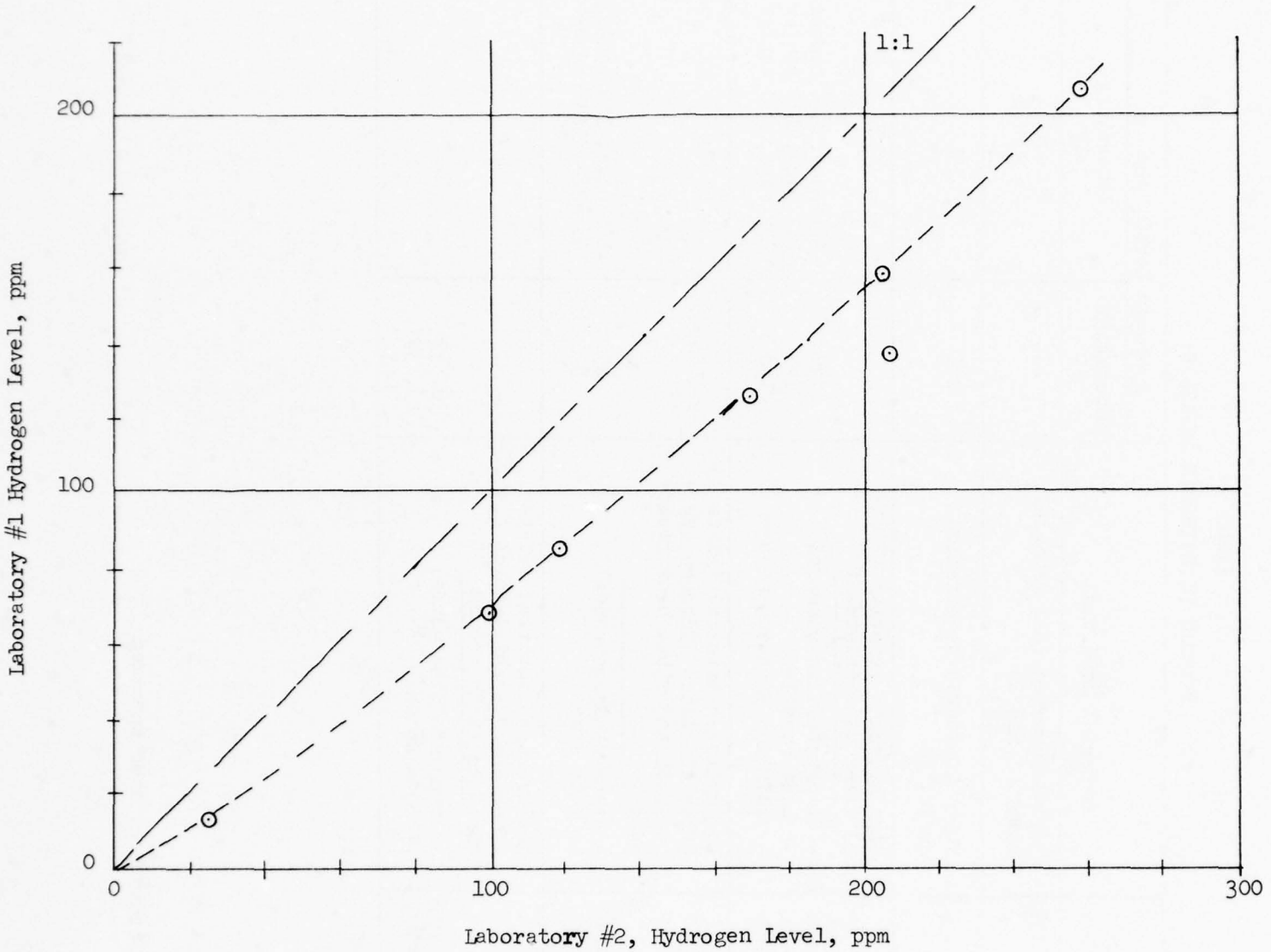

Figure 2. Comparison of Hydrogen Analysis Between Laboratories

fusion unit. Laboratory #2 used a vacuum fusion analysis employing a NRC vacuum fusion unit. Both laboratories used NBS standards SRM 352, 353, and 354 (unalloyed titanium blocks with 32, 98, and 215 ppm hydrogen, respectively) to verify equipment operation and calibration. No judgment of the relative accuracies can be made at this point in time. The results did show, however, that an additional vacuum degas was needed for the low hydrogen plate material.

Since the time during the 1400°F stabilization cycle reportedly has little effect on the properties[35], an extension of the stabilization consisting of four hours at 1400°F in vacuum was selected to degas the low hydrogen plate material. The cycle used was as follows:

Low Hydrogen Plate Material: 4 hours at 1400°F in vacuum, back filled with argon and the furnace opened, fan cooled.

High Hydrogen Plate Material (Except STA Heat Treated Material): 4 hours at 1400°F in argon, fan cooled.

Samples were then machined from the mid-plane of a block from the RA and β heat treated low hydrogen material and the RA high hydrogen material for hydrogen analysis at commercial laboratory #1. The results are also presented in Table 3 and show the low hydrogen plate material was degassed to ~30 ppm of hydrogen. Note that the high hydrogen RA material was reported at 166 ppm.

Specimens were then machined to maintain schedule. The final specimen thickness for the Phase I materials was 1.4 inch. The final thickness for the Phase II material was 0.375 inch nominal.

To resolve the apparent discrepancy in hydrogen level measurements prior to testing, one specimen from each of the final RA and β heat treated sets of both the high and low hydrogen level material was cut under controlled conditions to produce four identical sets of samples. These samples were sent to four laboratories for hydrogen analysis. Results of these hydrogen measurements are shown in Table 4. Test piece identification shown in parenthesis,( ),

TABLE 4

HYDROGEN LEVEL MEASUREMENTS ON SAMPLES REMOVED FROM THE SAME SPECIMEN

Specimen	Hydrogen Measurement Results				
	(1) LAB #2	(2) LAB #1	(3)LAB #3	(4) LAB #4	Avg. of Labs 2,3,4
1-B1 High Hydrogen,Beta Annealed Plate	192,194 (E) *	122 (D)	219 (B)	185.3, 185.5 (C)	199 ± 20
3-A1 High Hydrogen, Recrystallize Annealed Plate	242,254 (A)	162 (E)	250 (B)	236.8, 235.6 (D)	245 ± 10
103-B1 Low Hydrogen, Beta Annealed Plate	34,23 (B)	19 (A)	23 (C)	19.2, 19.2 (D)	24 ± 5
101-A1 Low Hydrogen, Recrystallize Annealed Plate	82,84 (D)	57 (C)	68 (E)	69.9, 67.5 (A)	72 ± 11

* Identification code of piece location submitted for analysis.

indicates the sequential location of the test sample through the thickness of the original specimen, (A) coming from the top surface through (E) which came from the lower surface. Examination of Table 4 shows generally consistent results for all laboratories except Lab #1 where results are increasingly low with increasing hydrogen levels. No effect of specimen location through the plate thickness was observed.

Based on these results, the beta annealed material was shown to have hydrogen levels near the target values of 20 and 150 ppm. The RA material hydrogen levels are higher than originally targeted, indicating that the RA material was not as effectively degassed during the four hours at 1400°F in vacuum as was the beta annealed material. Since a significant difference in hydrogen level between the low (72 ppm) and high (245 ppm) hydrogen content RA material had been achieved, testing was initiated.

2. PHASE I AND PHASE II MATERIAL CHARACTERIZATION

Metallographic sections were prepared from 1 x 3 x 1½-inch material blocks, one of which accompanied each of the five heat treat runs. Three orthogonal sections from each specimen were polished and etched with a solution of 5% HF in methyl alcohol for the RA and β heat treatments and 1% HF + 2% HNO_3 in methyl alcohol for the STA material. Photomicrographs of the specimen surface planes are shown in Figures 3 through 7. Examination indicates the microstructures are typical of the respective heat treatments. Figure 3 shows equiaxed primary alpha typical of the solution treated and aged condition. Figures 4 and 6 both exhibit equiaxed alpha in a transformed beta matrix containing coarse, acicular alpha, typical of the recrystallized annealed condition. Figures 5 and 7 both show a typical transformed beta microstructure typical of beta annealed material.

Texture evaluations for the RA, beta and STA materials were conducted. Basal pole figures for RA (72 ppm hydrogen) and STA (206 ppm hydrogen) are presented in Figures 8 and 9. The results indicate the presence of a definite texture of ~1 to 4X normal for both heat treatments, a somewhat surprising result for 1½

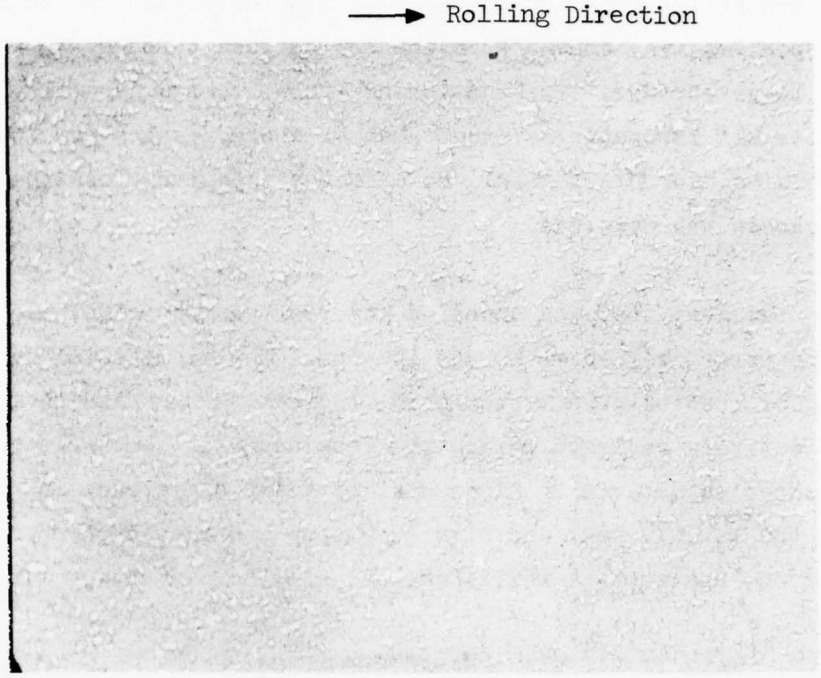

2181-1 100X

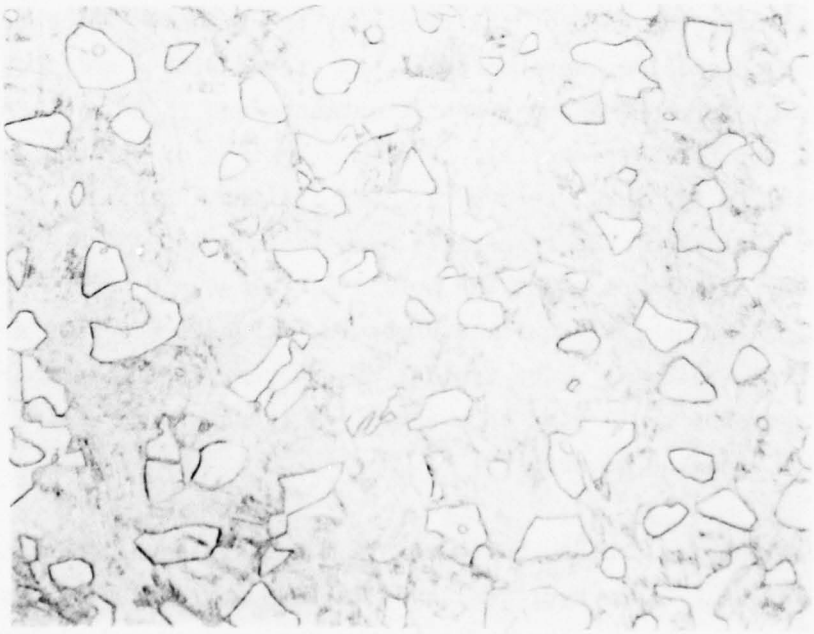

2181-4 500X

Figure 3. Typical Microstructure of the High Hydrogen (206 ppm) Solution-treated and Aged (STA) Material, Plate Surface Plane

→ Rolling Direction

2179-1

100X

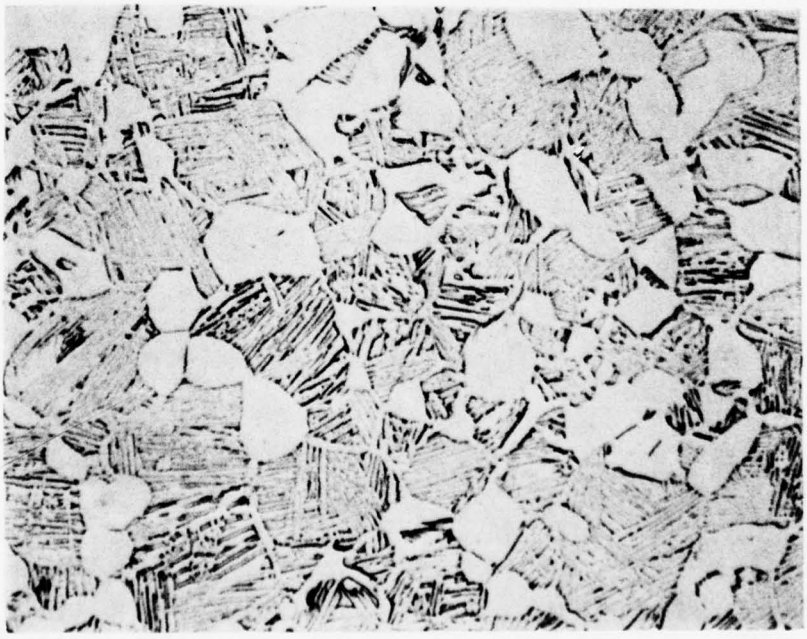

2179-4

500X

Figure 4. Typical Microstructure of the High Hydrogen (245 ppm) Recrystallize Annealed (RA) Material, Plate Surface Plane

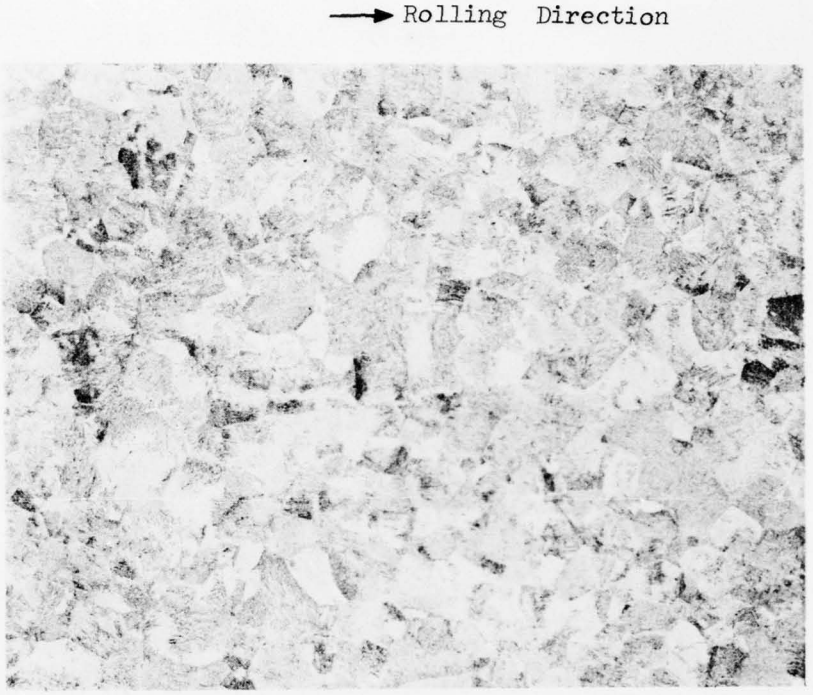

2180-7 25X

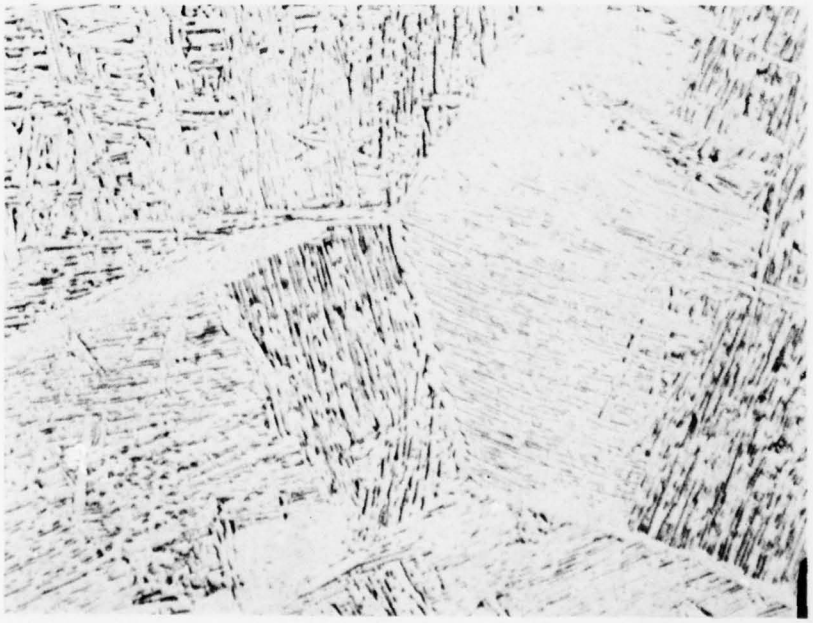

2180-4 500X

Figure 5. Typical Microstructure of the High Hydrogen (199 ppm) Beta Annealed Material, (β), Plate Surface Plane

→ Rolling Direction

2182-1 100X

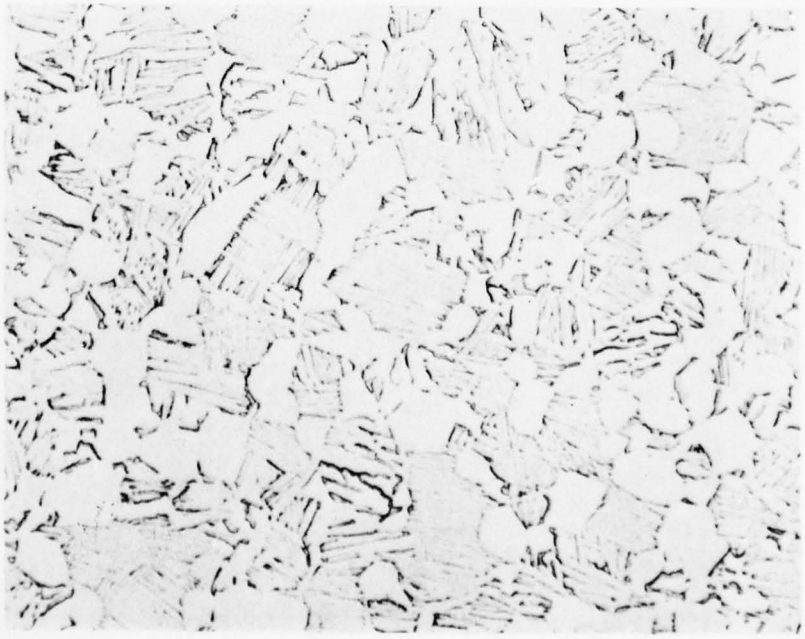

2182-4 500X

Figure 6. Typical Microstructure of the Low Hydrogen (72 ppm) Recrystallize Annealed (RA) Material, Plate Surface Plane

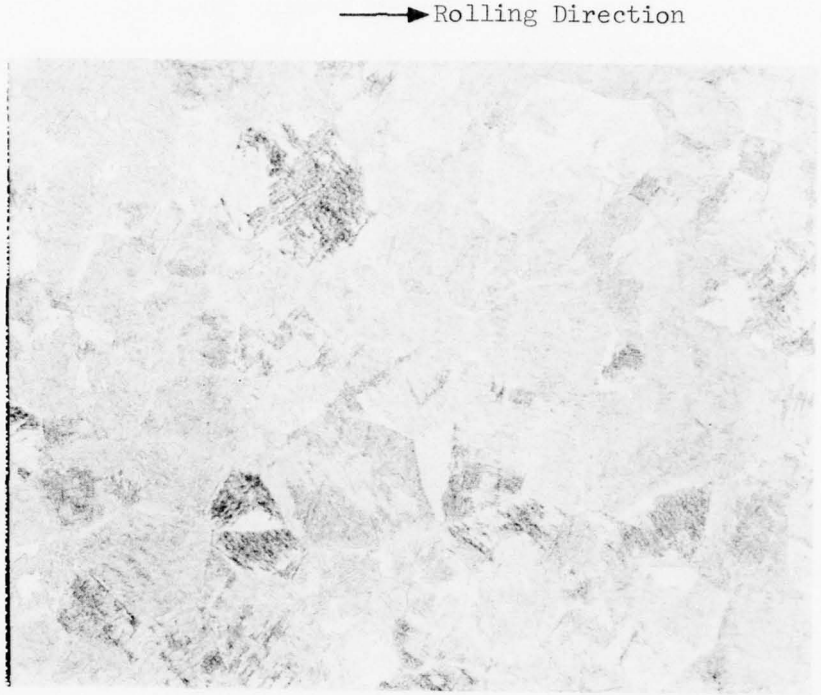

2183-7 25X

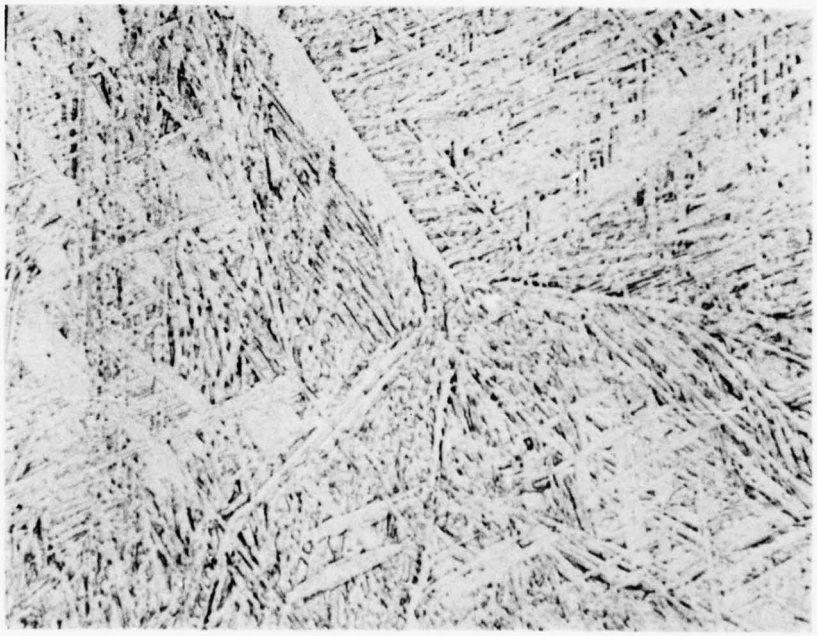

2183-4 500X

Figure 7. Typical Microstructure of the Low Hydrogen (24 ppm) Beta Annealed (β) Material, Plate Surface Plane

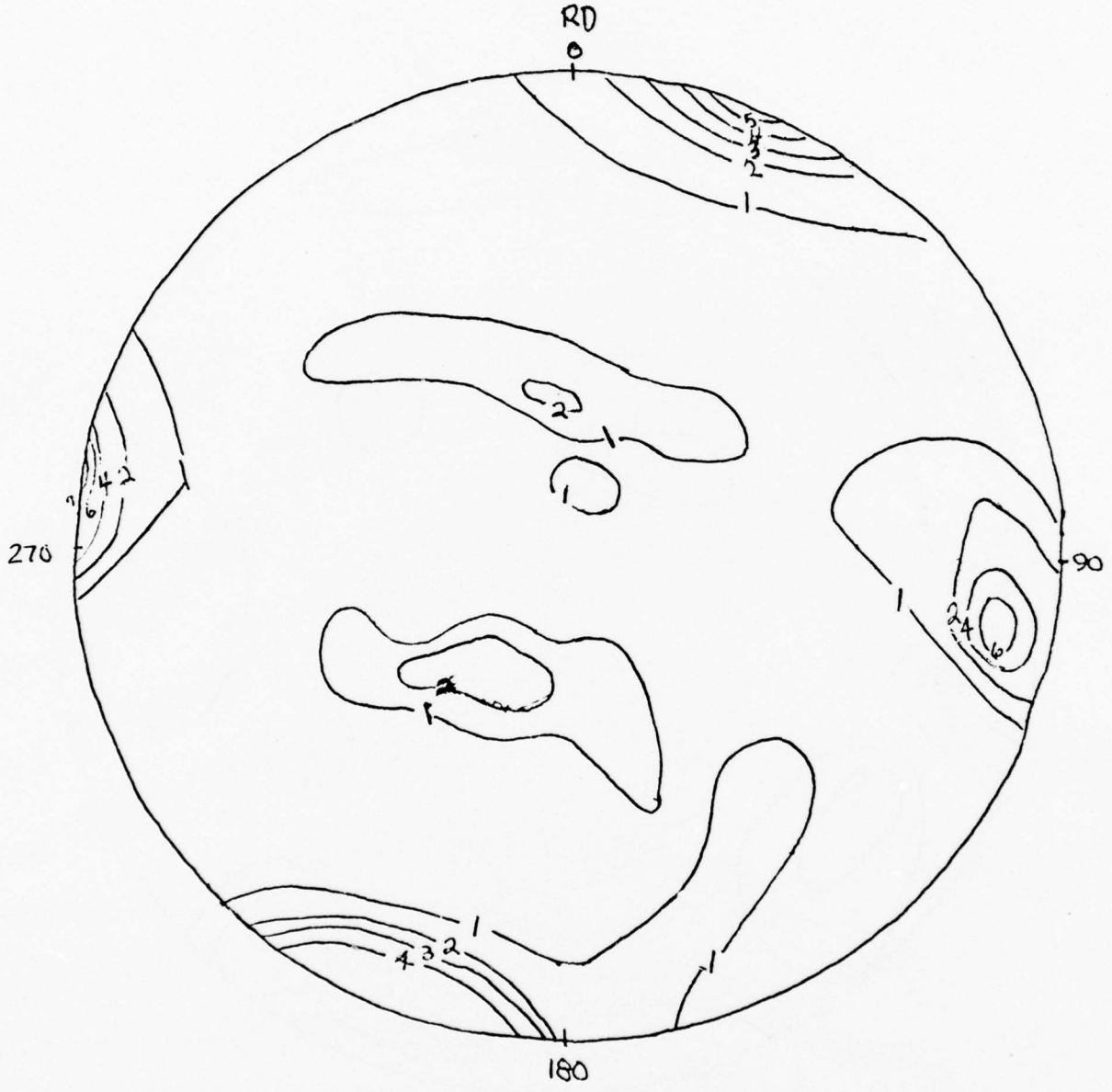

Figure 8. Basal Plane Pole Figure for Recrystallize Annealed Ti-6Al-4V Plate (72 ppm Hydrogen). Numbers are Times Random.

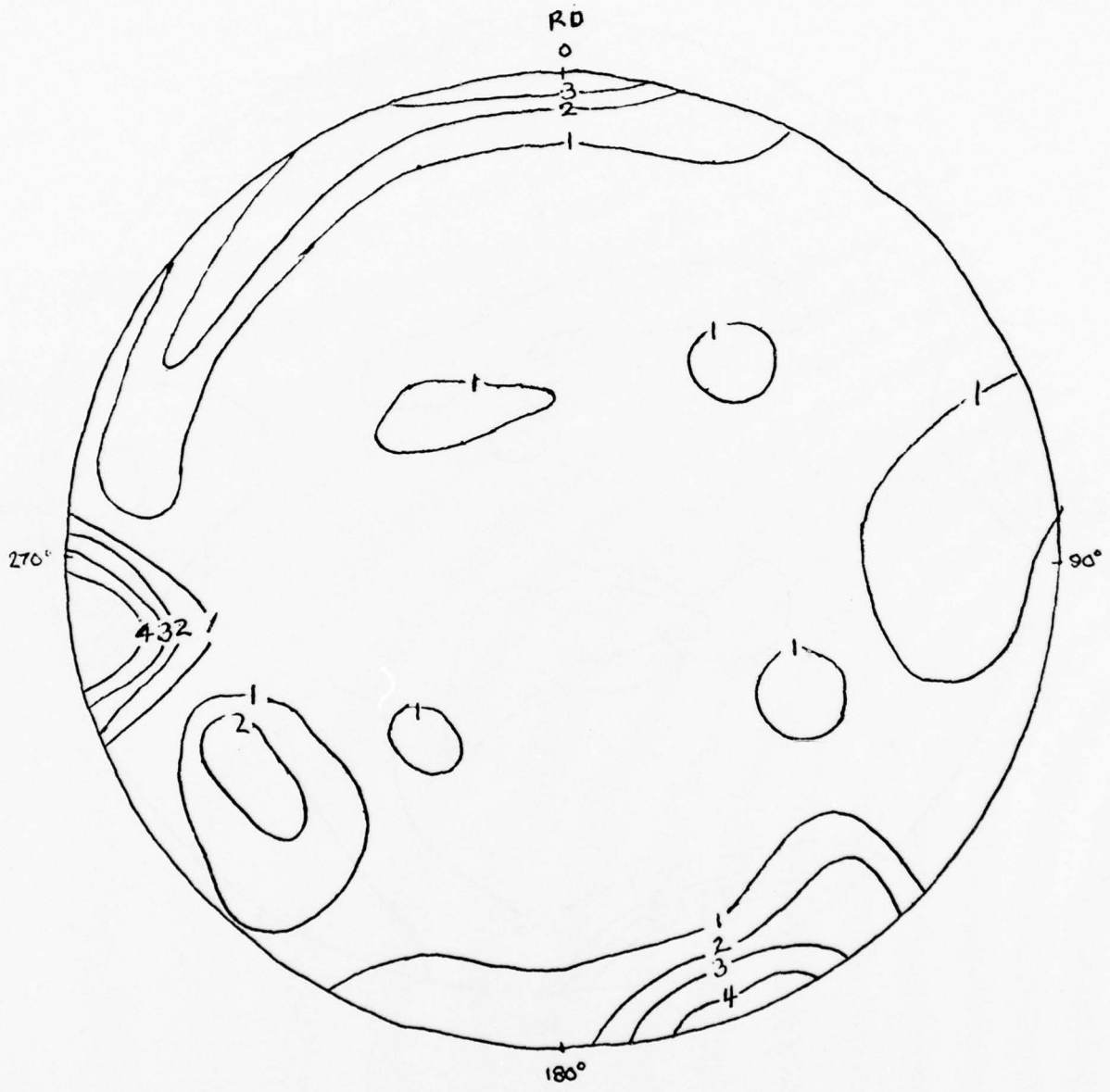

Figure 9. Basal Plane Pole Figure for Solution Treated and Aged Ti-6Al-4V Plate (206 ppm Hydrogen). Numbers are Times Random.

inch plate where all samples for texture analysis were removed from a location 1/4 inch below the surface. Pole figure results for the β annealed (248 ppm hydrogen) material are presented in Figure 10 for the basal (0001) α phase and in Figure 11 for the (200) β phase. A high degree of texture is indicated. Note, however, that this may be an artifact of the large grain size of the material.

Duplicate tensile tests were conducted as per ASTM E8[36] using standard 0.505 inch diameter round specimens for each microstructure. The results are presented in Table 5. Comparison of the results with minimum acceptable values[37,38] show all properties to be acceptable. Duplicate K_{Ic} tests were conducted on standard compact tension specimens for each of the five test materials. All tests were conducted in accordance with ASTM E-399-74[40]. Results of these tests are presented in Table 6.

Comparison of the fracture toughness values with those reported in Reference 41 shows the STA and Beta annealed toughness to be in the range anticipated. The recrystallize annealed materials generally show slightly lower toughness values than the 69-85 ksi $\sqrt{in.}$ reported. This may be a result of the somewhat higher strength (yield ~ 135 ksi) of the current material as compared to the typical 120 ksi yield strength reported in Reference 41.

3. PHASE III MATERIAL CHARACTERIZATION

The Ti-6Al-4V alloy for Phase III was originally purchased from the B-1 Division of Rockwell International* as 3/8 x 36 x 96 inch plate for use in a previous program, Reference 13. The material was purchased to Rockwell International Specification ST0170LB0032, Revision B, for the recrystallized anneal (RA) condition. The heat treatment sequence for the 3/8 inch material including heating at 1750°F for 1-1/2 hour and air cooling. The chemical analysis results for the material are presented in Table 7. Note that using

*Rockwell-International B-1 Airplane Division, International Airport, Los Angeles, California 90009. The 3/8 inch plate was supplied by Titanium Metals Corporation of America, 195 Clinton Road, West Caldwell, N.J. 07606, as Heat K9548.

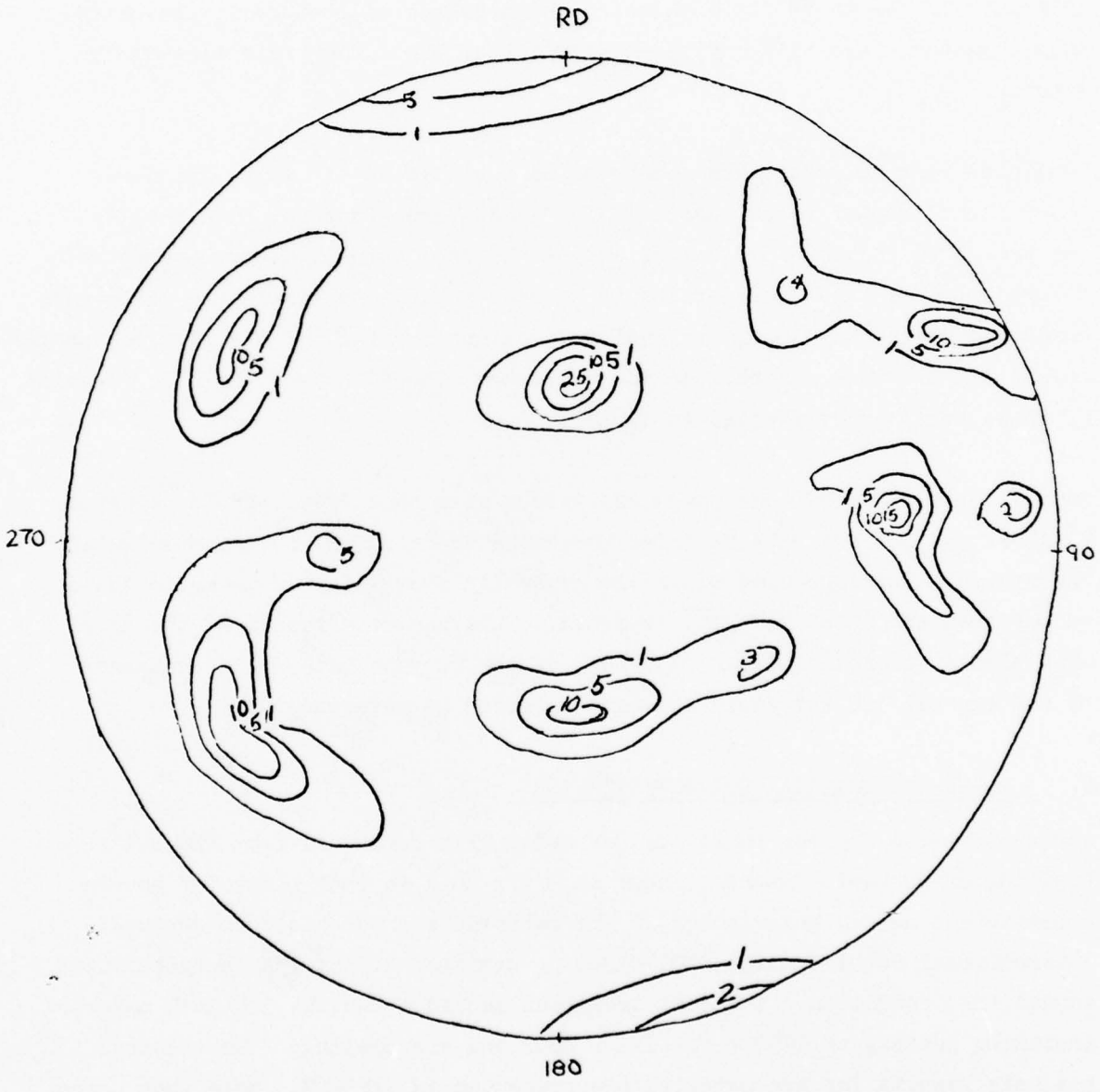

Figure 10. Basal Pole Figures for Beta Annealed Ti-6Al-4V Plate (24 ppm Hydrogen). Numbers are Time Random

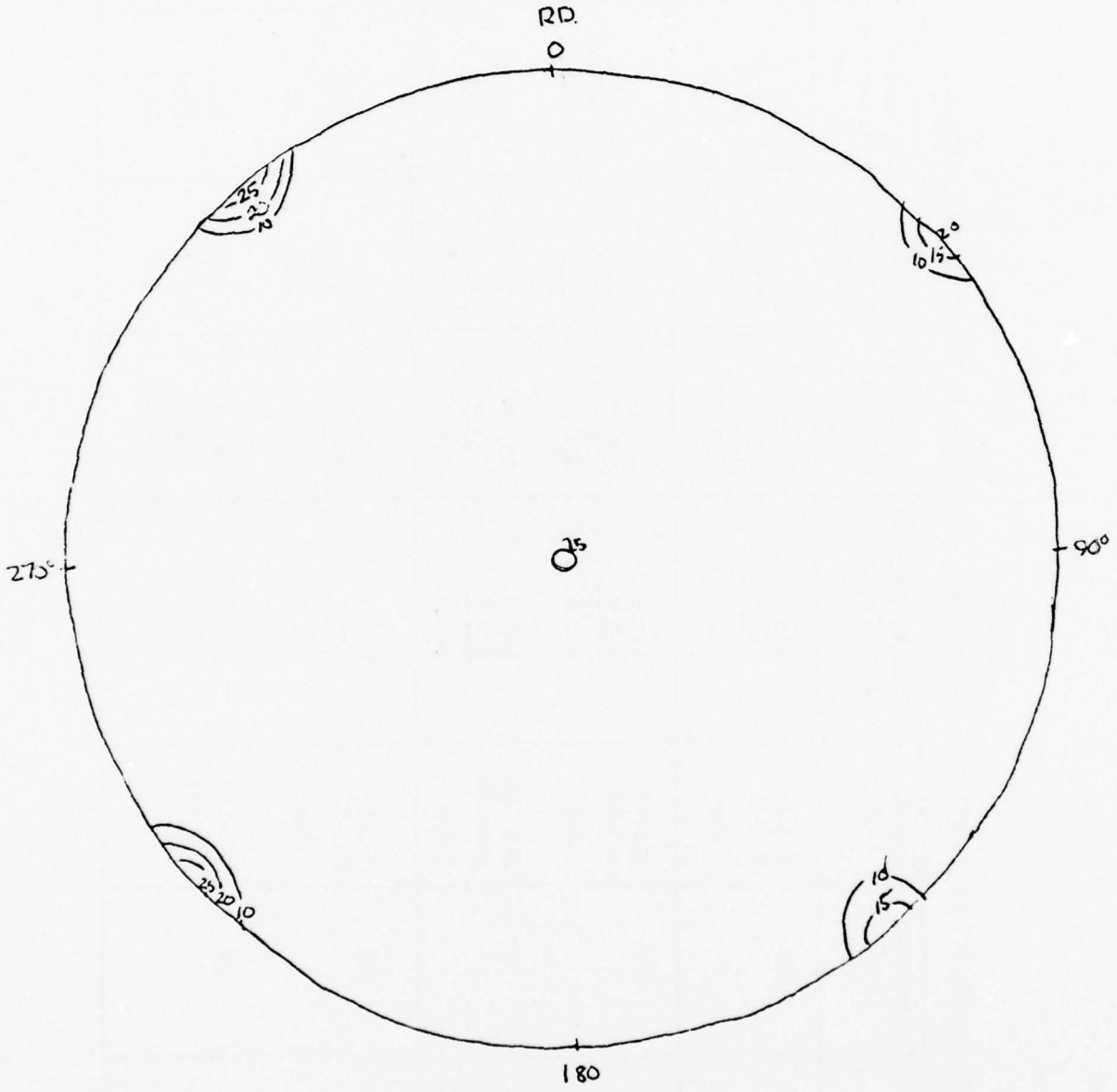

Figure 11. (200) Pole Figure for Beta Phase of Ti-6Al-4V(8) Plate. Numbers are Times Random.

TABLE 5

SUMMARY OF TRANSVERSE ORIENTATION TENSILE DATA FOR Ti-6Al-4V 1.5-INCH PLATE MATERIAL

Heat Treatment	Hydrogen Level, ppm	Specimen Number	Ultimate Tensile Strength, ksi	0.2% Yield Strength, ksi	Percent Elongation in 2 inch	Percent Reduction in Area	Apparent Modulus 1000 ksi
Solution Treatment and aged, STA	206	S-3-55	168.1	159.2	15.0	36.3	17.5
		S-3-56	165.6	158.9	15.0	34.7	17.4
		Ave	166.8	159.0	15.0	35.5	17.4
Recrystallize Annealed, RA	245	A-1-53	146.6	138.8	12.0	24.0	17.4
		A-1-54	146.4	138.0	12.5	24.8	-
		Ave	146.5	138.4	12.2	24.4	17.4
	72	A-1-196	145.9	135.3	15.0	21.8	18.8
		A-1-198	144.1	134.8	12.0	21.0	17.8
		Ave	145.0	135.0	13.5	21.4	18.3
Beta Annealed, β	199	B-1-57	143.4	133.5	12.0	22.3	17.0
		B-1-58	146.1	136.0	11.5	15.7	18.0
		Ave	144.8	134.8	11.8	19.0	17.5
	24	B-1-194	137.6	127.5	9.5	12.3	16.3
		B-1-195	139.3	128.6	10.0	14.3	16.6
			138.4	128.0	9.8	13.3	16.4

TABLE 6

FRACTURE TOUGHNESS RESULTS FOR PHASE I Ti-6Al-4V MATERIALS
REMOVED FROM $1\frac{1}{2}$-INCH THICK PLATE, T-L ORIENTATION

Material	Avg. Hydrogen Level * ppm	Specimen Number	Thickness, B inch	Width, W inch	Crack Length, a inch	P_Q, lbs.	Max Load, P_{max} lb.	Fracture Toughness K_{Ic} ksi $\sqrt{in.}$	Valid per ASTM E-399
High Hydrogen Solution-treated and Aged (STA)	206	S-3-35	0.998	2.812	1.508	9,615	10,000	61.6	Yes
		S-3-34	0.998	2.802	1.506	9,390	9,750	60.7	Yes
								Avg.61.2	
High Hydrogen Beta Annealed (β)	199	B-1-6	1.403	2.794	1.433	19,800	20,250	84.1	Yes
		B-1-20	1.405	2.790	1.480	18,900	19,300	85.0	Yes
								Avg.84.6	
High Hydrogen Recrystallize Annealed (RA)	245	A-1-32	1.406	2.795	1.511	14,750	15,600	68.5	* Yes
		A-1-4	1.409	2.816	1.487	16,250	16,725	72.0	Yes
								Avg.70.2	
Low Hydrogen Beta Annealed (β)	24	B-1-116	1.402	2.801	1.418	20,000	21,000	83.4	Yes
		B-1-118	1.405	2.794	1.435	20,600	21,500	87.8	Yes
								Avg.85.6	
Low Hydrogen Recrystallize Annealed (RA)	72	A-1-119	1.380	2.783	1.519	13,275	14,450	64.0	Yes
		A-1-120	1.394	2.797	1.508	13,900	14,575	64.7	Yes
								Avg.64.4	

*Based on average of all laboratory results excluding Lab #1 data

TABLE 7

CHEMICAL ANALYSIS OF Ti-6Al-4V(RA) ALLOY - PHASE III MATERIAL (Ref. 13)

Element	Specification Requirements, wt. % (RI ST0170LB00032-B)	Heat K9548*	Accuracy as per MIL-T-009046
Al	5.5 - 6.2	6.4	±0.4
V	3.5 - 4.5	4.0	———
Fe	Max 0.25	0.14	———
C	Max 0.08	0.026	———
O	0.09 - 0.13	0.13	±0.02
N	Max 0.030	0.014	———
H	Max 0.0125	0.010	±0.002, -0.0

* TMCA Certificate of Test, Chemical Analysis, 4-27-72

the accuracy ranges for the determination of Al, O_2, and H_2 percentages in titanium alloys as given in MIL-T-009046, the material could be considered to meet the requirements of RI ST0170LB00032-B although results are marginal, both the aluminum and oxygen being slightly on the high side. Metallographic sections were taken and the microstructure found to consist of equiaxed primary alpha separated by retained beta at the grain boundary. Detailed microstructural evaluation is presented in Reference 13 and the typical microstructure is shown in Figure 12.

This material was previously found[13] to possess a very strong crystallographic texture, the basal hexagonal planes being oriented as shown in Figure 13. This texture was consistent with the very high tensile strength in the transverse orientation and the significantly lower tensile strength in the longitudinal orientation.

Tensile test results are presented in Table 8. Fracture test results using compact tension specimens and procedures as per ASTM E-399 test specifications are presented in Table 9. All results are mixed mode and invalid for K_{Ic}.

4. PHASE IV MATERIAL CHARACTERIZATION

The Ti-6Al-6V-2Sn alloy was purchased* as 3/8 x 36 x 96 inch plate in the solution-treated-and-overaged (STOA) condition obtained by the following heat treatment cycle: heat at 1700°F for one hour and water quench; anneal at 1400°F for one hour and air cool. Samples were removed from the corner, submitted for chemical analysis, and the results compared to specification requirements. As shown in Table 10, the material met the specification requirements for each element within the appropriate limits.

*Titanium Metals Corporation of America, 195 Clinton Road, West Caldwell, New Jersey 07006. Heat K9197

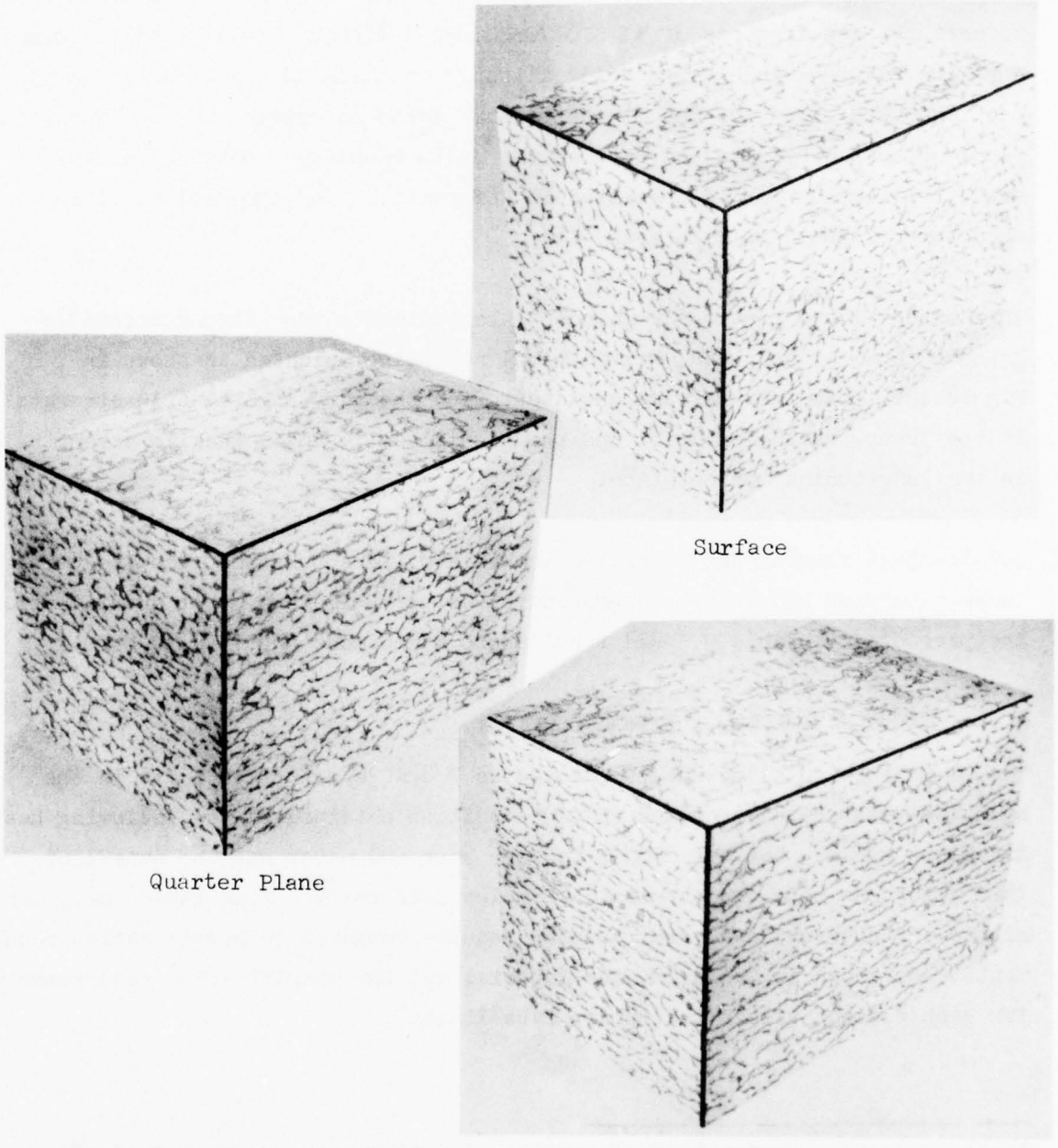

Figure 12. Typical Microstructure of Phase III Ti-6Al-4V(RA) Material, Surface, Quarter Plane and Midplane, as etched.

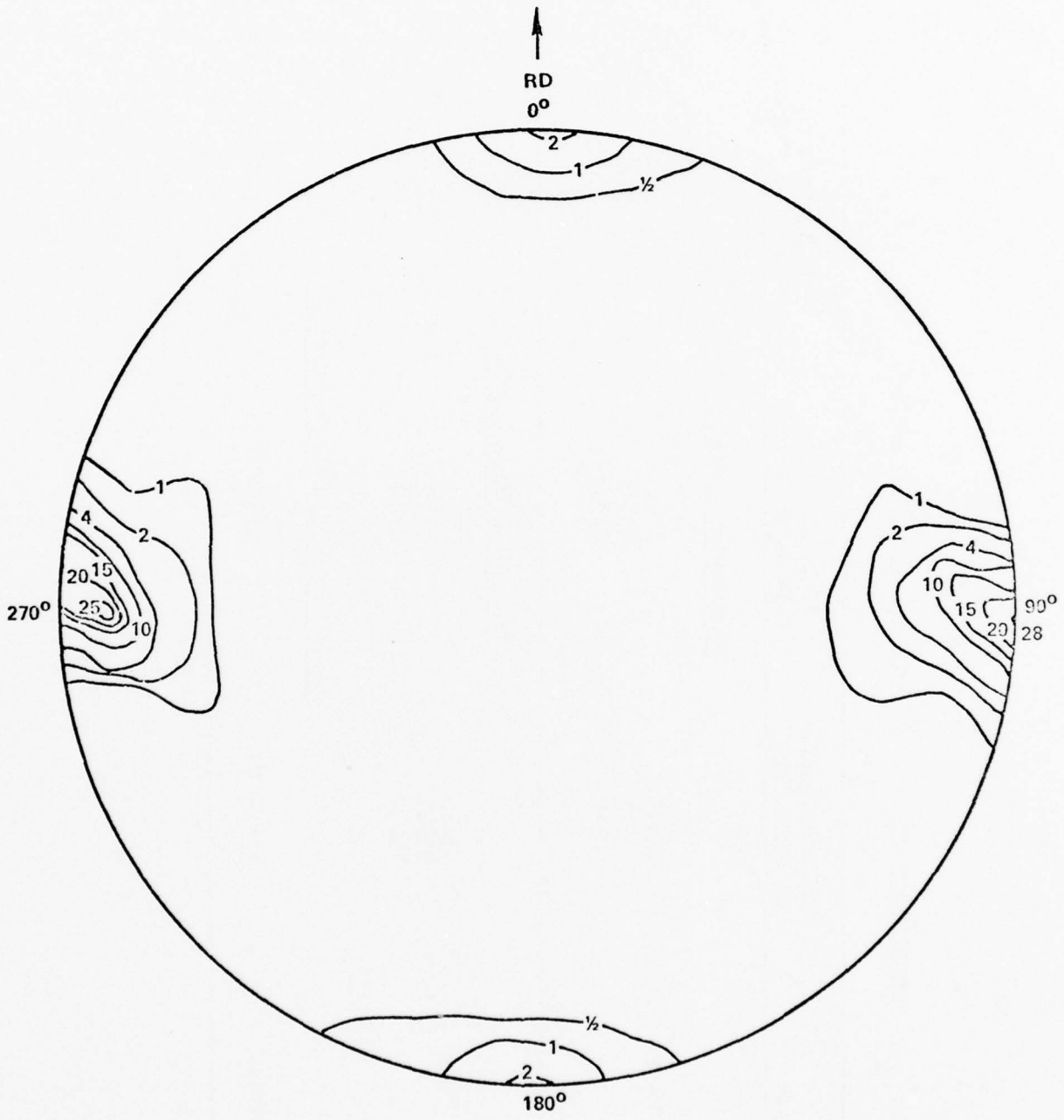

Figure 13. Crystallographic Texture of the 3/8 in. Ti-6Al-4V(RA) Plate (Heat No. K 9548), (0001) Pole Figure, Numbers are Times Random

TABLE 8

TENSILE RESULTS FOR 3/8 INCH Ti-6Al-4V(RA) MATERIAL (Ref. 13)

Data Source	Ultimate Tensile Strength, ksi	Yield Strength 0.2% Offset, ksi	Elongation, Percent in 2 inch
		Longitudinal, Heat K-9548	
Present Study	131.3	119.1	13.0
	131.4	118.6	10.0
	132.6	119.6	12.0
		Transverse, Heat K-9548	
Present Study	151.0	141.0	16.0
	152.4	142.0	16.0
	152.1	142.2	15.0
		Specification RI ST 0170LB00032-B	
Specification	130.0 Min.	120-145	10.0 min.

TABLE 9

SUMMARY OF FRACTURE TOUGHNESS VALUES OF Ti-6Al-4V(RA) 3/8-INCH THICK PLATE AS DETERMINED ACCORDING TO ASTM E399 REQUIREMENTS (Ref. 13)

Orientation	Specimen Number	Fracture Toughness* K_Q, ksi $\sqrt{in.}$	Strength Ratio, R_{SC}
T-L	D25	92.3	1.134
	D27	81.9	1.166
	D24	90.4	1.023
	Average	88.2	1.108
L-T	D21	95.4	1.250
	D22	92.1	1.163
	Average	93.8	1.206

* $B < 2.5 \left(\frac{K_Q}{S_y}\right)^2$

TABLE 10

CHEMICAL ANALYSIS OF Ti-6Al-6V-2Sn(STOA) 3/8-INCH PLATE

Element	Specification Requirements, wt. % (MIL-T-9046H)	Analysis of Materials, wt. %
		3/8 x 36 x 96 in. Plate
Al	5.0 - 6.0	5.4
V	5.0 - 6.0	5.6
Sn	1.5 - 2.5	1.8
Fe	.35 - 1.0	0.54
Cu	.35 - 1.0	0.54
C	max 0.05	0.022
O	max 0.20	0.18
N	max 0.050	0.017
H	max 0.015	0.009

Additional samples were removed from the surface, quarterplane and midplane of the 3/8-inch plate and the three orthogonal sections were examined. All sections showed primary alpha in a matrix of transformed beta, with the amount of primary alpha increasing from 30% at the center to 40% at the surface. However, the primary alpha showed a nonuniform distribution at the surface where there were large prior beta grains that were deficient in primary alpha, and some grain boundary alpha present. Complete microstructural characterization of the material has been previously reported in Reference 13. A typical micrograph is shown in Figure 14.

Tensile test results for the material are presented in Table 11. A summary of the fracture toughness results using compact tension specimens and the procedures of ASTM E399 for plane strain fracture toughness testing are presented in Table 12. All fracture toughness values meet the requirements of ASTM E399 for plane strain K_{Ic} values.

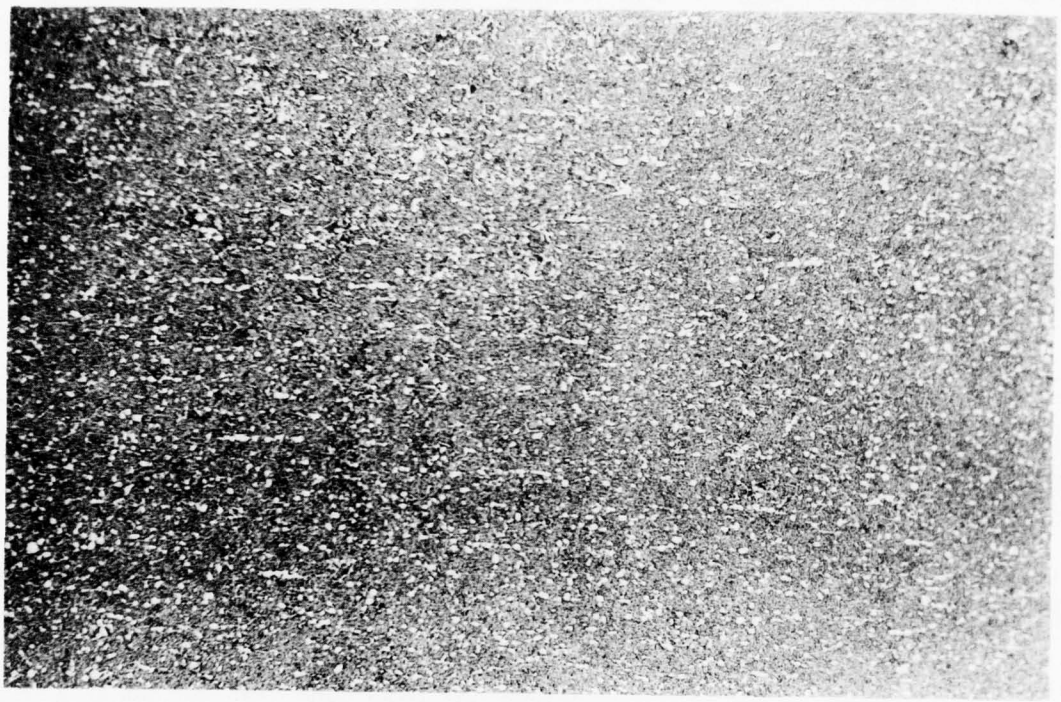

100X

500X

Figure 14. Typical Microstructure of Ti-6Al-6V-2Sn(STOA) Material[13]

TABLE 11

TENSILE RESULTS FOR Ti-6Al-6V-2Sn(STOA) 3/8-INCH THICK PLATE SPECIMENS (Ref. 13)

Plate Orientation	Ultimate Strength, ksi	0.2% Yield Strength, ksi	% Elongation in 2 Inch
Longitudinal	165.5	152.6	14.0
Longitudinal	168.3	--	14.0
Longitudinal	167.8	158.7	15.0
Average	167.2	156.5	14.7
Transverse	168.8	163.0	13.5
Transverse	167.4	160.2	15.0
Transverse	167.4	157.8	16.0
Average	167.8	160.3	14.8

TABLE 12.

SUMMARY OF FRACTURE TOUGHNESS VALUES OF Ti-6Al-6V-2Sn(STOA)
3/8-INCH PLATE AS DETERMINED ACCORDING TO ASTM E-399 REQUIREMENTS (Ref. 13)

Orientation	Specimen Number	Fracture Toughness K_{Ic} ksi $\sqrt{in.}$
T-L	C54	48.3
	C55	44.0
	C56	49.1
	C57	42.9
	Average	46.1
L-T	C53	42.5
	C51	41.9
	C52	44.3
	Average	42.9

SECTION V

EXPERIMENTAL PROCEDURES

1. SPECIMEN CONFIGURATION

Two basic test procedures were used. The primary test procedure used was constant load testing of compact tension specimens of the type described in ASTM E-399-74 and shown in Figure 15A. This specimen was loaded monotonically to a predetermined load and the load held constant. This procedure results in an increasing stress intensity field with increasing crack length, i.e., $dK/da > 0$. The secondary procedure examined used a modified WOL bolt loaded specimen of the type shown in Figure 15B. For this bolt loaded specimen, the stress intensity field decreases with increasing crack length, i.e., $dK/da < 0$.

2. CONSTANT LOAD CRACK GROWTH TEST PROCEDURES

Compact tension specimens were fatigue precracked in laboratory air to an initial a/W ratio of from 0.3 to 0.4. Precracking was conducted at a range ratio, R = 0.1, at a frequency of 10 Hz. The final precrack load range was such that the maximum stress intensity of the precrack was less than or equal to 0.6 K_{Ic} or the subsequent test K_{Ii} level, whichever is lower.

Each specimen was then sealed in a clear polyethylene bag which permitted optical viewing of the crack at all times. The specimen was then installed in a Satec creep machine (capacity selected from 6 to 20 kip) at zero load and the test environment stabilized. The specimen was then loaded to the test load. Crack length was monitored using both optical comparators to measure surface crack length and with an MTS compliance gage to check for subsurface growth until failure or 200 hours had elapsed. Specimens which did not fail in 200 hours were refatigue cracked and fractured. Subsurface crack extension was then measured from the fracture surface of the specimen at both surfaces, the midplane and both quarterplane locations using a tool maker's microscope.

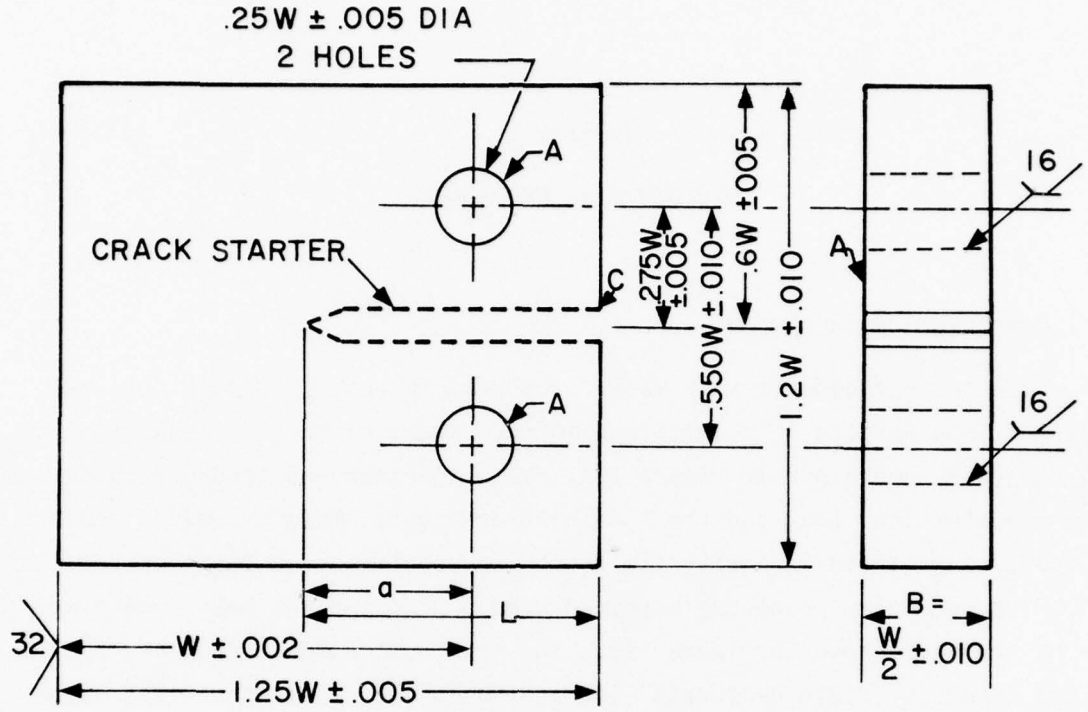

A. Compact Specimen (CT) Configuration (For B = 1.4 inch)

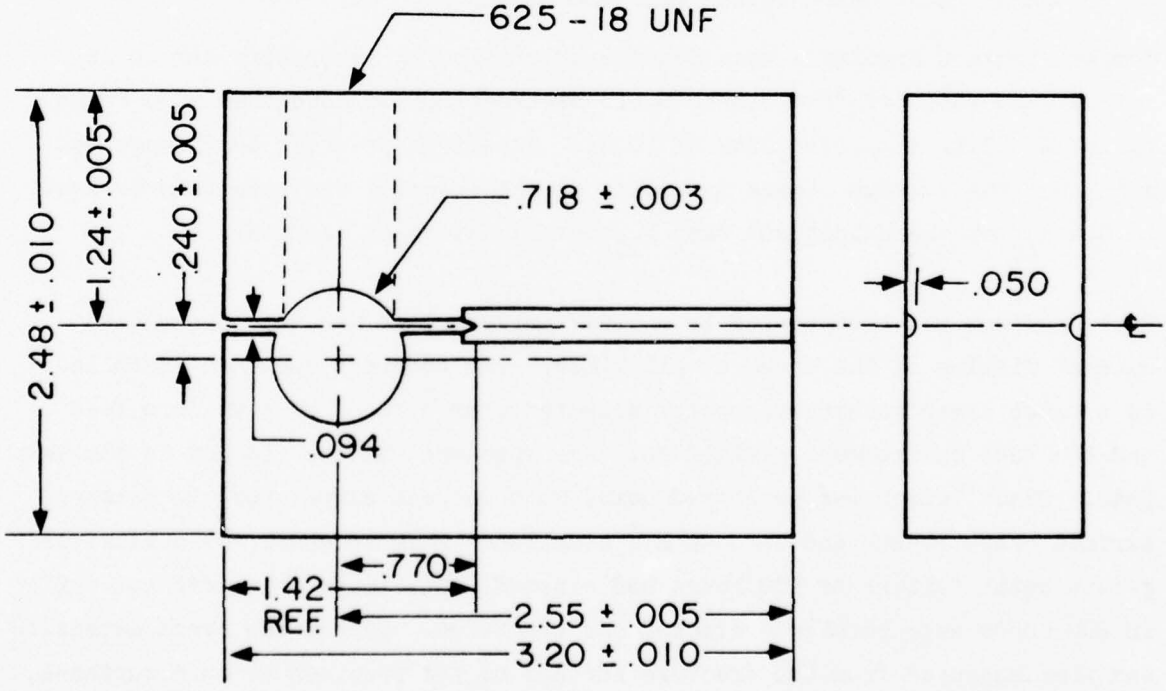

B. Mod-WOL Specimen Configuration

Figure 15. Specimen Configuration

3. TEST ENVIRONMENTS

The three environments which were included in this program were dry argon, high humidity air, and 3.5% NaCl solution. The environments were contained by a sealed clear polyethylene bag attached around the specimen, which permitted viewing of the crack during test and assured that the entire specimen test section was exposed to the environment. The details of the environmental controls are presented below for each of the three environments.

a. Dry Argon

Research quality argon gas with a certified purity of 99.996% and a dewpoint of -70°F which conforms to Mil Spec A-184558 was used. All valves and lines were ultrasonically cleaned and the system purged for five minutes prior to the start of each test. The sealed bag on the specimen was evacuated using a roughing pump and back filled with the dry argon. This procedure was then repeated twice more. A positive argon pressure was then maintained in the bag to prevent any leaking in of laboratory air during the test. Laboratory temperature was continuously controlled at 71 $\pm$ 2°F.

b. High Humidity Air

The high humidity air environment was generated by runring shop air through a filter to remove impurities and then bubbling the air through a saturated copper sulfate/distilled water solution. This procedure produced an environment with ~98% relative humidity. The same procedure for maintaining the environment in the test chamber as previously described for the dry argon was used.

c. 3.5% NaCl Solution

This solution was made by adding laboratory purity NaCl to deionized water to form a 3.5% NaCl solution. A continuous flow of the solution was maintained through the bag on the test specimen by a gravity feed flow system. Rate of flow was controlled at approximately 0.1 gal/hr.

4. DATA REDUCTION FOR CONSTANT LOAD TESTS

The expression used to determine the stress intensity factor was the newly revised ASTM expression for the compact tension specimen[39].

$$K = \frac{P}{B\,W} \frac{(2 + a_1)}{(1 - a_1)^{3/2}} (0.886 + 4.64a_1 - 13.32a_1^2 - 5.6a_1^4)$$

where a_1 = a/W; expression valid for a/W > 0.2

B = specimen thickness, inch

W = specimen width, inch

P = applied load, pounds

a = crack length

Note that this expression is valid over a larger range ($0.3 \leq a/W \leq 0.7$) than the expression in ASTM E-399-72, where $0.45 \leq a/W \leq 0.55$ was the originally intended range of application. The new expression permits the obtaining of valid da/dt measurements over a much larger range of crack lengths.

As will be discussed in the Results Sections, extensive crack tunneling occurred in many specimens. For these conditions, the COD based crack length was computed using the results of Newman[42] for CT specimens

$$\frac{B \cdot E \cdot COD}{P} = 120.7 - 1065.3(a/W) + 4098(a/W)^2 - 6688(a/W)^3 + 4450.5(a/W)^4, \text{ for } 0.35 \leq a/W \leq 0.60.$$

where COD = crack opening displacement

E = modulus of electricity

5. SUSTAINED DEFLECTION CRACK GROWTH TEST PROCEDURES

Modified WOL specimens were fatigue precracked in laboratory air for at least 0.2 inch beyond the machined slot. Precracking was conducted at an R ratio (minimum load/maximum load) of +0.1 and at a frequency of 10 Hz. The final precrack maximum load range was selected such that the final precrack maximum stress intensity was less than or equal to the initial maximum stress intensity of the subsequent test condition.

The specimen was self-loaded by bolts and loading pins to the desired stress intensity level in a manner similar to that described by Novak and Rolfe[43]. The specimens were then placed in the test environment such that the crack tip was immersed in the environment (if liquid) and the bolt and loading pin are above the environmental fluid level. Specimens were periodically measured for crack growth. Maximum test time in the environment was 200 hours.

The K_{Iscc} determination procedure followed that outlined by Novak and Rolfe[43]. Subsequent to the sustained load test, the crack length was marked by fatigue in air and then the specimen fractured for measurement of crack extension and arrest as evidenced by fracture surface markings.

The initial and final induced stress intensities in the modified WOL specimen used in the stress corrosion cracking tests were calculated by the following equation[44]:

$$K_I = \frac{C_3 P}{B\sqrt{a}}$$

where C_3 is given by:

$$C_3 = 30.96\left(\frac{a}{W}\right) - 195.8\left(\frac{a}{W}\right)^2 + 730.6\left(\frac{a}{W}\right)^3 - 1186.3\left(\frac{a}{W}\right)^4 + 754.6\left(\frac{a}{W}\right)^5$$

SECTION VI

PHASE I TEST RESULTS

Three different heat treatments, STA, RA and 8, of a common Ti-6Al-4V plate were examined in this phase. Two of the heat treatments, the RA and 8, were each studied at two hydrogen levels while the STA material was studied only in the higher hydrogen level condition. Results for this phase are presented in the following sections by heat treat condition.

1. SUSTAINED LOAD TEST RESULTS FOR THE SOLUTION-TREATED AND AGED MATERIAL (STA)

The sustained load test results for the STA material (206 ppm of hydrogen) are summarized in Table 13. Examination of the post-test fracture surfaces confirmed optical surface measurements and COD readings made during testing which indicated that the major growth occurred subsurface in all environments, as illustrated in Figure 16. This "crack-tunneling" characteristic makes optical crack length measurements misleading and unusable for crack growth rate determination. Similarly, use of the compliance data for crack-growth rate determination must be approached with care since a straight crack front geometry is also assumed in the formulation of compliance relationships between crack length and crack-opening-displacement, COD. As a result, the "effective crack length" computed based on COD readings may not correspond well to any measured physical crack length, the COD response depending on the extent of crack tunneling at a given point in time. The crack growth rate data presented in the following sections was developed using the COD data. As a result, the data is presented in terms of the "effective crack growth rate" defined as the time rate of change of the effective crack length as defined by the crack opening displacement. The stress intensity factor is also presented in terms of an "effective stress intensity factor" computed using standard expressions and the average "effective crack length" in the interval. Based on these procedures, the effective crack growth rate

TABLE 13. SUSTAINED LOAD CRACK GROWTH RESULTS FOR 1.0 INCH THICK Ti-6Al-4V(STA) PLATE MATERIAL

Specimen	Environment	Initial Stress Intensity K_{Ii}, ksi$\sqrt{in.}$	$\frac{K_{Ii}}{K_{Ic}}$	Test Duration Hours	Observed Crack Growth Δa, inch				
					Surface	1/4 Plane	1/2 Plane	3/4 Plane	Surface
	T-L Orientation, K_{Ic} = 60.1 ksi $\sqrt{in.}$								
S-3-36	High Humidity Air	55.9	0.93	166.8 DNF*	0.007	0.266	0.270	0.196	0.021
S-3-38	High Humidity Air	51.2	0.85	238.3 DNF	0.004	0.005	0.005	0.006	0.006
S-3-37	High Humidity Air	45.3	0.75	215.5 DNF	~0.001	~0.001	0.002	0.002	~0.001
S-3-39	Dry Argon	57.2	0.95	236.9 DNF	0.057	0.300	0.353	0.323	0.041
S-3-40	Dry Argon	43.6	0.72	195.6 Failed	0.10	0.23	0.47	0.50	0.25
S-3-41	Dry Argon	36.6	0.61	195.5 DNF	0	0.013	0.029	0.027	0.001
S-3-60R	Dry Argon	30.1	0.50	212.8 DNF	~ 0	~ 0	~ 0	~ 0	~ 0
S-3-61R	3-1/2% NaCl Solution	43.8	0.73	4 minutes	~0.38	~0.50	~0.46	~0.40	~0.42
S-3-42	3-1/2% NaCl Solution	36.9	0.61	234.7 DNF ***	0.021	0.014	0.032	0.089	0.101
S-3-61	3-1/2% NaCl Solution	31.7	0.53	67 DNF **	0.017	0.011	0.025	0.025	0.008

* DNF - Did Not Fail

** Chamber failed, test stopped

*** Grew initially and then arrested

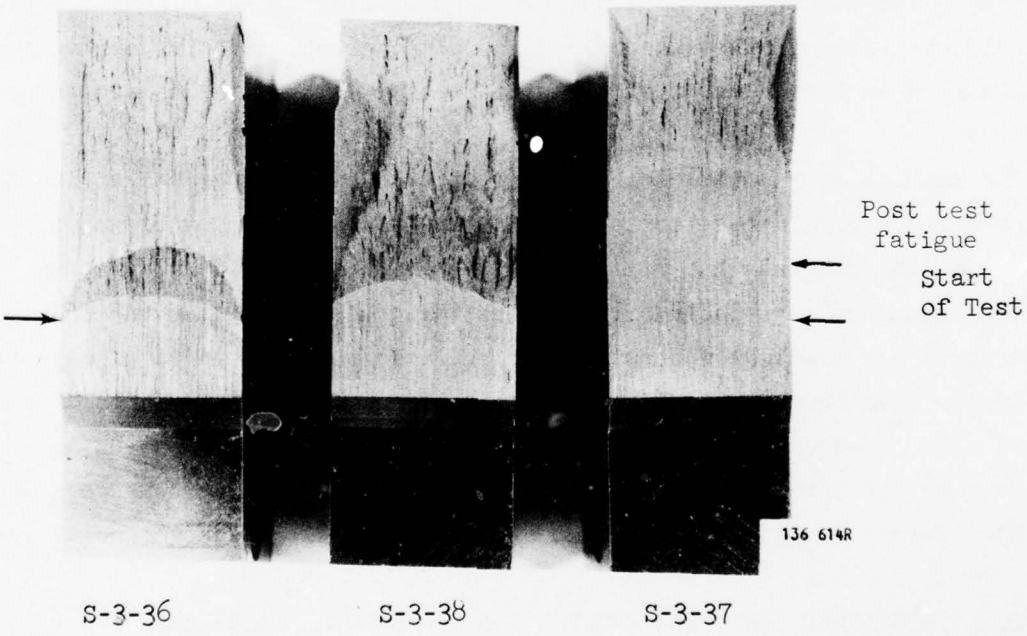

Figure 16. Typical Fracture Surface Appearance for Ti-6Al-4V(STA) Specimens S-3-36, S-3-37, and S-3-38 Tested in High Humidity Air

behavior for the Ti-6Al-4V(STA) material is presented in Figure 17.

Examination of the results shown in Table 13 and Figure 17 show sustained load cracking to occur at lower stress intensities in the dry argon than in high-humidity air even though the upper shelf rates appear to be equivalent. For the results in dry argon, the apparent threshold stress intensity is ~35 ksi $\sqrt{\text{in.}}$ as compared to a value of ~50 ksi $\sqrt{\text{in.}}$ in high-humidity air. It is of interest to note in Table 13 that specimen S-3-39 tested at K_{Ii} = 57.2 ksi $\sqrt{\text{in.}}$ did not fail in 236.9 hours (but did grow) while specimen S-3-40 tested at K_{Ii} = 43.6 ksi $\sqrt{\text{in.}}$ failed in 195.6 hours. This is believed due to the larger plastic zone formed on loading to the higher K_{Ii} level which remained in the wake of the tunneling crack. Similar behavior was also observed in the RA material and will be discussed in the subsequent section.

The results in 3½% NaCl solution exhibited slow crack growth at low K_{Ii} which occurred early in the test and then arrested. This behavior was also observed in the RA materials and will be discussed in the subsequent section. Above the "apparent" threshold (i.e., where the crack propagates to failure with no arrest) the crack growth rate upper shelf is several orders of magnitude faster than observed in high-humidity air and dry argon. It is of interest to note, however, that the apparent threshold in 3½% NaCl solution is the same as the threshold value in dry argon although some growth does occur and then arrest in 3½% NaCl solution at lower initial stress intensity levels.

2. SUSTAINED LOAD TEST RESULTS FOR THE RECRYSTALLIZE ANNEALED (RA) MATERIAL

The two hydrogen levels of the RA materials studied were 245 $\pm$ 10 ppm for the high hydrogen material and 72 $\pm$ 18 ppm for the low hydrogen material. Tables 14 and 15 present the results for the high and low hydrogen level RA materials, respectively. Results of both materials show the tests in high humidity air exhibited only minor crack growth tendencies, the behavior of the two hydrogen levels being essentially equivalent. Test results in dry argon show sustained load cracking to occur only at very high K_{Ii} levels in the low hydrogen level material. In the high hydrogen material, however, growth occurred over a

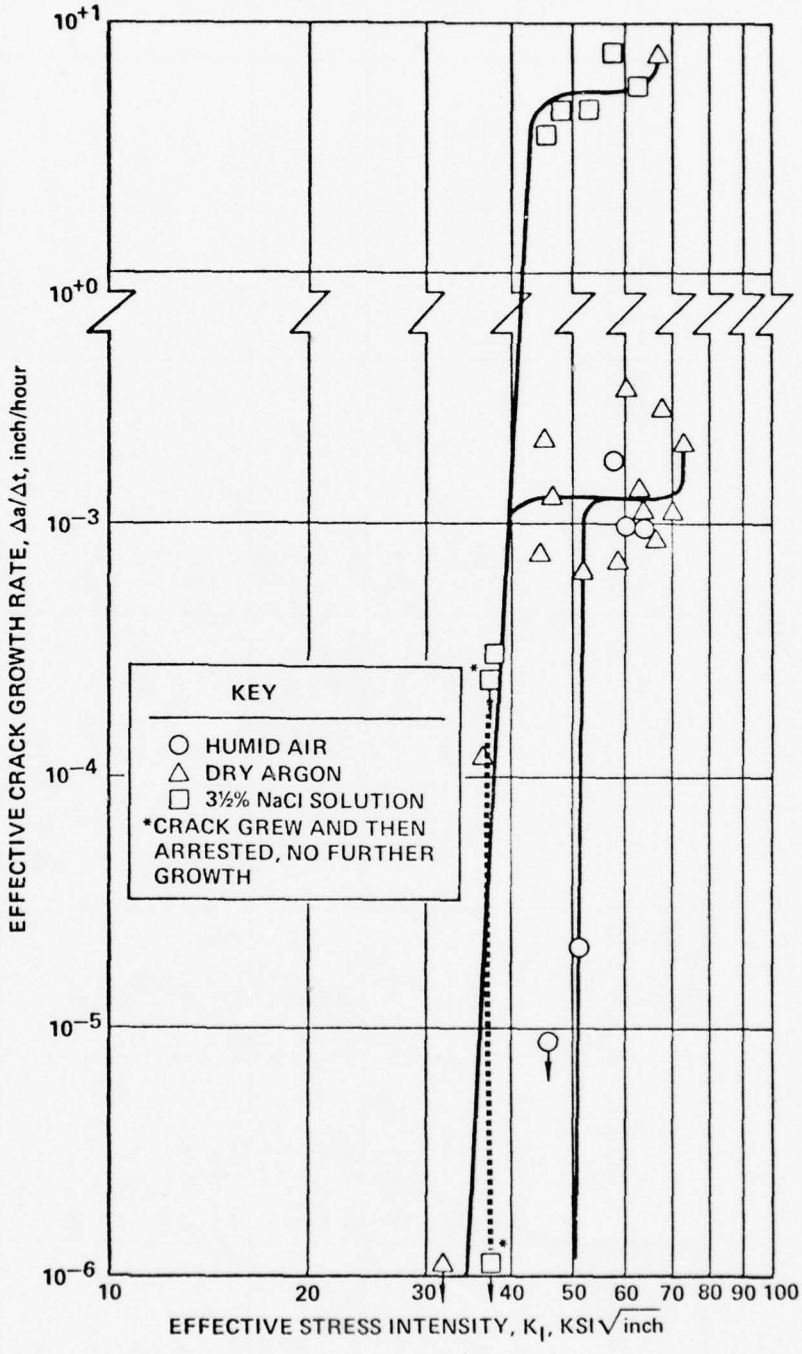

Figure 17. Effective Crack Growth Rate Behavior of Ti-6Al-4V(STA) Material (206 ppm)

TABLE 14. SUSTAINED LOAD CRACK GROWTH RESULTS FOR HIGH HYDROGEN (245 ± 10 ppm)
Ti-6Al-4V(RA) PLATE MATERIAL, B = 1.4 INCH

Specimen	Environment	Initial Stress Intensity K_{Ii}, ksi/in.	Ratio $\frac{K_{Ii}}{K_{Ic}}$	Test Duration Hours	Observed Crack Growth Δa, inch				
					Surface	1/4 Plane	1/2 Plane	3/4 Plane	Surface
	T-L Orientation, K_{Ic} = 70.2 ksi $\sqrt{in.}$								
A-1-23	High Humidity Air	70.0	0.99	Failed on Loading	-	-	-	-	-
A-1-26	High Humidity Air	65.1	0.93	210.8 DNF*	0.005	0.040	0.020	0.017	0.002
A-1-31	High Humidity Air	61.7	0.88	209.9 DNF*	0.004	0.012	0.018	0.008	0.008
A-1-17	High Humidity Air	51.2	0.73	215.1 DNF	0.002	0.002	0.005	0.001	0.001
A-1-28	Dry Argon	69.5	0.99	123.0 DNF **	0.003	0.030	0.023	0.030	0.015
A-1-19	Dry Argon	65.1	0.93	204.6 DNF **	0.010	0.140	0.170	0.130	0.005
A-1-21	Dry Argon	53.9	0.77	132.0 FAILED	~0.20	~0.60	~0.60	~0.53	~0.13
A-1-25	Dry Argon	43.2	0.62	191.1 DNF	0	0	0.001	0.001	0
A-1-18	3-1/2% NaCl Solution	53.1	0.76	105 sec. Failed	0.39	0.34	0.31	0.29	0.28
A-1-10	3-1/2% NaCl Solution	42.2	0.60	464 sec. Failed	0.55	0.64	0.62	0.54	0.58
A-1-12	3-1/2% NaCl Solution	37.2	0.53	162.2 DNF **	0.141	0.162	0.301	0.320	0.146
A-1-5	3-1/2% NaCl Solution	33.4	0.48	109.3 DNF **	0.056	0.114	0.104	0.072	0.128
A-1-11	3-1/2% NaCl Solution	28.0	0.40	196.6 DNF	***	***	***	***	***

* DNF = Did not fail

** Grew initially and arrested.

*** Crack front indistinct, COD indicates ~0.30 inch change during test (see text).

TABLE 15. SUSTAINED LOAD CRACK GROWTH RESULTS FOR LOW HYDROGEN (72 ± 18 ppm) Ti-6Al-4V(RA) PLATE MATERIAL, B = 1.4 INCH

Specimen	Environment	Initial Stress Intensity K_{Ii}, ksi$\sqrt{in.}$	Ratio $\frac{K_{Ii}}{K_{Ic}}$	Test Duration Hours	Observed Crack Growth Δa, inch				
					Surface	1/4 Plane	1/2 Plane	3/4 Plane	Surface
	T-L Orientation, K_{Ic} = 64.4 ksi $\sqrt{in.}$								
A-1-122	High Humidity Air	62.0	0.96	Failed on Loading	-	-	-	-	-
A-1-124	High Humidity Air	60.3	0.94	208.5 DNF **	0	0.070	0.055	0.055	0.005
A-1-111	High Humidity Air	54.0	0.84	233.0 DNF*	0.008	0.011	0.007	0.008	0.006
A-1-104	Dry Argon	67.1	1.04	42 seconds	-	-	-	-	-
A-1-117	Dry Argon	65.4	1.0	76.2 DNF **	0.065	0.046	0.060	0.066	0.010
A-1-105	Dry Argon	56.0	0.87	142.8 DNF	0.003	0.009	0.008	0.011	0.010
A-1-113R	3-1/2% NaCl Solution	48.9	0.76	0.12 Failed	~0.33	~0.36	~0.29	~0.33	~0.30
A-1-113	3-1/2% NaCl Solution	39.1	0.61	44.3 DNF **	0.096	0.102	0.090	0.085	0.050
A-1-115	3-1/2% NaCl Solution	24.8	0.39	203.4 DNF**	~0.040	~0.110	~0.140	~0.130	~0.090

* DNF = Did not fail

** Grew initially and then arrested.

range of K_{Ii} values, but failure occurred only in a narrow range of K_{Ii} values, no growth to failure occurring below or above this range. At very high K_{Ii} values, extensive multiple cracking was found to occur at the crack tip in both hydrogen level materials as shown in Figure 18. This crack tip shattering blunted the effective crack tip sufficiently to prevent crack extension in the low $\frac{dK}{da}$ gradient in the specimen. As the K_{Ii} value was lowered, crack splitting decreased and crack growth to failure occurred in the high hydrogen level material, the low hydrogen level material exhibiting only minor growth.

The effective crack growth rate results for the high and the low hydrogen level materials are presented in Figure 19. Crack growth rates in the high humidity air are minor below ~0.95 K_{Ic} and are essentially equivalent for both hydrogen levels. In addition, the low hydrogen material shows the same rate behavior in dry argon as in high humidity air. The results in dry argon show a definite decrease in the threshold with an increase in the internal hydrogen level, the threshold dropping to ~45 ksi $\sqrt{\text{in.}}$ for the 245 ppm material compared to ~55 ksi $\sqrt{\text{in.}}$ for the 72 ppm material. This difference is even larger if normalized to account for the difference in fracture toughness for the two materials, the threshold being ~0.64 K_{Ic} for the high hydrogen level material compared to ~0.85 K_{Ic} for the low hydrogen level material.

Results for both materials in $3\frac{1}{2}\%$ NaCl solution showed rapid crack extension to occur to failure at initial stress intensities greater than an apparent threshold value. At initial stress intensities below the apparent threshold, a region is encountered where the crack grows rapidly at the start of the test, the growth rate then slowing and finally going to zero after approximately 10 to 15 minutes, no further crack growth then occurring for the duration of the test. Post test examination of the crack path of specimens that arrest showed the formation of multiple "fingers" of crack growth all along the crack front as shown schematically in Figure 20. This indicates that as the cracking causes splitting along grain boundaries parallel to the

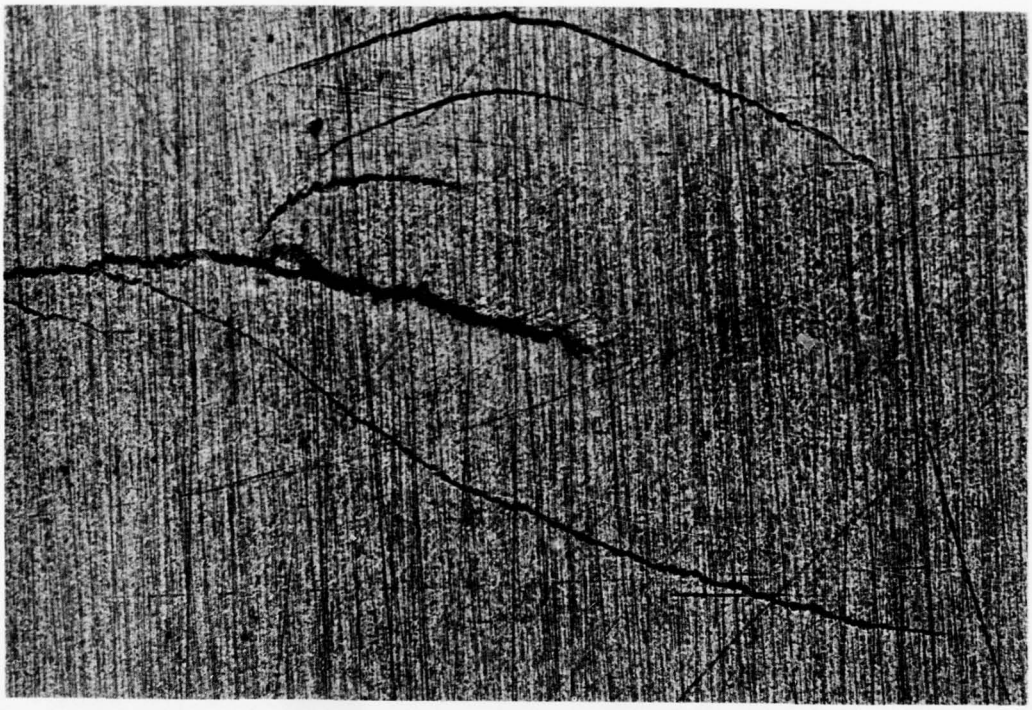

Rear Surface 25X

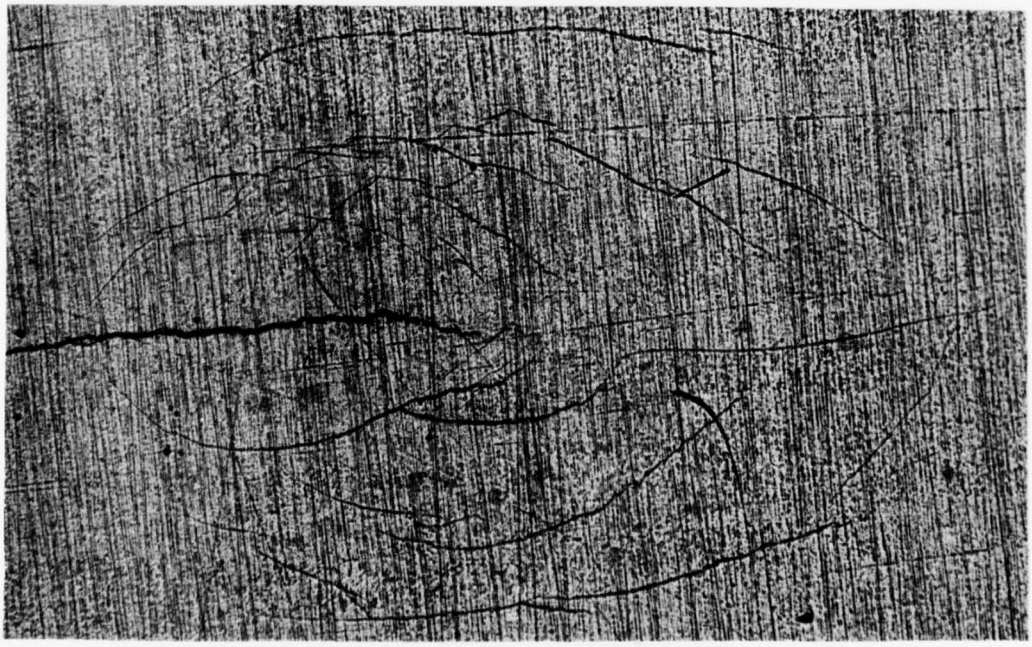

Front Surface 25X

Figure 18. Typical Crack Tip Cracking in Dry Argon for RA Materials, Specimen A-1-117

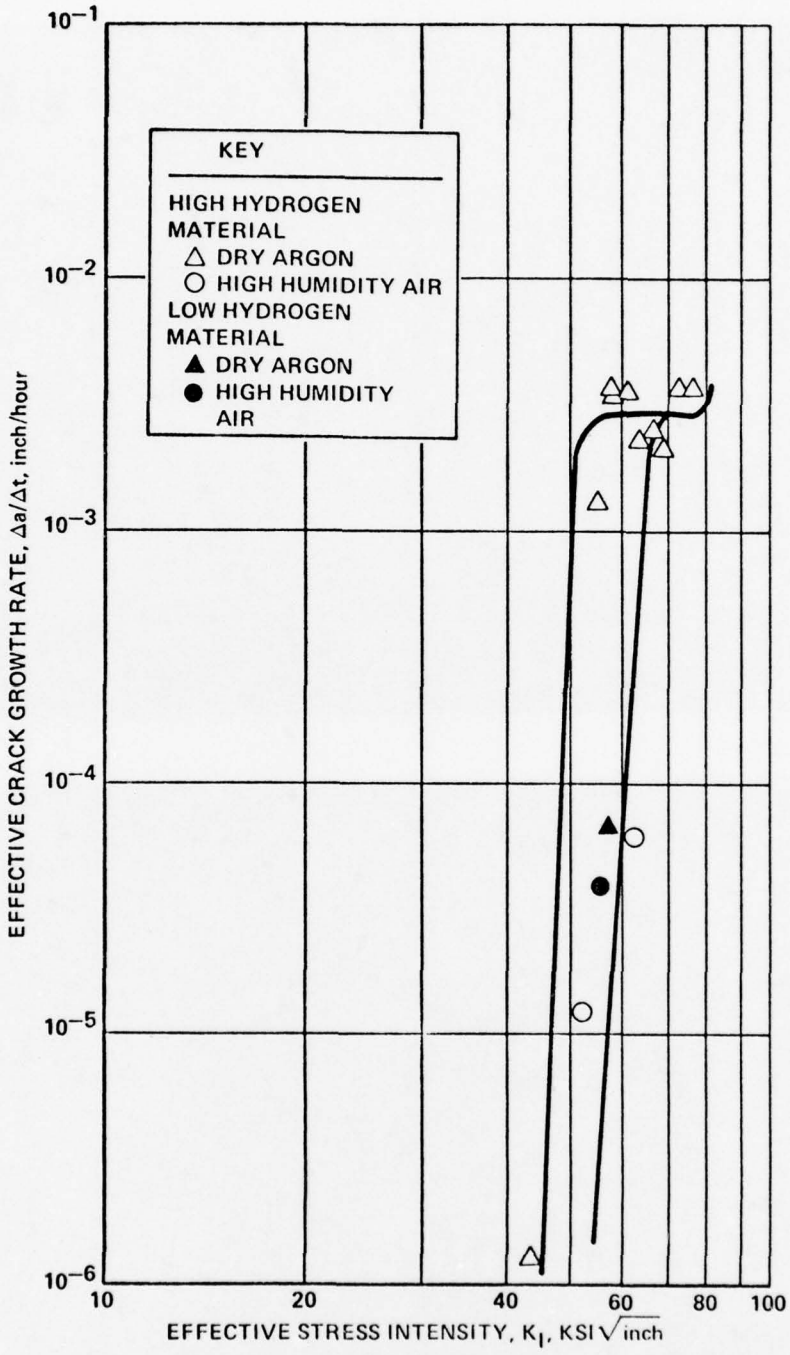

Figure 19. Ti-6Al-4V(RA) Crack Growth Rates in Dry Argon and High Humidity Air

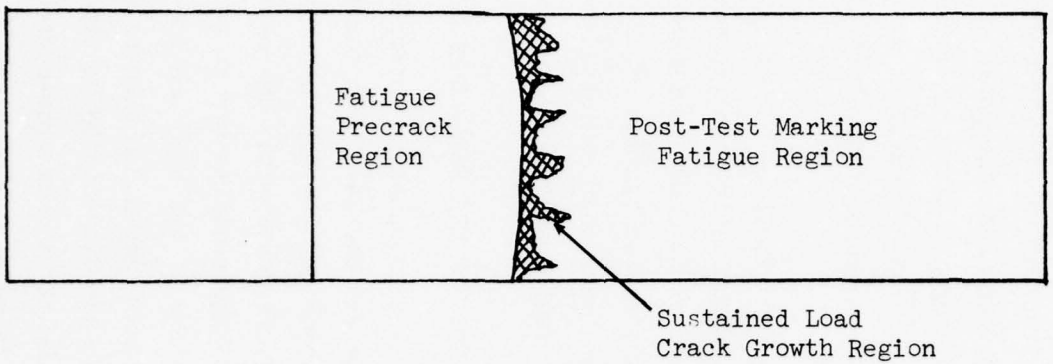

Figure 20. Schematic of Post-Test Fracture Surface of 1.4 inch thick RA Materials Tested in 3-1/2% NaCl Solution

specimen surface, the crack becomes self arresting in low $\frac{dK}{da}$ specimens. In addition, little of the crack extension was visible on the specimen surface. As the initial stress intensity is decreased still farther, a region is encountered where the crack grows continuously at a low rate for the test duration of 200 hours, as shown in Figure 21. In general, the behavior in $3\frac{1}{2}\%$ NaCl solution was similar for the two hydrogen level materials, the main difference being the lower "apparent threshold" level of the high hydrogen material. For the high hydrogen content material, the "apparent threshold" was approximately 41 ksi $\sqrt{\text{in.}}$ as compared to a value of approximately 47 ksi $\sqrt{\text{in.}}$ for the low hydrogen content material.

Examination of the fracture surfaces of the specimens after fatigue marking and fracturing shows a distinctly different appearance of the specimens tested at the lowest K_{Ii} level as shown in Figure 22. The "rough" appearing sustained load crack growth region typical of the rapid crack growth behavior is not apparent on the specimens that exhibited the continuing slow growth behavior, the slow growth region appearing much smoother.

3. SUSTAINED LOAD RESULTS FOR THE BETA ANNEALED (β) MATERIAL

The hydrogen levels for the beta annealed materials examined were 199 ± 20 ppm for the high hydrogen material and 24 ± 5ppm for the low hydrogen material. Results for the high hydrogen and low hydrogen beta annealed materials are shown in Tables 16 and 17, respectively. The beta annealed material is shown to be more susceptible to high humidity air at both hydrogen levels than was the RA material. Examination of the high and low hydrogen level material effective crack growth rates shown in Figures 23 and 24, respectively, shows the behavior in high humidity air to be similar, the high hydrogen level material showing slightly higher growth rates. Both materials show a threshold value in the range of 60 to 65 ksi $\sqrt{\text{in.}}$

Test results in dry argon show the crack growth rates in the high hydrogen level materials to vary widely at K_{Ii} values greater than ~70 ksi $\sqrt{\text{in.}}$ or 0.82 K_{Ic}. In general, the dry argon data exhibited a higher maximum crack growth rate than observed in high humidity air, but the rate increases

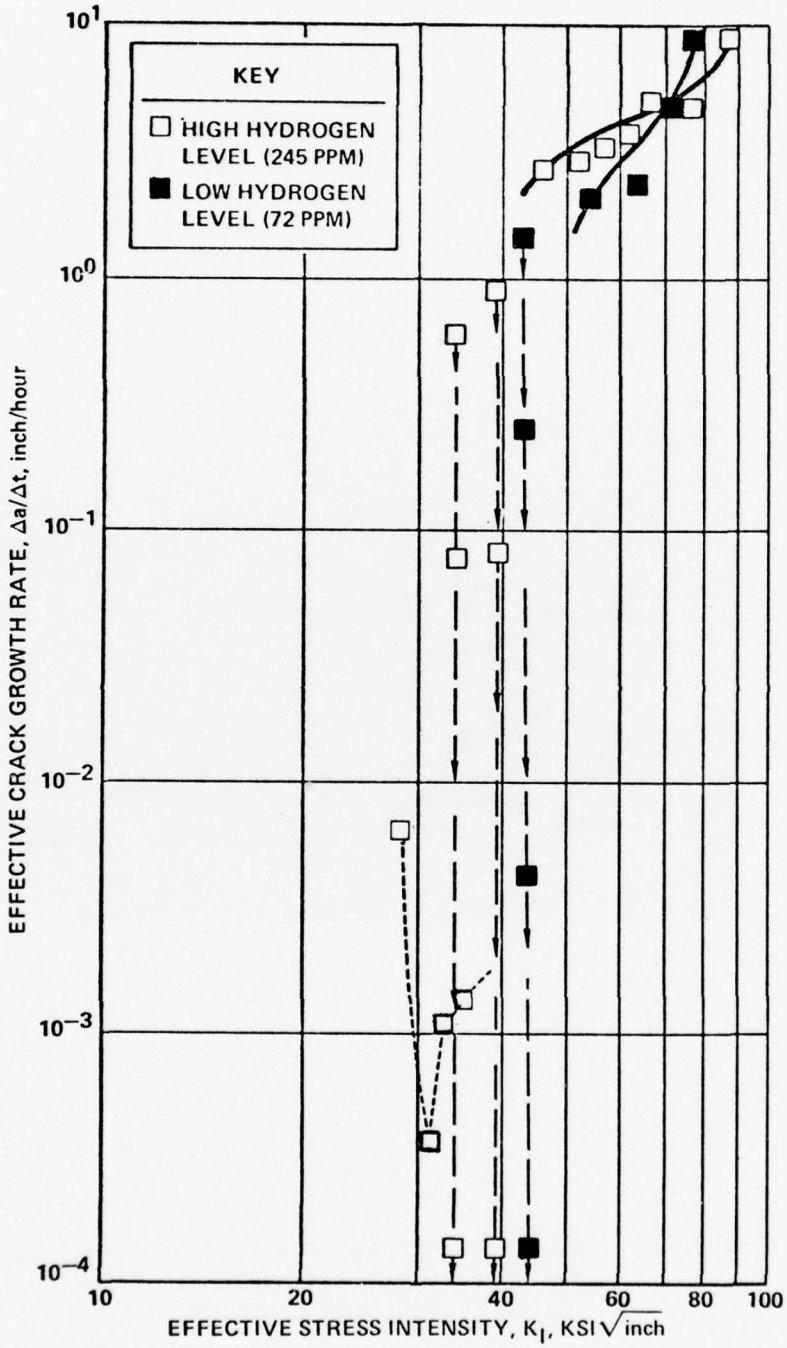

Figure 21. Sustained Load Crack Growth Rates in $3\frac{1}{2}\%$ NaCl Solution as a Function of Hydrogen Level in Ti-6Al-4V(RA)

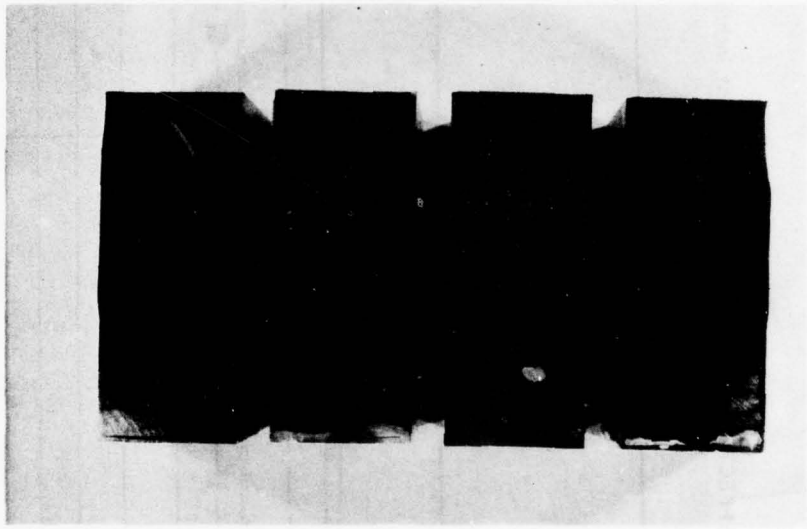

	A-1-11	A-1-5	A-1-12	A-1-10
K_{Ii}, ksi $\sqrt{in.}$	28.0	33.4	37.2	42.2

Figure 22. Variation in Fracture Surface Appearance for Ti-6Al-4V(RA) Material (245 ppm) Tested in $3\frac{1}{2}\%$ NaCl Solution

TABLE 16. SUSTAINED LOAD CRACK GROWTH RESULTS FOR HIGH HYDROGEN (199 ± 20 ppm) BETA ANNEALED Ti-6Al-4V PLATE MATERIAL, B = 1.4 INCH

Specimen	Environment	Initial Stress Intensity K_{Ii}, ksi$\sqrt{in.}$	Ratio $\frac{K_{Ii}}{K_{Ic}}$	Test Duration, Hours	Observed Crack Growth Δa, inch				
					Surface	1/4 Plane	1/2 Plane	3/4 Plane	Surface
	L-T Orientation, K_{Ic} = 84.6 ksi $\sqrt{in.}$								
B-1-24	High Humidity Air	81.6	0.96	166.0, failed	~0.06	~0.15	~0.21	~0.14	~0.04
B-1-7	High Humidity Air	70.5	0.83	211 DNF *	0.040	0.272	0.331	0.342	0.032
B-1-22	High Humidity Air	61.0	0.72	215 DNF	~0 **	~0 **	~0 **	~0 **	~0 **
B-1-29	Dry Argon	81.5	0.96	0.10, failed	-	-	-	-	-
B-1-22R	Dry Argon	75.0	0.87	171.5, failed	-	-	-	-	-
B-1-30	Dry Argon	70.9	0.83	171.6 DNF	0.019**	0.019**	0.019**	0.019**	0.019**
B-1-8	Dry Argon	59.9	0.71	258.9 DNF	0.004	0.002	0.006	0.004	0.000
B-1-9	Dry Argon	48.8	0.58	190.7 DNF	~0.001	~0.001	~0.001	~0.001	~0.001
B-1-13	3-1/2% NaCl Solution	51.1	0.60	10-5/6 min. failed	-	-	-	-	-
B-1-16	3-1/2% NaCl Solution	40.3	0.48	142.2 DNF	0.076	0.148	0.108	0.132	0.082

* DNF = Did not fail

** Crack front indistinct, Δa based on COD readings

TABLE 17. SUSTAINED LOAD CRACK GROWTH RESULTS FOR LOW HYDROGEN (24 ± 5 ppm) BETA ANNEALED Ti-6Al-4V PLATE MATERIAL, B = 1.4 INCH

Specimen	Environment	Initial Stress Intensity K_{Ii}, ksi/in.	Ratio $\frac{K_{Ii}}{K_{Ic}}$	Test Duration Hours	Observed Crack Growth Δa, inch				
					Surface	1/4 Plane	1/2 Plane	3/4 Plane	Surface
	L-T Orientation, K_{Ic} = 85.6 ksi $\sqrt{in.}$								
B-1-114	High Humidity Air	79.3	0.93	0.67 Failed	-	-	-	-	-
B-1-106	High Humidity Air	74.0	0.86	234.2 DNF*	0.010	0.070	0.110	0.089	0.026
B-1-109	High Humidity Air	60.6	0.71	209.9 DNF	~0.001	~0.002	~0.003	~0.001	~0.001
B-1-123	Dry Argon	78	0.91	176.4 DNF**	0.030	0.040	0.035	0.035	0.050
B-1-121	Dry Argon	72	0.84	217.0 DNF**	0.010^X	0.010^X	0.010^X	0.010^X	0.010^X
B-1-107	Dry Argon	57.6	0.67	258.9 DNF	~ 0	~ 0	~ 0	~ 0	~ 0
B-1-112	3-1/2% NaCl Solution	54.7	0.64	0.54 Failed	0.50	0.45	0.45	0.49	0.51
B-1-108	3-1/2% NaCl Solution	42.4	0.50	114.8 DNF	0.058	0.186	0.175	0.128	0.197

* DNF = Did not fail

** Crack grew initially and arrested

X Based on COD

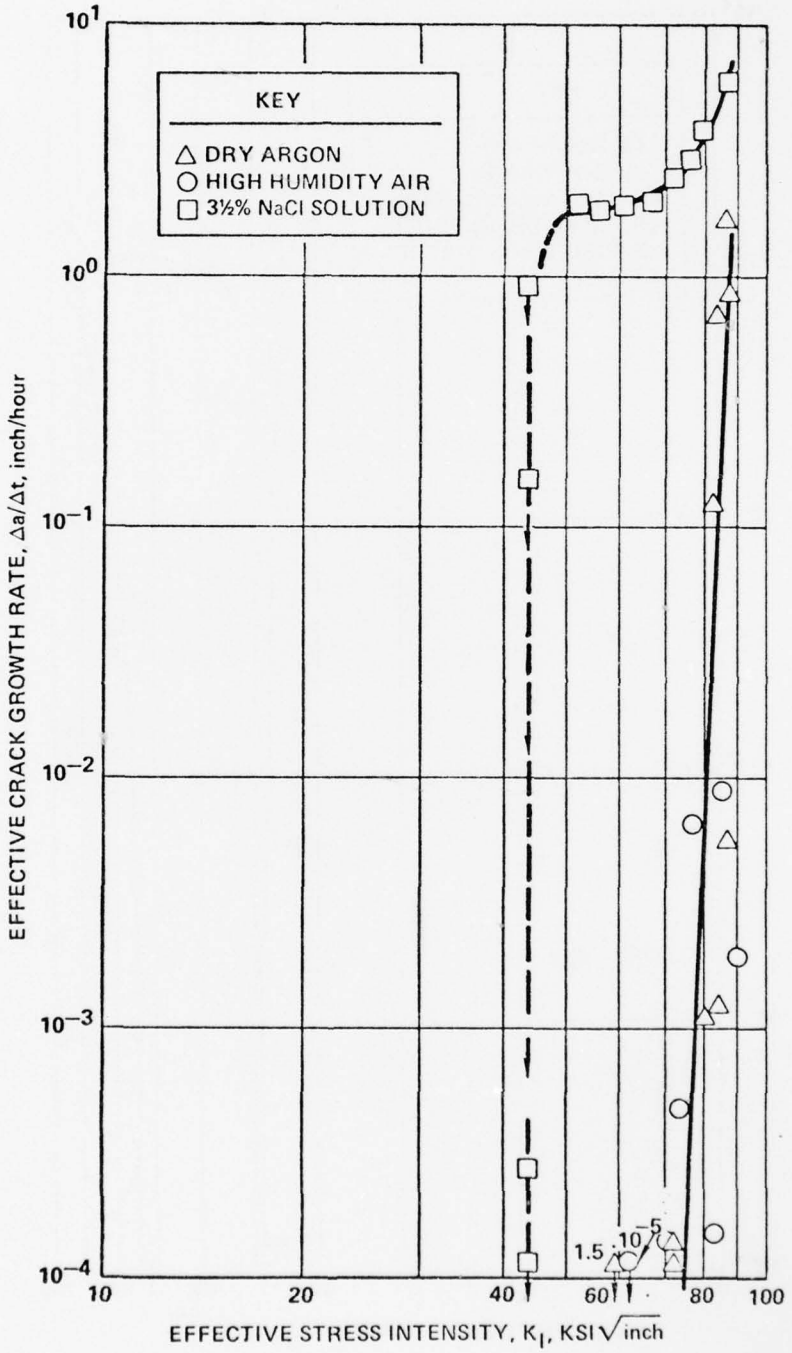

Figure 23. High Hydrogen Level Ti-6Al-4V(β) Crack Growth Rate Results (199 ppm)

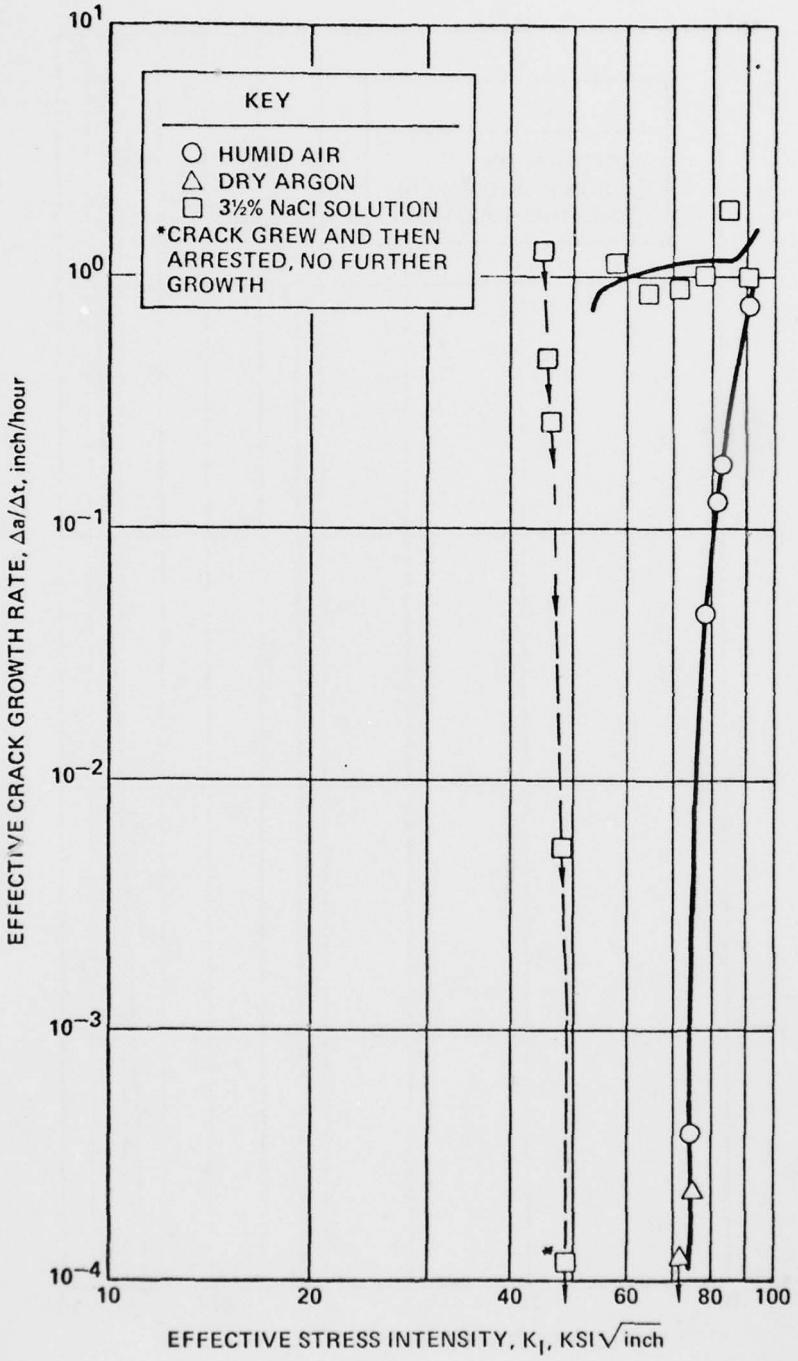

Figure 24. Low Hydrogen Level Ti-6Al-4V(β) Crack Growth Rate Results (24 ppm)

rapidly with fairly wide scatter at these higher stress intensity levels. Less tendency for rapid crack growth is apparent in the low hydrogen material, but the end threshold value still appears to be similar between the dry argon and high humidity air test results. Note that for the low hydrogen level material tested in dry argon, the cracks tended to exhibit growth early in the test and then to arrest. This type of behavior was not observed in the high hydrogen level material.

Sustained load cracking behavior in 3½% NaCl solution showed initial crack extension and arrest at K_{Ii} values below the apparent threshold value for fracture for both materials. A typical COD vs. time trace is shown in Figure 25. This behavior is similar to that previously noted for the RA heat treated material. The apparent threshold values for the two hydrogen level materials show the low hydrogen material to be slightly lower (~55 ksi $\sqrt{\text{in.}}$) than the high hydrogen material (~57 ksi $\sqrt{\text{in.}}$). Crack growth rate behavior was similar for the two hydrogen level materials, the high hydrogen level material showing a slightly faster upper shelf crack growth rate.

4. SUSTAINED DEFLECTION TEST RESULTS

A limited number of modified WOL specimens were tested for the Ti-6Al-4V(RA) material to examine the effect of a decreasing $\frac{dK}{da}$ gradient in the measured crack growth threshold values. The results of these tests are summarized in Table 18. For the high hydrogen material in high humidity air and in dry argon, the apparent crack growth threshold values from the constant load and constant deflection tests are in good agreement for the limited data. The results for the tests in 3½% NaCl solution show that the sustained deflection specimen propagated a small distance and arrested, just as occurred in this K_{Ii} range for the specimen tested under constant load. Note that this results in a non-conservative estimate of the threshold value. The low hydrogen material tests in high humidity air exhibited very asymmetric crack growth, crack growth occurring on one side only. The resulting K_{If} value is viewed as suspect and its significance is questionable.

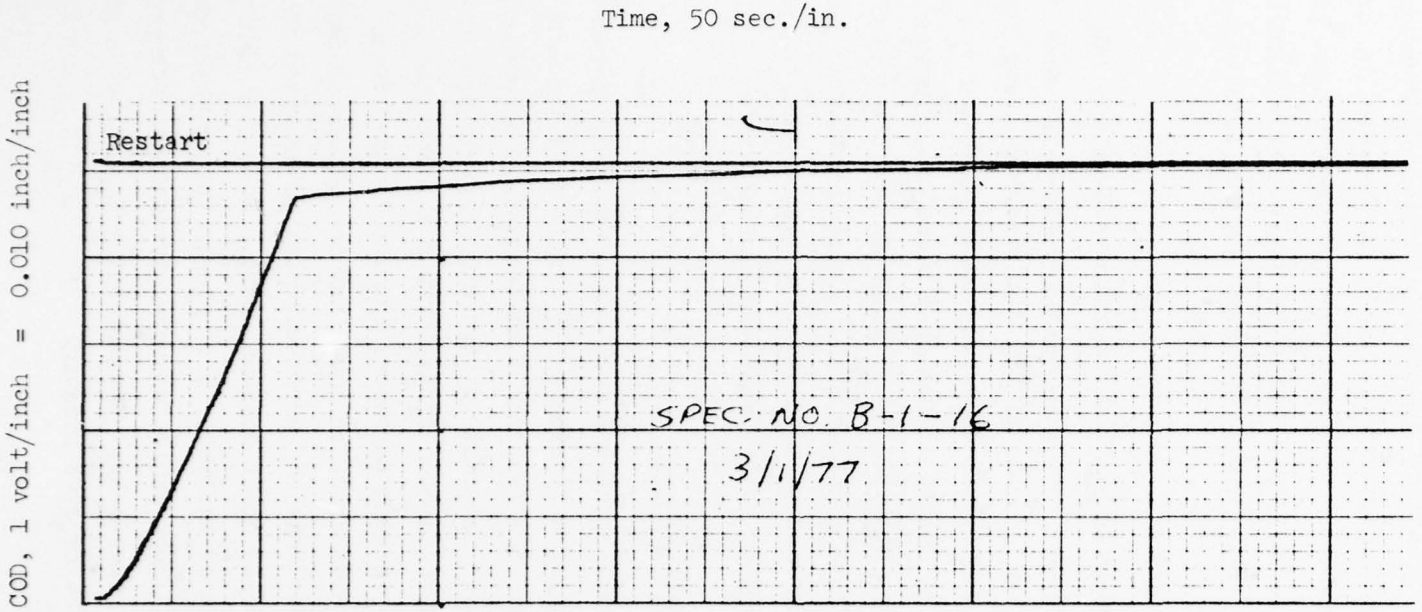

Figure 25. Typical Load vs COD Trace for Crack Growth Arrest Specimen B-1-6, 3-1/2% NaCl Solution

TABLE 18. COMPARISON OF CRACK GROWTH THRESHOLD VALUES FOR CONSTANT LOAD AND CONSTANT DEFLECTION SPECIMENS OF Ti-6Al-4V(RA).

Specimen Number	Test Environment	Initial Stress Intensity, K_{Ii}, Ksi $\sqrt{\text{inch}}$	Test Duration, Hours	Final Stress Intensity, K_{If}, Ksi $\sqrt{\text{inch}}$	Threshold Stress Intensity from Constant Load Tests, K_{Ith}, Ksi $\sqrt{\text{inch}}$
A-1-52 (245 ppm)	High Humidity Air	65.0	555.0	55.1	50 to 55
A-1-51 (245 ppm)	Dry Argon	60.0	550.0	49.7	45 to 50
A-1-50 (245 ppm)	3½% Nacl Solution	40.0	553.5	35.4	>25 (see text).
A-1-131 (72 ppm)	High Humidity Air	58.0	552.0	44.9*	50 to 55
A-1-130 (72 ppm)	Dry Argon	**	**	**	50 to 55

*Crack grew on one side only, see text.

**Specimen failed during precrack-overload.

Based on these results, the constant load and constant deflection test methods seem to give equivalent results for those conditions where the crack grows as a uniformly increasing crack to failure above the threshold value. The constant deflection tests give non-conservative threshold values for the case of $3\frac{1}{2}\%$ NaCl solution where the material results in crack arrest after an initial increment of growth. This is due to multiple cracking at microstructural features that blunt the crack tip and decrease the effective stress intensity. For tests conducted under constant load at K_{Ii} values below the apparent threshold level, extensive crack growth is still observed prior to arrest in low $\frac{dK}{da}$ specimens. Smaller specimens with high $\frac{dK}{da}$ tested under constant load would be expected to yield significantly lower threshold values.

5. FRACTOGRAPHY RESULTS FOR THE TASK I MATERIALS

Following the completion of testing, selected specimens of each microstructural condition were examined using metallurgical sections normal to the crack plane and by scanning-electron-microscopy (SEM) of the fracture surface. These results are presented in the following sections.

a. Ti-6Al-4V(RA) Results

Examination of the fracture surfaces showed no significant difference between specimens with 72 ppm and 245 ppm hydrogen when tested in dry argon as shown in Figures 26 and 27. The results show a mixture of ductile rupture with some cleavage of the alpha grains and at the alpha/beta interface. Specimens tested in $3\frac{1}{2}\%$ NaCl showed a marked increase in the amount of cleavage present as shown in Figures 28 and 29. Note that in Figure 28 a region of marked crack splitting is observed a short distance into the sustained load crack growth region. This corresponds to the approximate crack growth region where the crack slowed and arrested when tested at lower K_{Ii} values, thus providing further evidence of the crack arrest mechanism.

b. Ti-6Al-4V(β) Results

Metallographic sectioning and SEM results for the high hydrogen level material (199 ppm) are shown in Figures 30 through 33 for the three test environments

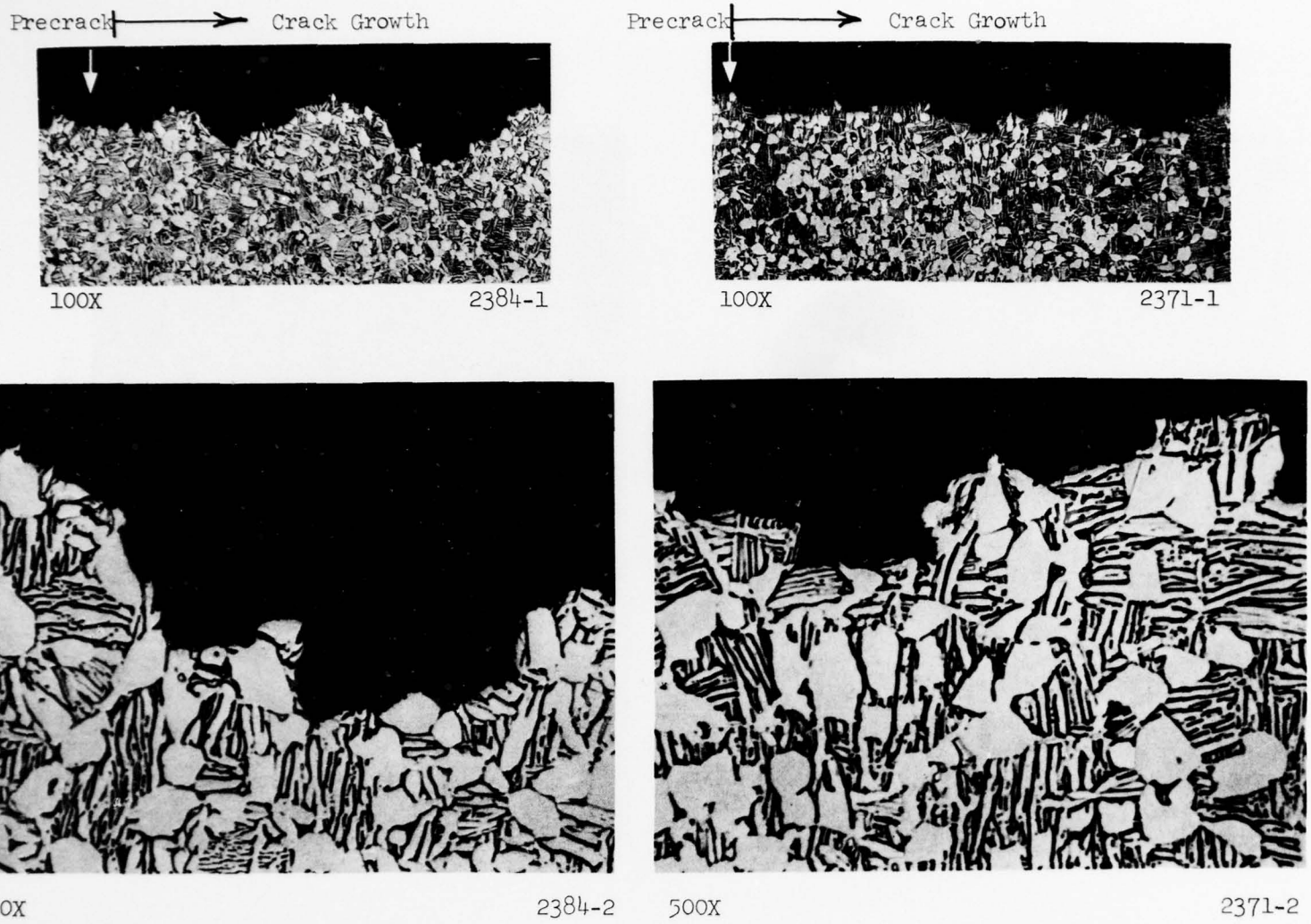

a. Specimen A-1-117 (72 ppm Hydrogen)

b. Specimen A-1-21 (245 ppm Hydrogen)

Figure 26. Metallographic Section Results for Ti-6Al-4V(RA) Material Tested in Dry Argon

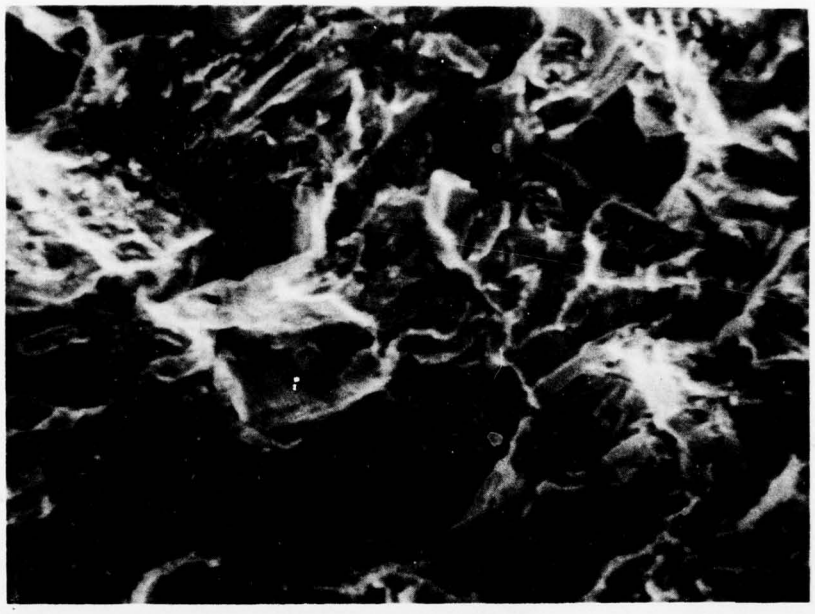

a. Specimen A-1-117 (72 ppm hydrogen)

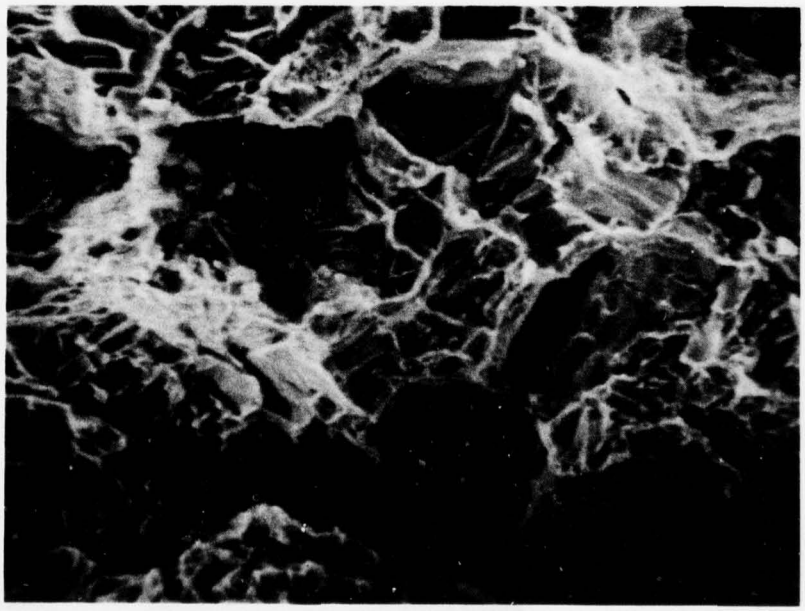

b. Specimen A-1-21 (245 ppm hydrogen)

Figure 27. SEM Results for Ti-6Al-4V(RA) Material Tested in Dry Argon, 1000X

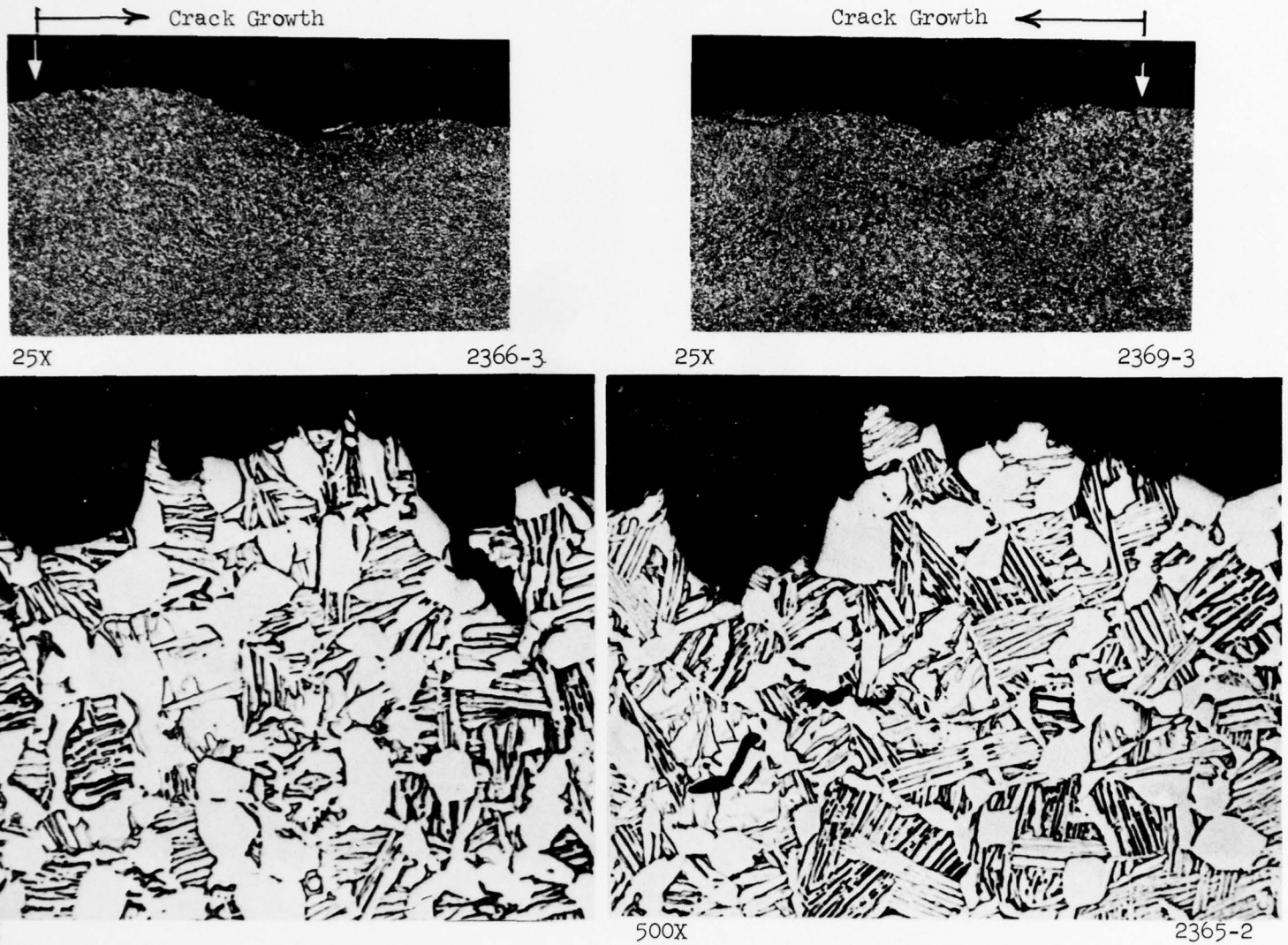

a. Specimen A-1-113 (72 ppm Hydrogen)

b. Specimen A-1-12 (245 ppm Hydrogen)

Figure 28. Metallographic Section Results for Ti-6Al-4V(RA) Material Tested in $3\frac{1}{2}\%$ NaCl Solution

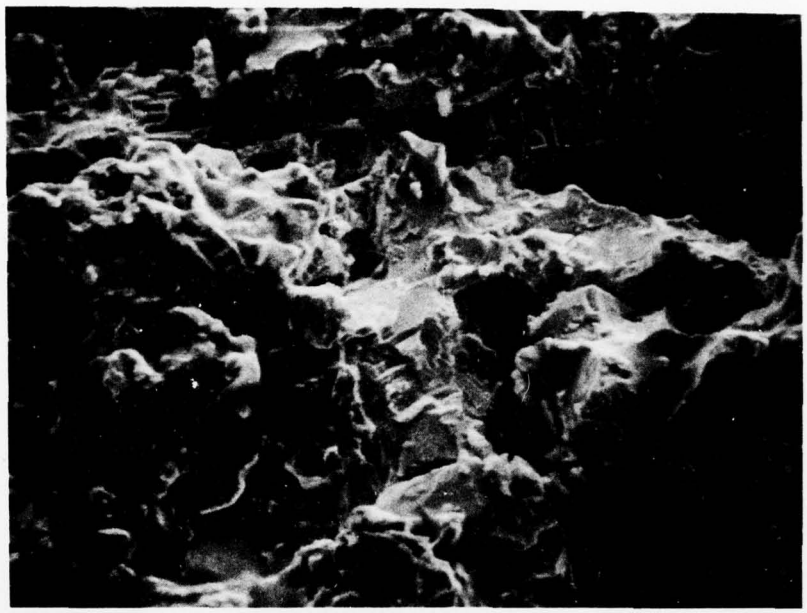

a. Specimen A-1-113 (72 ppm hydrogen)

b. Specimen A-1-12 (245 ppm hydrogen)

Figure 29. SEM Results for Ti-6Al-4V(RA) Material Tested in $3\frac{1}{2}\%$ NaCl Solution, 500X

a. Specimen B-1-7, High Humidity Air, K_{Ii} = 70.5 ksi $\sqrt{in.}$

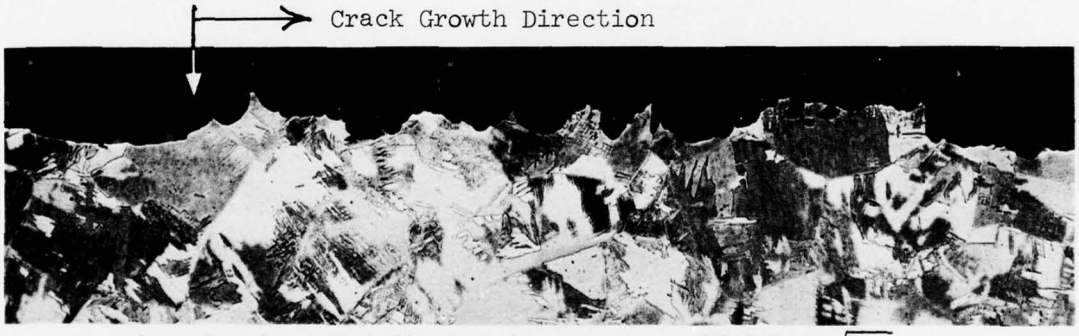

b. Specimen B-1-22, Dry Argon, K_{Ii} = 75.0 ksi $\sqrt{in.}$

c. Specimen B-1-16, $3\frac{1}{2}\%$ NaCl Solution, K_{Ii} = 40.3 ksi $\sqrt{in.}$

Figure 30. Metallographic Sections Showing Crack Propagation Regions in Ti-6Al-4V(β) Material (199 ppm Hydrogen), 25X

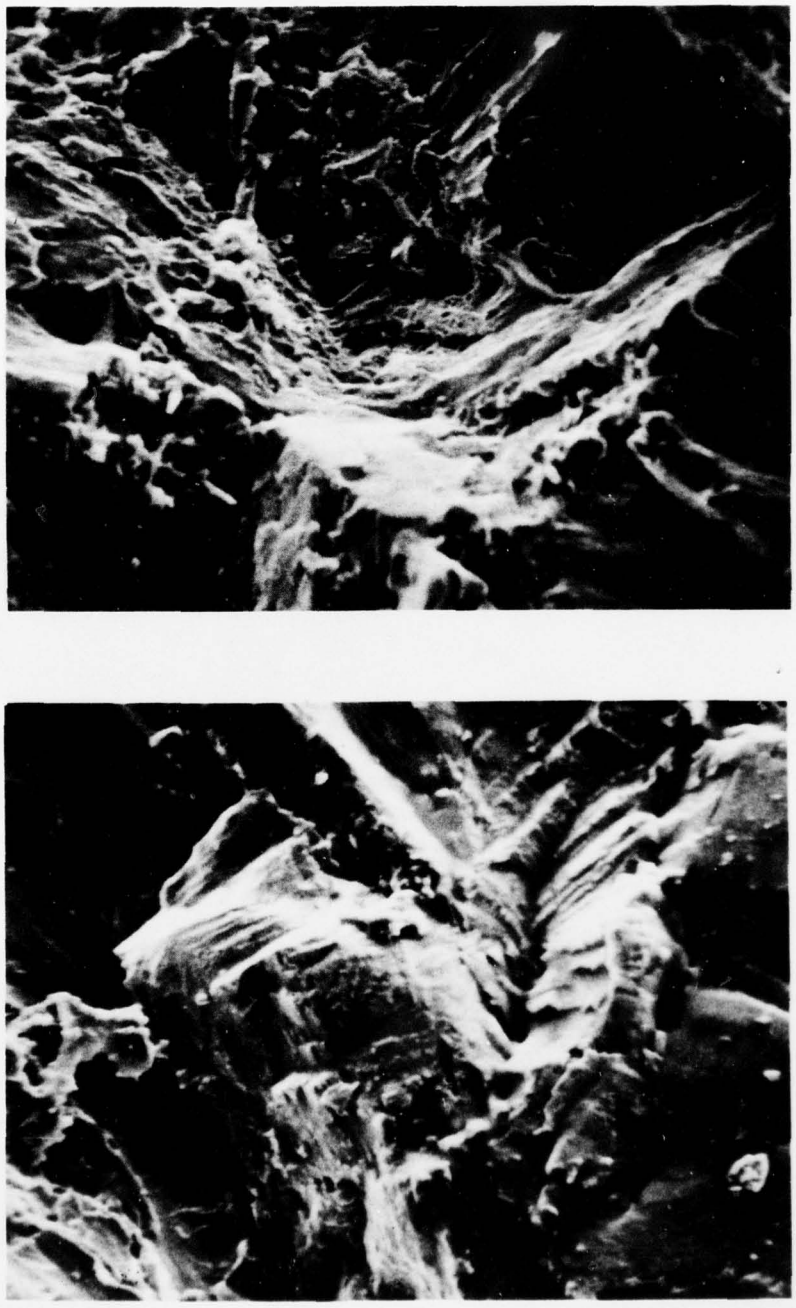

Figure 31. Sustained Load Crack Growth Fracture Surface of Specimen B-1-7 Tested in High Humidity Air, 500X

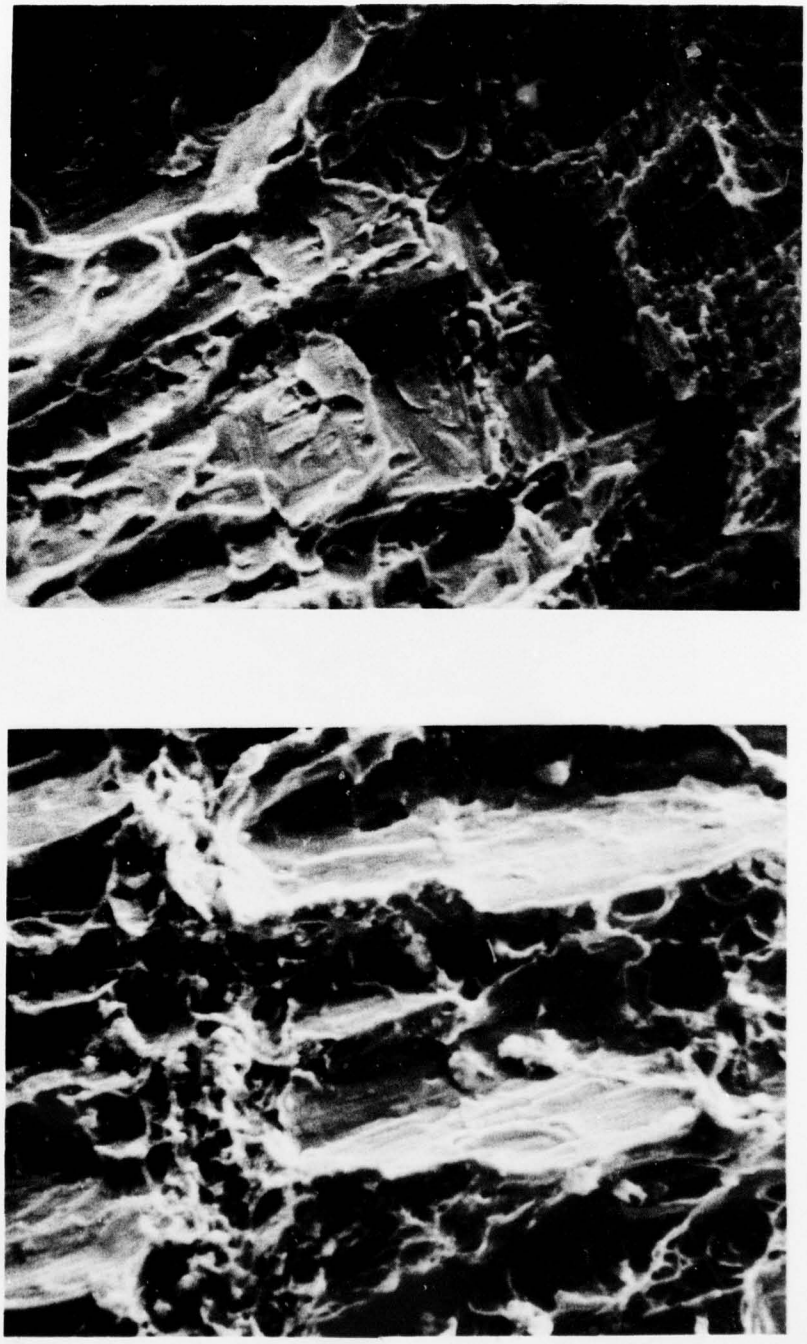

Figure 32. Sustained Load Crack Growth Fracture Surface of Specimen B-1-22 Tested in Dry Argon, 1000X

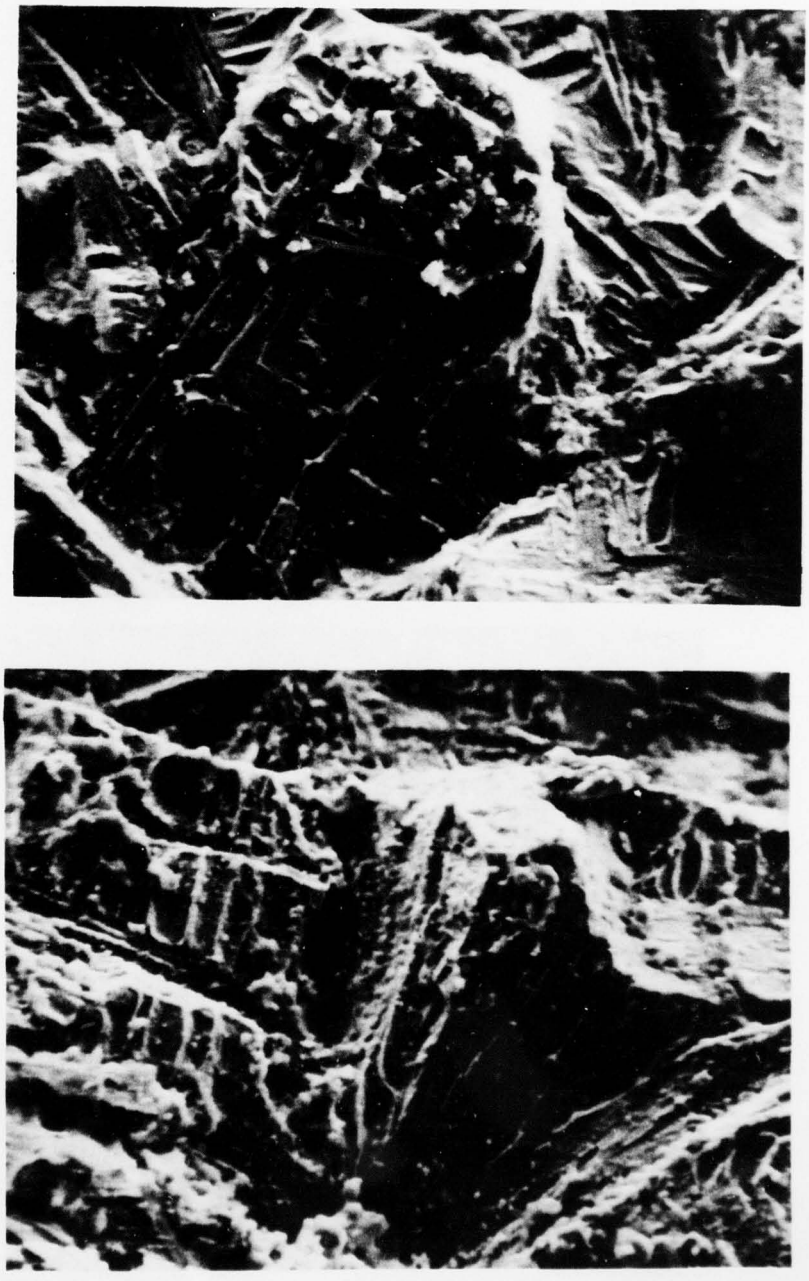

Figure 33. Sustained Load Crack Growth Fracture Surface of Specimen B-1-16 Tested in 3½% NaCl Solution, 500X

studied. The results show similar fracture surface features of specimens tested in the high humidity air and dry argon environments, the results in dry argon showing somewhat more ductile rupture mixed with the cleavage. Results in $3\frac{1}{2}\%$ NaCl solution for specimen B-1-16 (which grew and arrested) show extensive crack tip branching in the region of crack arrest. Fracture surfaces show primarily cleavage features, the majority of which occur normal to the alpha colonies. Examination of the fracture surface features of the low hydrogen level material (24 ppm) shown in Figures 34, 35 and 36 reveals fracture features essentially the same as those found in the high hydrogen material tested in the same environment.

c. Ti-6Al-4V(STA) Results

Figure 37 shows the metallographic sections through the sustained load crack growth region in various environments. The results are consistent with those of the RA and beta materials in that the extent of cleavage of the alpha is more extensive in $3\frac{1}{2}\%$ NaCl solution. The results in high humidity and dry argon are again similar.

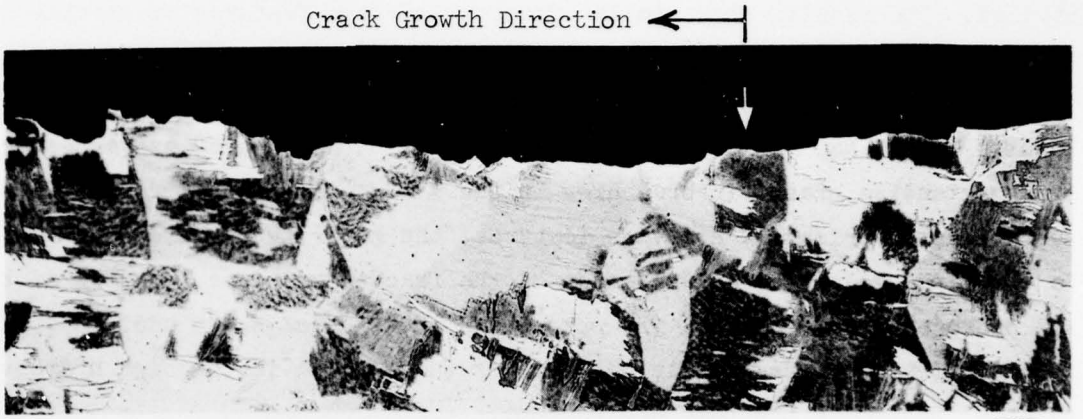

a. Specimen B-1-114, High Humidity Air, K_{Ii} = 79.3 ksi $\sqrt{in.}$

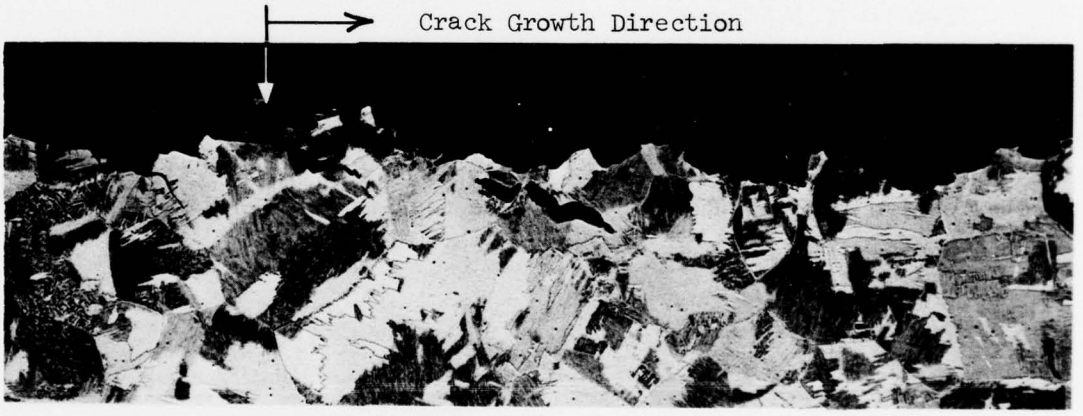

b. Specimen B-1-123, Dry Argon, K_{Ii} = 78.0 ksi $\sqrt{in.}$

c. Specimen B-1-112, 3½% NaCl Solution, K_{Ii} = 54.7 ksi $\sqrt{in.}$

Figure 34. Metallographic Section Results for Low Hydrogen Level (24 ppm) Beta Annealed Materials, 25X

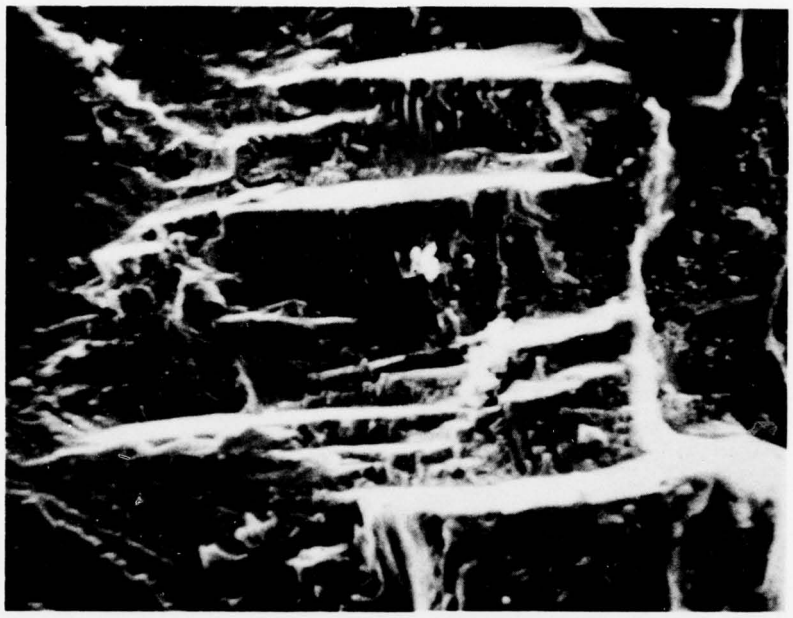

a. Specimen B-1-114 tested in High Humidity Air, K_{Ii} = 79.3 ksi $\sqrt{in.}$

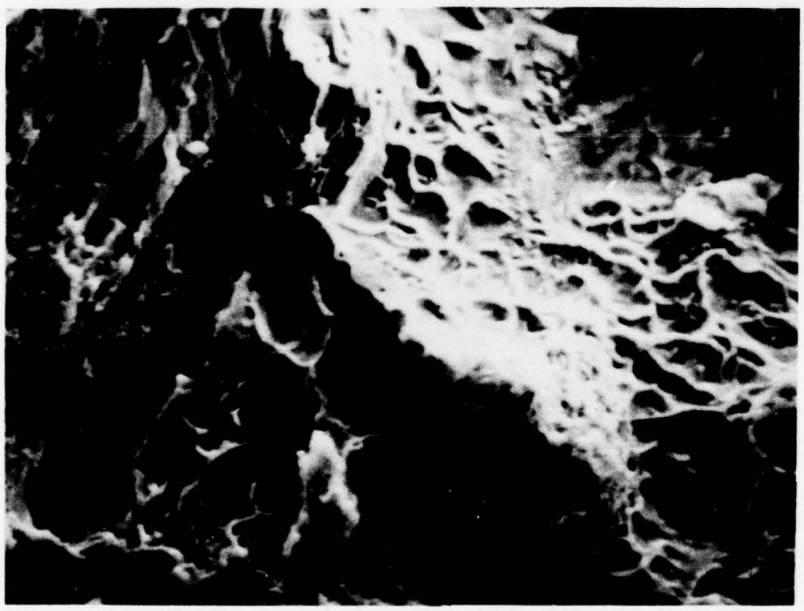

b. Specimen B-1-123 tested in Dry Argon, K_{Ii} = 78 ksi $\sqrt{in.}$

Figure 35. Sustained Load Crack Growth Fracture Surfaces in High Humidity Air and Dry Argon, 1000X

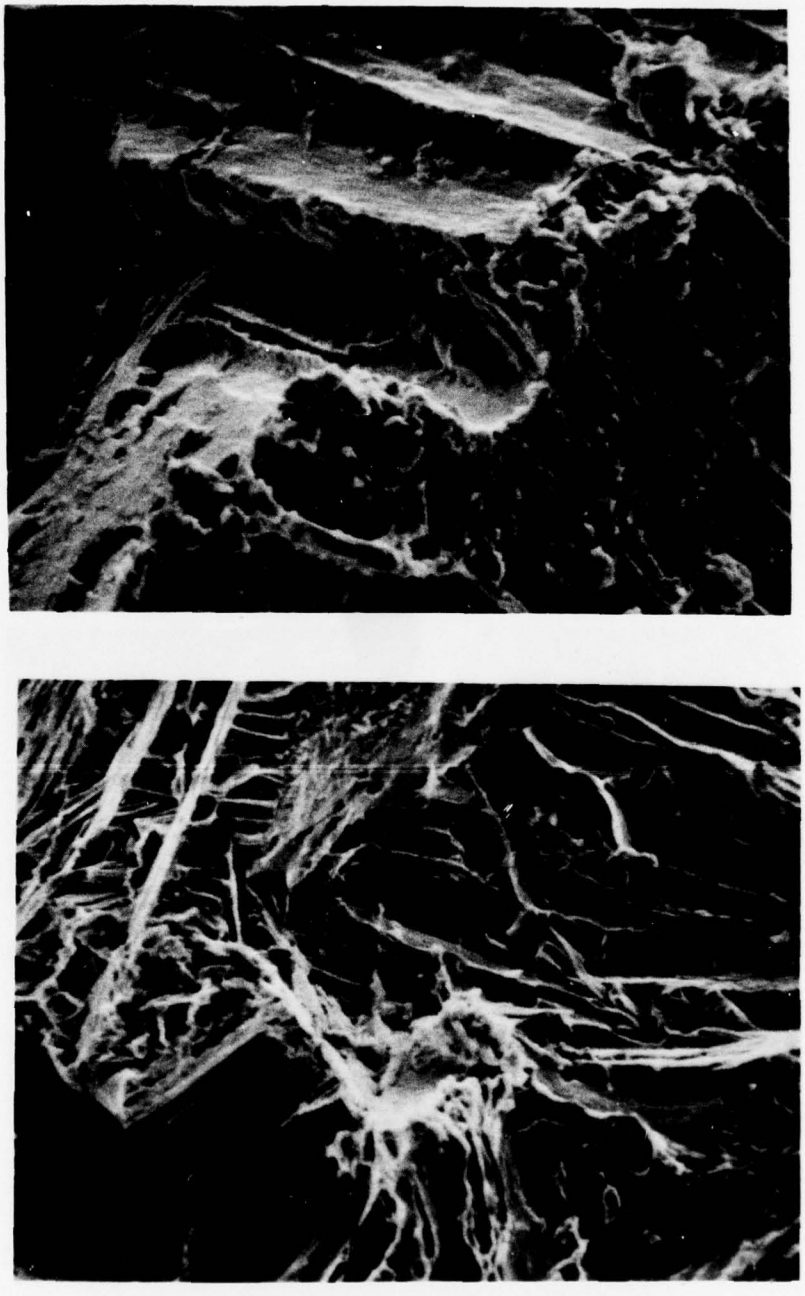

Figure 36. Sustained Load Crack Growth Fracture Surface of Specimen B-1-112 Tested in 3½% NaCl Solution, 500X

a. Specimen S-3-36, High Humidity Air, K_{Ii} = 55.9 ksi $\sqrt{in.}$

b. Specimen S-3-39, Dry Argon, K_{Ii} = 57.2 ksi $\sqrt{in.}$

c. Specimen S-3-61, $3\frac{1}{2}\%$ NaCl Solution, K_{Ii} = 31.7 ksi $\sqrt{in.}$

Figure 37. Metallographic Sections of Sustained Load Crack Growth Region in Ti-6Al-4V(STA), 500X

SECTION VII

PHASE II: THICKNESS EFFECT RESULTS

The objective of the Phase II tests was to compare the plane strain results (B = 1.4 inch) with the results of the same material tested in a plane strain/plane stress transition thickness. Specimens were machined to a nominal thickness of 0.375 inch from the 1.5 inch base Ti-6Al-4V high hydrogen recrystallize annealed (RA) material following heat treatment. Tests were then conducted in high humidity air and in dry argon.

As discussed in Section VI, the fracture results for the thick (B = 1.4 inch) Ti-6Al-4V(RA) material with 245 ppm hydrogen was K_{Ic} = 70.2 ksi $\sqrt{in.}$ In addition ~ 0.018 inch of sustained load crack growth had been observed in high humidity air at an initial stress intensity of 61.7 ksi $\sqrt{in.}$ As a result the first test in Phase II (A-2-44) was conducted at a $K_{Ii} \approx 60$ ksi $\sqrt{in.}$ in high humidity air. Following the test, the specimen was refatigue-cracked 0.15 inch and a static fracture test conducted to determine the K_{IQ} and RSC values as per ASTM E399 and to verify the mixed mode test condition. The load vs COD results of the fracture test are shown in Figure 38 and are typical of mixed mode fracture behavior. Analysis of the results give values of K_{IQ} = 79.6 ksi $\sqrt{in.}$ and RSC = 0.84.

Sustained load crack growth results for the 3/8 inch thick high hydrogen level Ti-6Al-4V(RA) material are presented in Table 19. As has been previously reported[13], the sustained load cracking behavior of the 3/8 inch thick material resulted in extensive crack tunneling at the midplane with little observed crack extension at the surfaces. The COD readings indicate that the crack extension occurred rapidly at the start of the test and decreased in rate as the tunneling became more pronounced, the crack extension finally

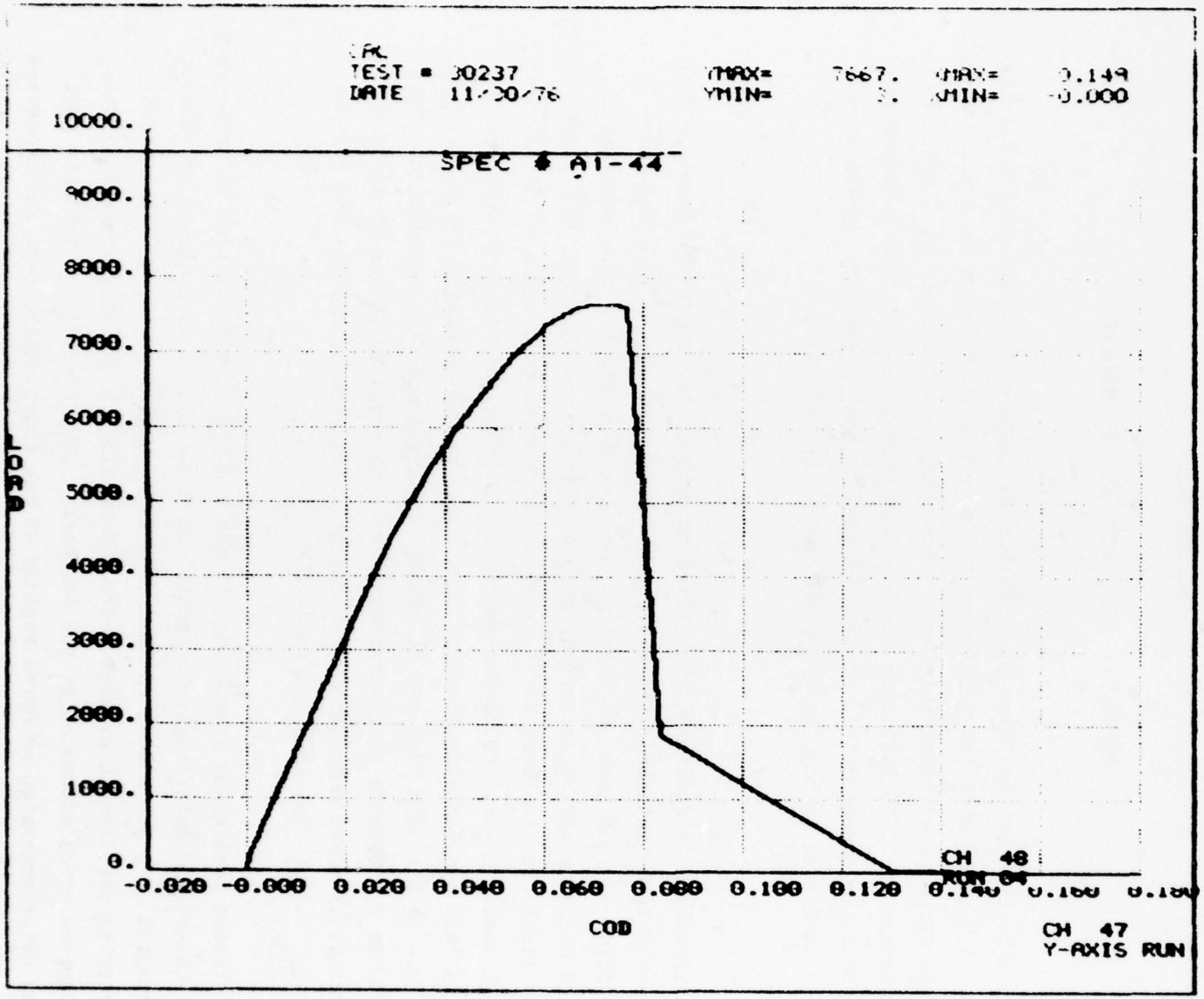

Figure 38. Fracture Results for 3/8 Inch Thick High Hydrogen RA Material

TABLE 19. SUSTAINED LOAD CRACK GROWTH RESULTS FOR 3/8 INCH THICK Ti-6Al-4V(RA) PLATE MATERIAL (245 ppm Hydrogen)

Specimen	Environment	Initial Stress Intensity K_{Ii}, ksi$\sqrt{in.}$	Ratio $\frac{K_{Ii}}{K_{I_Q}}$	Test Duration, Hours	Observed Crack Growth Δa, inch				
					Surface	1/4 Plane	1/2 Plane	3/4 Plane	Surface
	T-L Orientation, K_{I_Q} = 79.6 ksi $\sqrt{in.}$								
A-2-45	High Humidity Air	78.3	0.98	214.2 DNF*	0.021	0.095	0.152	0.138	0.045
A-2-49	High Humidity Air	72.6	0.91	224.8 DNF	0.001	0.004	0.004	0.004	0.003
A-2-44	High Humidity Air	59.8	0.75	153.4 DNF	~0.001	0.005	0.003	0.002	0.002
A-2-47	Dry Argon	73.0	0.91	209.9 DNF	0.041	0.117	0.152	0.087	0
A-2-46	Dry Argon	61.6	0.77	182.4 DNF	0.001	0.009	0.010	0.007	0.002
A-2-48	Dry Argon	52.2	0.65	219.5 DNF	0.003	0.003	0.002	0.003	0.002

*DNF = Did not fail

arresting completely. This behavior was identical for the Phase II and Phase III materials and will be described in more detail in Section VIII.

A comparison of Tables 14 and 19 show the high humidity air results of the 3/8 inch material to exhibit less sustained load cracking than was observed in the 1.4 inch thick specimen tested at comparable initial stress intensity values. Results in dry argon also indicate more extensive cracking in the thicker material.

SECTION VIII

PHASE III: TEXTURE EFFECT RESULTS

In this phase, the objective was to examine the effect of a heavy crystallographic texture on the sustained load crack growth behavior. The material used was a 3/8-inch thick Ti-6Al-4V(RA) plate with a known heavy crystallographic texture. Tests were conducted using both LT and TL oriented specimens.

1. SUSTAINED LOAD TEST RESULTS

Results of these tests are presented in Tables 20 and 21. Examination of these tables shows that no failures occurred at any initial stress intensity up to 0.95 K_{IQ} in any environment other than 3½% NaCl solution for either the LT and TL orientation. However, extensive subsurface crack growth was observed in both the high humidity air and dry argon environments for both orientations. Examination of the COD vs. time data for specimens that exhibited extensive subsurface growth showed the growth to occur primarily during the first few hours in all environments. The apparent crack growth rate then slowed and finally went to zero with additional time. This was found to be true for both orientations and environments. As a result, the computation of crack growth rates was not attempted for this material. Typical COD vs. time plots are shown in Figure 39. It should also be noted that larger crack extensions are observed at equivalent K_{Ii} values for the LT orientation compared to the TL orientation. It cannot be assumed, however, that this means a difference in cracking rates, the initial rates apparent from the COD readings both being similar. Rather it may be related to the strong crack front tunneling. The crack tunneling will place more strain on the uncracked surface ligaments in the crack wake. As a result of the large yield strength differential between the longitudinal (120 ksi) and transverse (145 ksi) directions, the resulting local strain field at the crack tip may well be considerably different as a function of the extent of tunneling for the two orientations. The lower yield strength in the longitudinal

TABLE 20. SUSTAINED LOAD CRACK GROWTH RESULTS FOR TEXTURED 3/8 INCH THICK Ti-6Al-4V(RA) PLATE MATERIAL

Specimen	Environment	Initial Stress Intensity K_{Ii}, ksi $\sqrt{in.}$	Ratio $\frac{K_{Ii}}{K_{IQ}}$	Test Duration, Hours	Observed Crack Growth Δa, inch				
					Surface	1/4 Plane	1/2 Plane	3/4 Plane	Surface
	T-L Orientation, K_{IQ} = 88.2 ksi $\sqrt{in.}$								
T-1R**	High Humidity Air	82.6	0.94	240.4 INF*	0.026	0.058	0.059	0.044	0.010
T-2	High Humidity Air	66.6	0.76	235.0 INF	0.004	0.020	0.020	0.012	0.005
T-1	High Humidity Air	60.5	0.69	214.3 INF	0.013	0.007	0.009	0.005	0 008
T-15R	High Humidity Air	52.1	0.59	192.0 INF	0.001	0.002	0.003	0.002	0.014
T-15	High Humidity Air	45.2	0.51	234.3 INF	~ 0	~ 0	~ 0	~ 0	~ 0
T-4	Dry Argon	82.7	0.94	257.4 INF	0.019	0.078	0.110	0.086	0.021
T-5	Dry Argon	69.1	0.78	133.1 INF	0.009	0.017	0.015	0.014	0.003
T-3	Dry Argon	60.1	0.68	205.8 INF	0.002	0.004	0.003	0.002	0.004

* INF = did not fail

** R = Retest

TABLE 21. SUSTAINED LOAD CRACK GROWTH RESULTS FOR TEXTURED 3/8 INCH THICK Ti-6Al-4V(RA) PLATE MATERIAL

Specimen	Environment	Initial Stress Intensity K_{Ii}, ksi$\sqrt{in.}$	Ratio $\frac{K_{Ii}}{K_{I_Q}}$	Test Duration Hours	Observed Crack Growth Δa, inch				
					Surface	1/4 Plane	1/2 Plane	3/4 Plane	Surface
	L-T Orientation, K_{I_Q} = 93.8 ksi $\sqrt{in.}$								
T-12	High Humidity Air	89.0	0.95	233.3 DNF*	0.000	0.055	0.134	0.053	0.002
T-13	High Humidity Air	81.8	0.87	170.9 DNF	0.000	0.035	0.098	0.039	0.000
T-11	High Humidity Air	71.9	0.77	213.5 DNF	0.001	0.046	0.090	0.032	0.000
T-14	High Humidity Air	61.9	0.66	169.1 DNF	0.000	0.030	0.067	0.027	0.001
T-16	High Humidity Air	54.0		258.3 DNF	0.003	0.008	0.017	0.013	0.001
T-18	High Humidity Air	42.9		214.0 DNF	~ 0	~ 0	~ 0	~ 0	~ 0
T-8R	Dry Argon	86.7	0.91	173.7 DNF	0.002	0.035	0.089	0.016	0.000
T-8	Dry Argon	71.3	0.76	192.2 DNF	0.001	0.035	0.061	0.028	0.000
T-6	Dry Argon	61.9	0.66	120.0 DNF	0.001	0.012	0.035	0.016	0.000
T-6R	Dry Argon	44.7	0.48	213.9 DNF	0	0	0	0	0
T-9	3-1/2% NaCl	20.6	0.22	112.2 DNF	0.046	0.076	0.075	0.052	0.029
T-9R (Retest)	3-1/2R NaCl	23.8	0.25	143.1 DNF	0.013	0.072	0.100	0.071	0.002
T-7	3-1/2% NaCl	30.8	0.33	0.37 **	Failed	Failed	Failed	Failed	Failed

* Did not Fail

** Specimen loaded 12.26 hours with no apparent growth when leak occurred in system. Specimen unloaded and leak repaired. Reloaded to same load and failed in 0.37 hours.

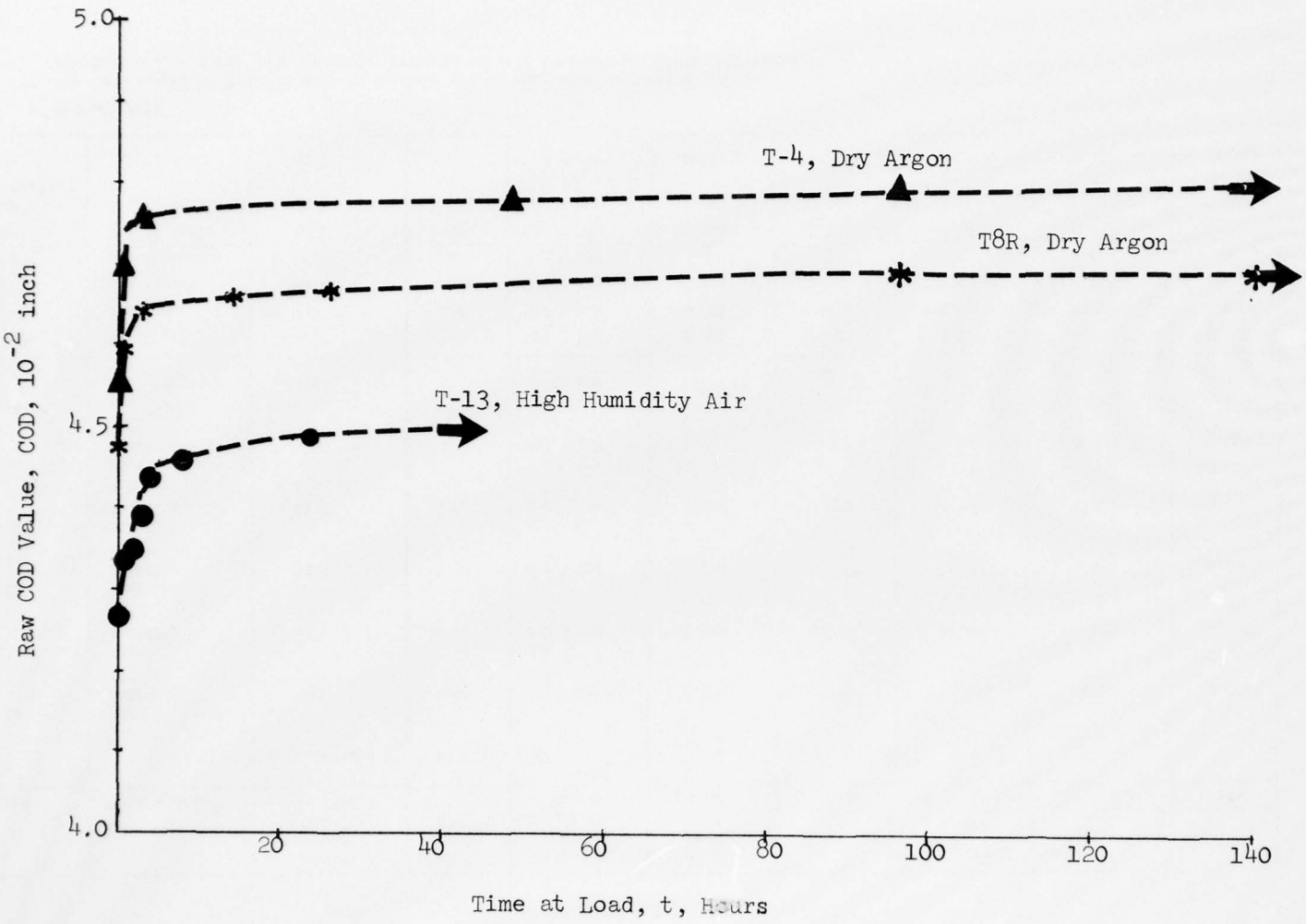

Figure 39. Typical COD vs. Time Data for 3/8 inch Textured Ti-6Al-4V(RA) Material

orientation could result in less restraint on the crack progression in the L-T orientation than results from the higher yield strength on crack progress in the T-L orientation. Examination of these results by environment show only slightly more crack extension to occur in high humidity air than in dry argon prior to crack arrest.

If the data from Reference 13 (shown in Table 22) for the same material is compared with the current results, one fact is noted. The previous data for W = 1.5 inch CT specimens did result in fracture at $K_{Ii} \approx 70$ ksi $\sqrt{\text{inch}}$ in the high humidity air environment where no fractures were obtained in the current study on W = 2.8 inch CT specimens. This is due to the dK/da gradient for the two specimens, the smaller W = 1.5 inch specimen resulting in a more rapid increase in K for a given increment of Δa. Thus in the smaller specimen the crack can become a propagating crack while in the larger specimen the extent of tunneling is not sufficient to elevate the driving force, K, to propagate the crack to failure. As a result, the dK/da of a given geometry can have a major influence on the observed sustained load crack growth behavior in the transition thicknesses of titanium alloys and other material/thickness conditions that tend to exhibit crack tunneling. In addition, comparison of time-to-failure data for different geometry specimens may show no correlation.

2. FRACTOGRAPHY RESULTS

The only major difference observed between the two specimen orientations was observed in the 3-1/2% NaCl solution tests. In this environment the L-T oriented specimen T-7 failed normal to the direction of the initial crack, the sustained load crack growth occurring in the T-L direction. Scanning electron fractorgaphs of the transition region of the precrack to sustained load cracking growth are shown in Figures 40 and 41. As anticipated, the crack growth region exhibited predominately cleavage features with some areas of intergranular fracture the same as previously observed[13] for crack growth in the T-L orientation specimens tested in 3-1/2% NaCl solution.

TABLE 22. SUSTAINED LOAD FLAW GROWTH TEST RESULTS OF 3/8 INCH Ti-6Al-4V(RA) (Ref. 13)

Thickness: 3/8 in.
W: 1.5 inch CT
K_{I_Q}: 88.2 ksi $\sqrt{in.}$

Specimen Orientation: T-L

Specimen Number	Calculation Designation*	Test Time, Hours	Average Surface Crack Length, a_s, in.	Surface Stress Intensity, K_{I_s},** ksi $\sqrt{in.}$	Average Subsurface Crack Length, a_{ss}, in.	Subsurface Stress Intensity, $K_{I_{ss}}$, ksi $\sqrt{in.}$	Initial Subsurface K/ Fracture Toughness, $K_{I_{ss}}/K_{I_Q}$
			Environment: Humid Air				
(1) D41	A	261.2	0.750	45.1	0.778	47.7	0.54
	B		***	-	***	-	
(2) D41	A	Failed in	0.819	68.2	0.843	72.1	0.82
	B	3 min.	***	-	***	-	
			Environment: 3.5% NaCl Solution				
(1) D35	A	308.9	0.740	9.6	0.787	10.5	0.12
	B		0.764	10.0	0.795	10.7	
(1) D36	A	315.3	0.753	17.7	***	-	-
	B		0.754	17.7	***	-	
D29	A	141.7	0.726	16.7	0.809	19.9	0.22
	B	(PC in NaCl)	0.825	20.6	0.856	22.2	
(2) D35	A	337.0	0.782	22.2	0.806	23.4	0.27
	B		0.791	22.6	0.824	24.3	
D39	A	Failed in	0.817	24.9	0.826	25.4	0.28
	B	5 min. (PC in NaCl)	1.232	95.3	1.192	81.5	
D33	A	Failed in	0.774	24.2	0.805	25.9	0.29
	B	4.25 min.	1.152	74.6	1.186	85.0	
D31	A	Failed	0.758	26.4	0.775	27.4	0.31
	B	on load application	1.132	78.2	1.147	82.8	
D32	A	Failed	0.753	44.1	0.762	44.9	0.51
	B	on load application	0.961	73.4	1.041	94.9	

*A = Initial conditions at start of test
B = Final conditions at end of test time under load

**K_{I_s} = based on surface readings
$K_{I_{ss}}$ = based on average of subsurface crack lengths at 1/4, 1/2, and 3/4 thickness locations

*** Crack length not measurable
**** PC in Env. = Precracked in environment

Specimen Orientation, T-7

B - Precrack Region

A - Sustained load crack growth in 3-1/2% NaCl Solution

800X

Figure 40. Scanning Electron Fractograph of Sustained Load Crack Growth Region of Specimen T-7 Tested in 3-1/2% NaCl Solution

Fractography of the specimens tested in high humidity air and dry argon all showed similar features for both orientations. Typical results are shown in Figure 42. The results show predominately equiaxed dimple rupture with minor isolated regions of cleavage.

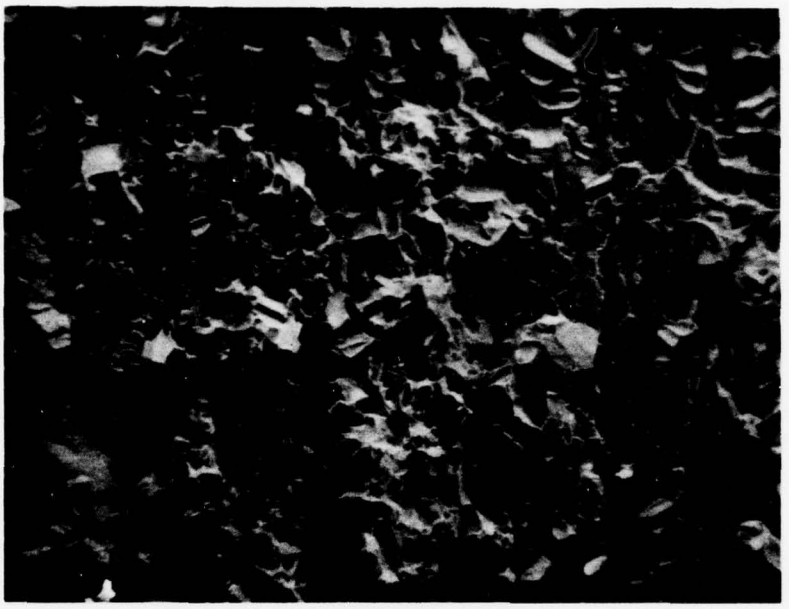

"A" Surface 300X

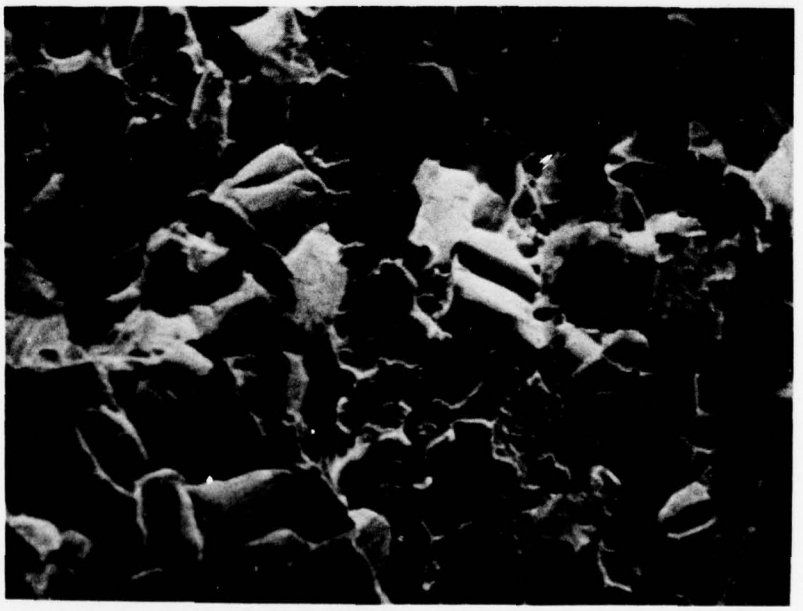

"A" Surface 1000X

Figure 41. Scanning Electron Fractograph of Sustained Load Crack Growth Region A of Specimen T-7

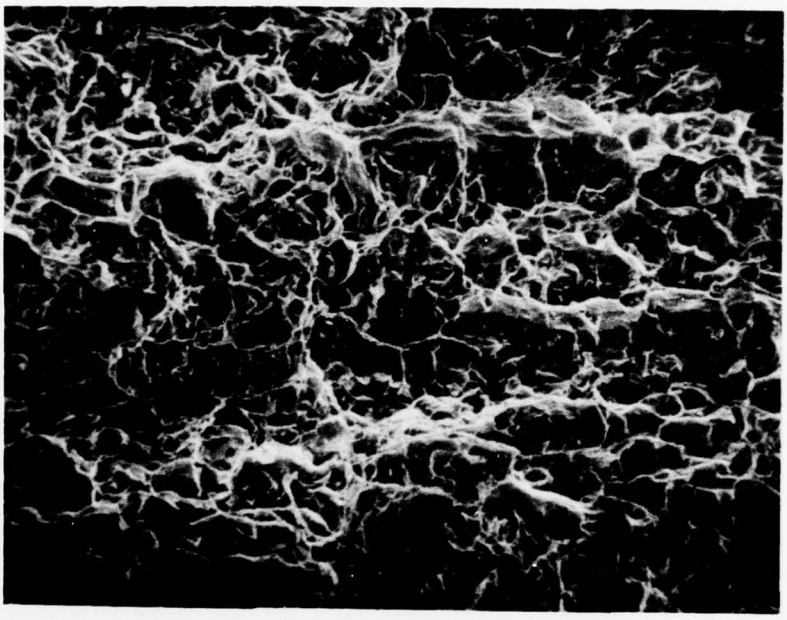

300X

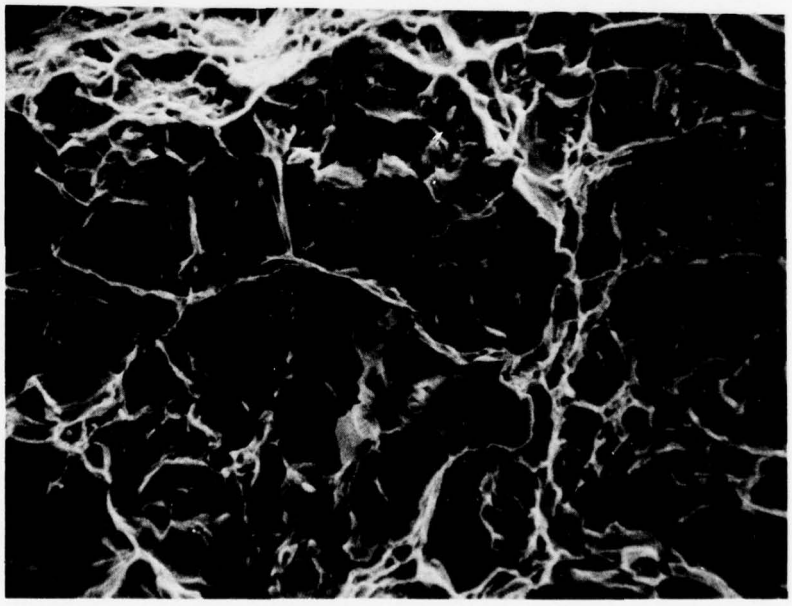

1000X

Figure 42. Typical Scanning Electron Fractographic Features in High Humidity Air and Argon. Specimen T-11

SECTION IX

PHASE IV: ALLOY EFFECT RESULTS

The objective of the Phase IV program was to examine the behavior of a second alloy system tested under the same conditions as the previous tests. In this phase 3/8 inch Ti-6Al-6V-2Sn(STOA) material was used.

1. SUSTAINED LOAD TEST RESULTS

For this material, full plane strain conditions occurred for the 3/8 inch thickness. For the T-L orientation tested, K_{Ic} = 46.1 ksi $\sqrt{in.}$ Sustained load test results for the 3/8 inch thick Ti-6Al-4V-2Sn(STOA) material are presented in Table 23. Unlike the 3/8 inch Ti-6Al-4V(RA) material, the crack growth in the Ti-6Al-6V-2Sn(STOA) material did not exhibit any tendency to tunnel, the COD and surface crack length measurements showing consistently good correlation. The results in Table 23 show the 3-1/2% NaCl solution to result in the lowest apparent threshold value, K_{Iscc}, with high humidity air the next most aggressive and the dry argon resulting in the highest K_{Iscc}. Typical time to failure curves are shown in Figure 43.

A computer program was developed to reduce the raw crack length, a, vs. time, t, data to crack growth rate, $da/_{dt}$, vs. stress intensity, K, plots. A composite plot of all the rate data by test environment is shown in Figure 44. Note that the specimen to specimen agreement is very good for a given environment. Figure 44 shows the effect of environment on the sustained load crack growth rates to have the same relative ranking as the apparent threshold values. These results are similar to those observed by others including Yoder et al [4] in Ti-6Al-4V tested in ambient air where threshold values were found to be from 11 to 35% lower than the rising load fracture values. Williams [11] has also seen indications that tests in air and vacuum yield similar times to failure.

TABLE 23

SUSTAINED LOAD TEST RESULTS FOR 3/8-IN. Ti-6Al-6V-2Sn(STOA) PLATE MATERIAL, TL ORIENTATION, K_{Ic} = 46.1 ksi$\sqrt{\text{in.}}$

Specimen Number	Environment	Initial Stress Intensity K_{Ii}, ksi $\sqrt{\text{in.}}$	Ratio K_{Ii}/K_{Ic}	Time to Failure t, Minutes	Average Subsurface Crack Growth, inch
U-1	High Humidity Air	33.4	0.72	142	to failure
U-3		28.8	0.62	249	to failure
U-2		25.4	0.55	12,912 DNF	$\Delta a = 0.006$
U-10		26.7	0.58	14,238 DNF	$\Delta a \approx 0.001$
U-5	Dry Argon	37.4	0.81	61	to failure
U-4		33.4	0.72	823	to failure
U-11		30.2	0.66	12,000 DNF	$\Delta a \approx 0.002$
U-6		27.7	0.60	9,120 DNF	$\Delta a \approx 0.002$
U-8	3-1/2% NaCl Solution	26.5	0.57	5.25	to failure
U-7		22.9	0.50	13,800 DNF	$\Delta a = 0.006$

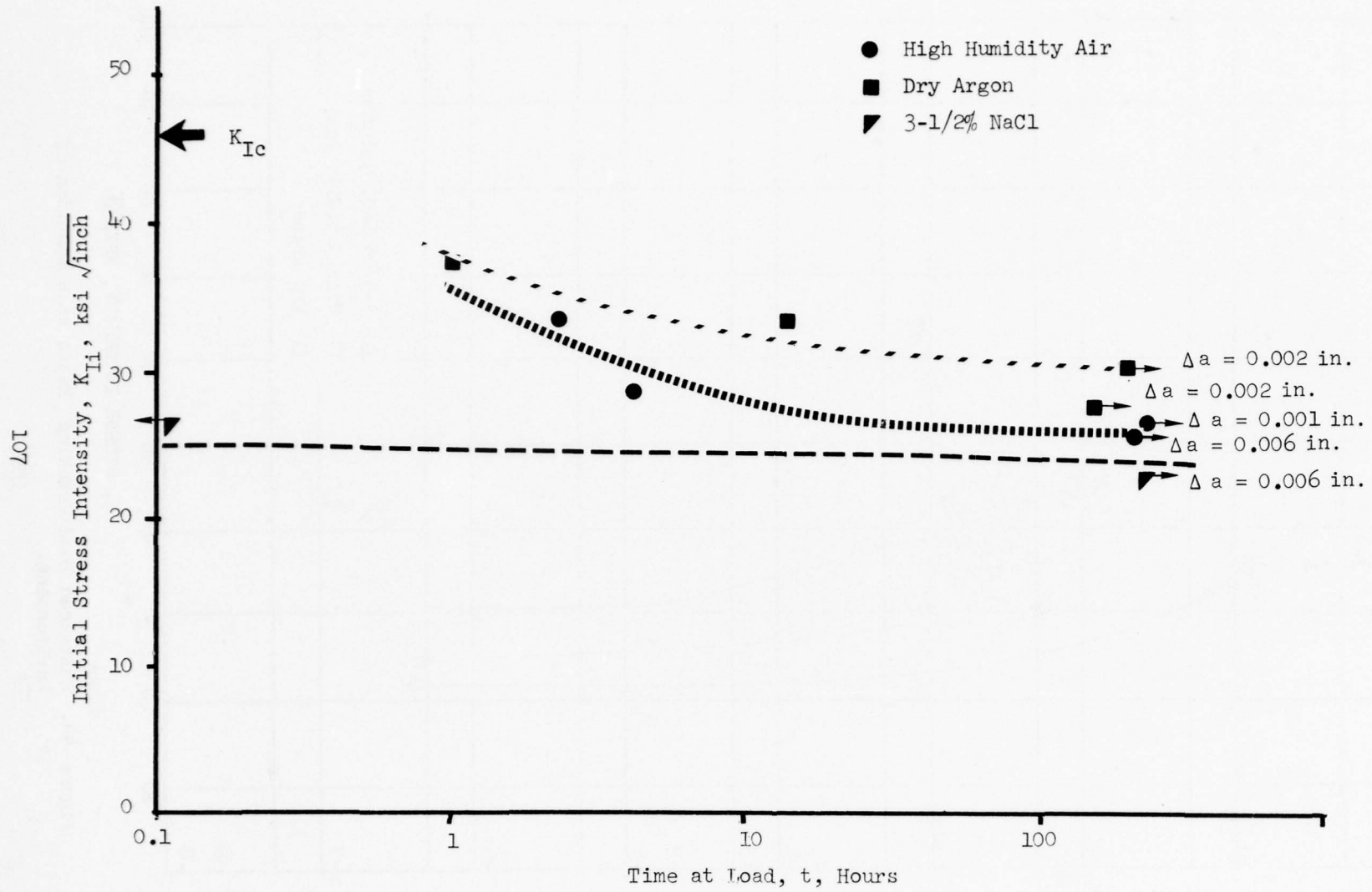

Figure 43. Typical Time to Failure Curves for Ti-6Al-6V-2Sn(STOA)

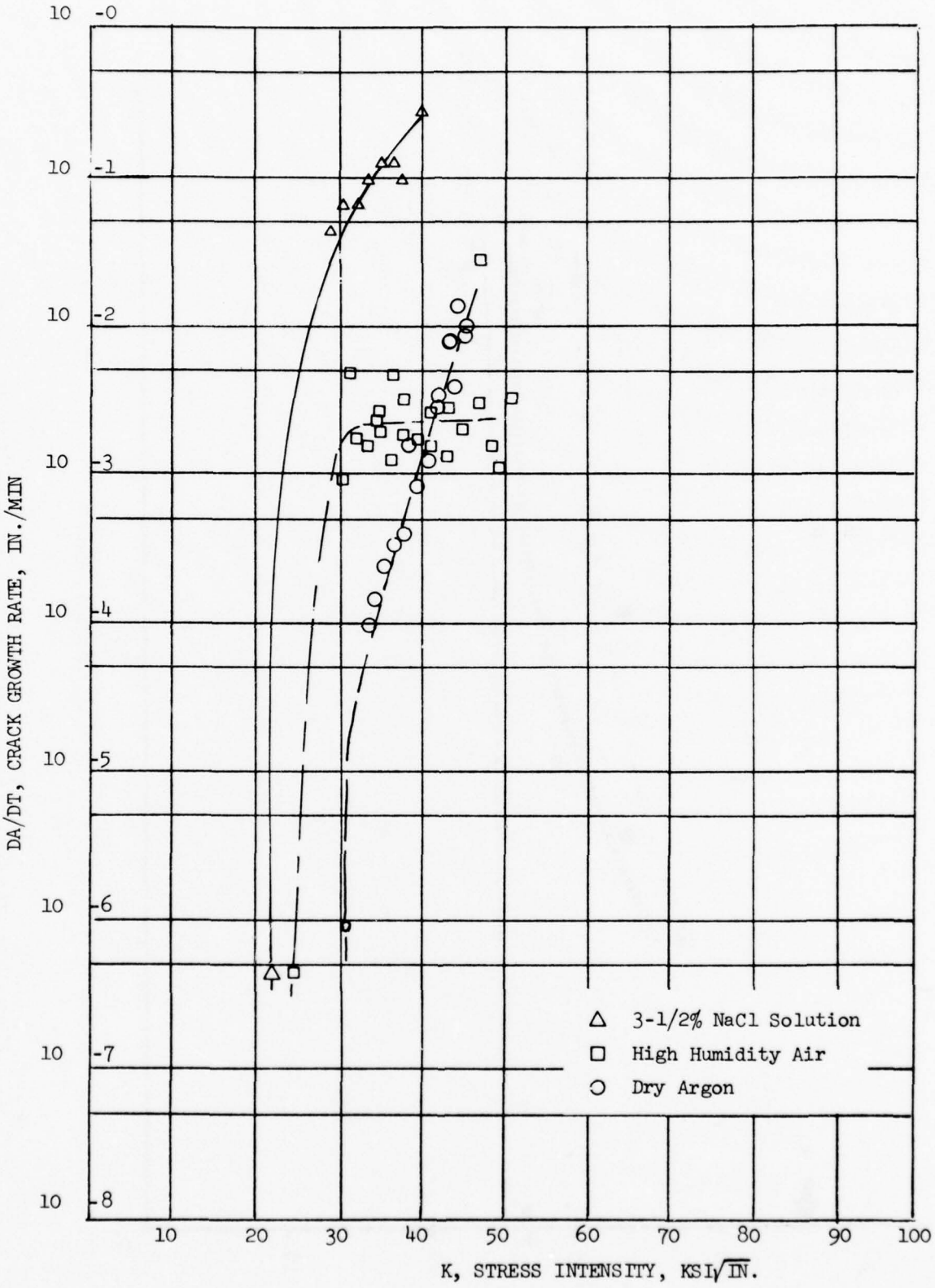

Figure 44. Sustained Load Cracking Rates as a Function of Environment

2. FRACTOGRAPHY RESULTS

Scanning electron microscope fractographs of specimens which failed in each of the three environments showed no significant differences in the region of sustained load crack growth. Typical results for the 3-1/2% NaCl, high humidity air, and dry argon specimens, Figures 45 through 47, respectively, exhibited predominantly equiaxed ductile rupture features with limited isolated areas of cleavage. These fracture surface features are similar to those observed by Meyn[8] and Yoder[4].

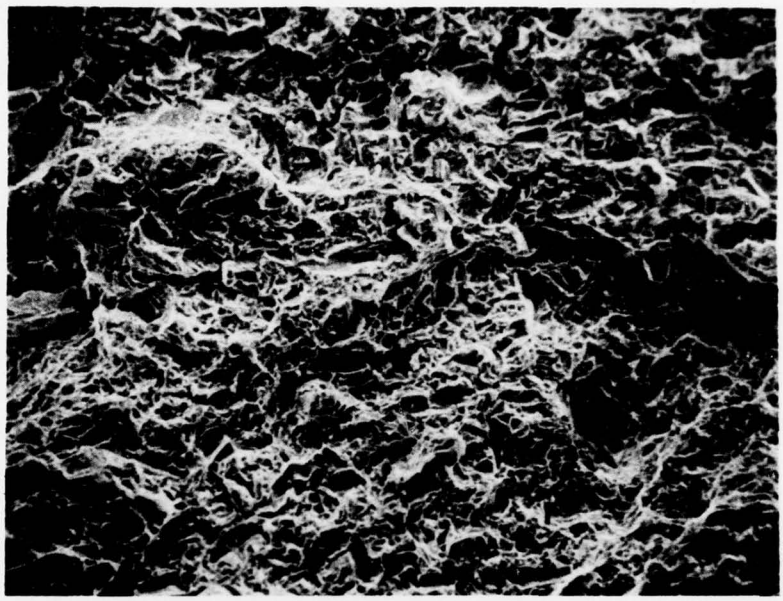

1 300X

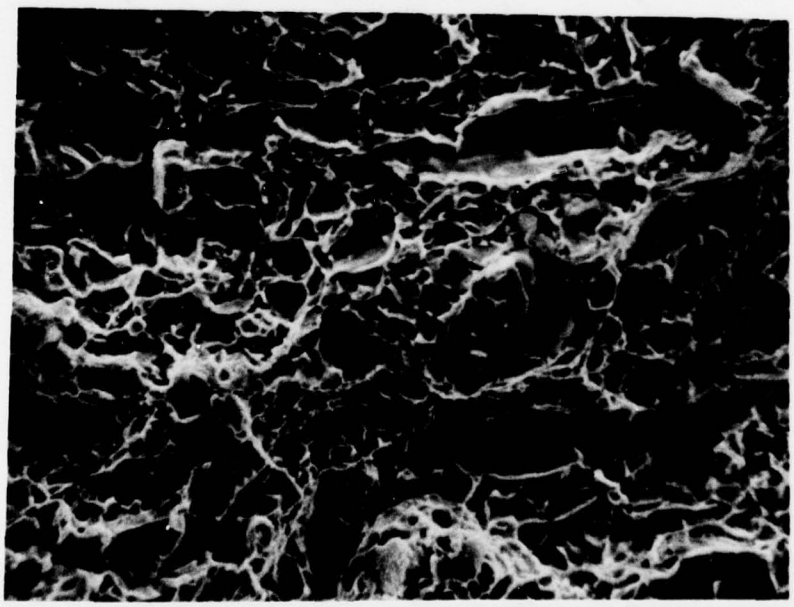

1 1000X

Figure 45. Fracture Surface of Crack Growth Region in Ti-6Al-6V-2Sn(STOA) in 3½% NaCl Solution, TL Orientation, Specimen U-8

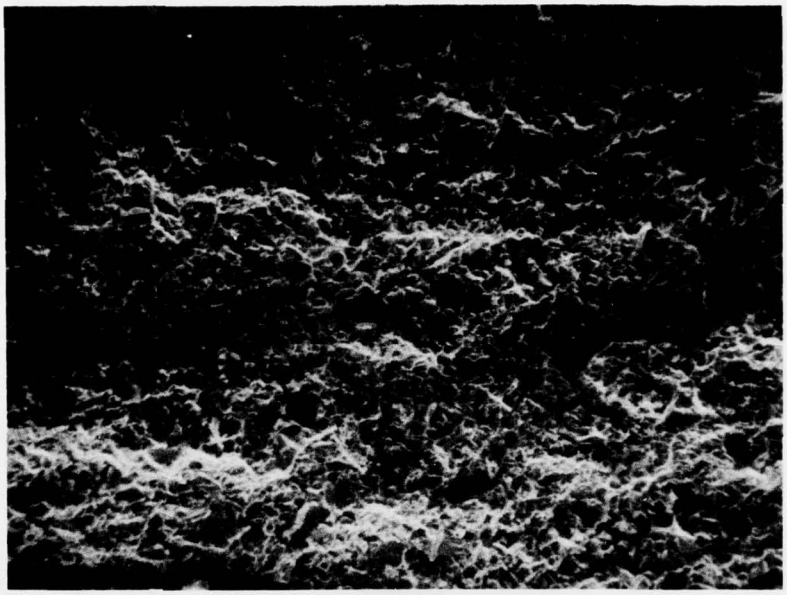

1 300X

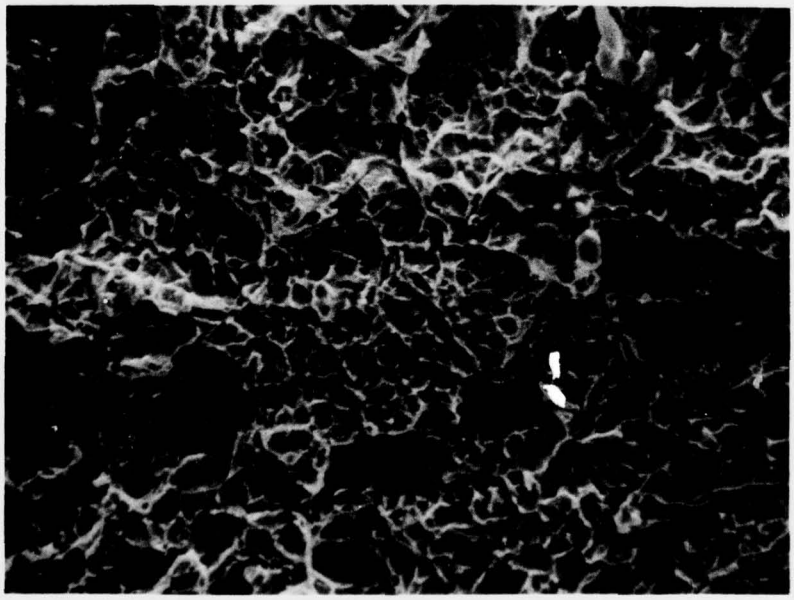

1 1000X

Figure 46. Fracture Surface of Crack Growth Region in Ti-6Al-6V-2Sn(STOA) in High Humidity Air, TL Orientation, Specimen U-3

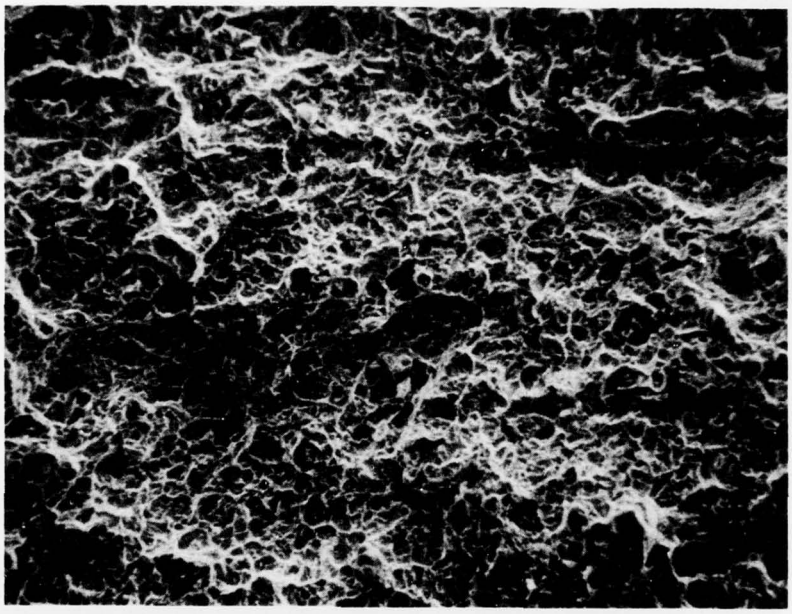

1 300X

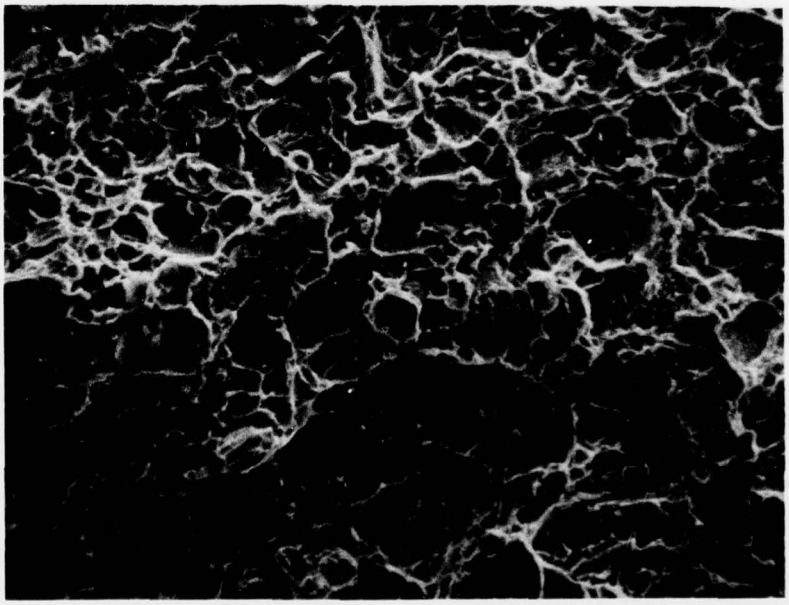

1 1000X

Figure 47. Fracture Surface of Crack Growth Region in Ti-6Al-6V-2Sn(STOA) in Dry Argon, TL Orientation, Specimen U-4

SECTION X

CONCLUDING REMARKS

The results developed in this program have been designed to provide further information on the complex phenomena of sustained load cracking in titanium alloys. These results, when examined along with other results from the literature provide a basis for an assessment of the major parameters involved in the phenomena of sustained load cracking.

The results show that sustained load cracking in titanium alloys can readily occur under certain conditions in assumedly inert environments such as dry argon. This is further supported by Williams' results[11] for tests conducted in vacuum on Ti-4Al-3Mo-1V. The extent and severity of cracking in the inert environment is, however, affected by both the state of stress, microstructure, alloy, and internal hydrogen level. In the current study, the STA and RA heat treatments of Ti-6Al-4V both show extensive cracking in dry argon when tested with internal hydrogen levels > 200 ppm. A drop in the hydrogen level to 72 ppm in the RA material, decreased the cracking tendency in dry argon. This is in agreement with Meyn's conclusion[6] that increasing the internal hydrogen level degrades the sustained load cracking behavior of the material. However, for the RA material the low hydrogen material showed a 10% lower K_{Ic} than did the high hydrogen material. The beta annealed material showed no effect of the hydrogen level on K_{Ic}. The Ti-6Al-4V(8) material showed similar sustained load cracking behavior in dry argon at hydrogen levels of 199 and 24 ppm. Note, however, that in both cases initial stress intensities greater than $\sim$ 75 ksi $\sqrt{\text{inch}}$ were required to initiate cracking. Sustained load cracking in dry argon was also shown to occur in the Ti-6Al-6V-2Sn(STOA) material (90 ppm hydrogen) at levels down to 30 ksi $\sqrt{\text{inch}}$.

A change in the test environment from dry argon to high humidity air resulted in some unexpected changes in behavior. If the roll of air (and/or humidity) is only to provide an additional external source of contaminating species,

then the high humidity air would be expected to increase the cracking tendency over that observed in dry argon. Indeed, this was the case for the Ti-6Al-6V-2Sn(STOA) material. If, however, the primary mechanisms of sustained load cracking is due to creep (in the absence of a liquid environment), then little difference would be anticipated between the dry argon and high humidity air results. This was the case for the Ti-6Al-4V(β) materials (both high and low hydrogen) and the low hydrogen Ti-6Al-4V(RA) material. However, for the high hydrogen Ti-6Al-4V(RA) and (STA) materials, the dry argon environments resulted in substantially more extensive sustained load cracking than did the high humidity air environment, the STA condition showing the dry argon threshold to be very near that found in $3\frac{1}{2}\%$ NaCl solution. If the controlling parameter was simply the interaction of the load (or K_{Ti}) and the internal hydrogen level, then these two high hydrogen materials would have been expected to show similar sustained load cracking behavior in high humidity air and dry argon. The results indicate a much more complex interaction involving the external environment and the microstructure. These results are not unlike the laboratory air results of Yoder et al[12] who found the sustained load cracking in titanium alloys in lab air to vary from 11 to 35% reduction from K_{IQ} values.

Metallographic and fractographic examination of the specimens show that at high K_{Ii} levels (in dry argon especially) extensive secondary cracking can occur at the crack tip which effectively blunts the crack tip and slows or arrests the crack. This was particularly noted in the RA and β Ti-6Al-4V materials which exhibits high K_{Ic} values. A similar crack growth arrest was noted at much lower stress intensities in all three heat treatments of Ti-6Al-4V tested in $3\frac{1}{2}\%$ NaCl solution. These results indicated that for specimens with low dK/da gradients, the secondary cracking at the crack tip can result in an "apparent" sustained load cracking threshold which is non-conservative. This effect is further confirmed by constant displacement tests ($\frac{-dK}{da}$) which show the results in $3\frac{1}{2}\%$ NaCl solution to also arrest at the "apparent" threshold from constant load tests. These results indicate the importance of the crack branching at the crack tip and its interaction with the dK/da field due to the specimen geometry.

These results indicate the level of complexity involved in the interpretation of the sustained load cracking behavior in titanium alloys. In addition to extensive crack tunneling which occurs, the microstructural features and their interaction with both the internal hydrogen and the external environment may result in local crack tip cracking which decreases the local stress intensity and the extent of the triaxial stress field. In addition, Sommer and Creager [45] have shown that Ti alloys which are slow cooled may also develop short-range-order (SRO) of the aluminum and oxygen atoms which results in degradation of the load carrying capability proportional to the product of the SRO and hydrogen concentration. Thus, furnace cooled material would be expected to show more degradation at a given hydrogen level than would rapidly cooled material.

Material used by Meyn [8] and by Williams [11] were all reported as being furnace cooled. If the hypothesis of Sommer and Creager [45] is correct on the effect of SRO, then it would be expected that the level of hydrogen required to significantly affect the sustained level cracking behavior might be very low. Meyn[8] has reported that hydrogen levels above the 35-50 ppm range seriously degrade the sustained load carrying capacity of his alloy B. Levels of greater than 9 ppm in alloy C yielded a constant apparent sustained load threshold while the fast fracture value increased $\sim$ 30% for hydrogen levels below 50 ppm. Material used by Williams [11] was also furnace cooled and contained only 10 ppm hydrogen but exhibited extensive sustained load cracking in moist air and in vacuum. Yoder et al [4] did not specify the final cooling rates for his material. In contrast to these results, the RA material of this study(which was fan cooled)showed an increase in resistance to sustained load cracking when the hydrogen level was decreased from 245 to 72 ppm, the 72 ppm value being higher than would be expected to improve the sustained load cracking behavior based on Meyn's results. This behavior seems to be strongly microstructure dependent, the highest sustained load cracking susceptibility occurring in $\alpha + \beta$ materials. Both the results of Yoder [4] and this study show the β materials to be more resistant to SLC than the $\alpha + \beta$

materials. The results of this study also show only minor effects of hydrogen level changes from 199 to 24 ppm for the β material.

It must be noted at this point that these results do not preclude Williams hypothesis [11] that a creep mechanism is the controlling factor in sustained load cracking of titanium. Krafft [5] has had reasonable success predicting the results of Yoder [4] using a model based on the plastic flow characteristics and a minor environmental effect. Note that this model, however, still fails to identify the crack arrest phenomena due to microstructure/environment crack tip branching.

Fractography of the failed specimens showed a mixture of ductile rupture and cleavage similar to that reported by Meyn [8]. In addition no significant difference in the fracture surface features could be found for different hydrogen levels of a common material, further confirming Meyn's results.

As the thickness of the Ti-6Al-4V(RA) 245 ppm hydrogen material was decreased, the propensity to crack under sustained load decreased; the thicker material showing increased cracking tendencies and lower sustained load cracking thresholds in air and argon. Comparison of the crack growth rates is difficult due to the extensive crack tunneling that was noted in the Ti-6Al-4V material tests, the tunneling being severe enough to arrest the crack in all of the Ti-6Al-4V 3/8 inch thick materials in high humidity air and dry argon. These results are similar to those of Williams [12] and of Beachem et al [7].

The textured Ti-6Al-4V(RA) results showed no clear effect of the texture on the sustained load cracking behavior in the high humidity air or dry argon, similar threshold values being found for both environments. This is due in part to the associated differences in yield strength in the orthogonal directions and the extensive tunneling which occurred in the 3/8 inch thick material. All crack growth occurred in the normal plane of crack growth (normal to load line) regardless of the orientation of the

specimen. However, in 3 1/2% NaCl solution the L-T specimens exhibited 90° crack rotation and failed in the T-L direction at K levels only slightly higher than threshold for the T-L specimens. These results are similar to those seen by Sommer and Creager [45]. The results also indicate the time-to-failure vs. initial stress intensity method of presenting data can be misleading and the time to failure curve may change its basic shape for different size or configuration of specimens due to the crack arrest effect of large trailing plastic zones at the surface. Fractographic results showed no significant differences between specimens of the two orientation tested in dry argon or high humidity air, all showing a mixture of equiaxed ductile rupture and minor areas of cleavage similar to that seen in the Task I materials. However, the specimens tested in 3 1/2% NaCl solution showed extensive cleavage with areas of intergranular cracking.

In contrast to the Ti-6Al-4V results, the Ti-6Al-6V-2Sn(STOA) material did not exhibit any tendency to tunnel under sustained load cracking but did exhibit crack growth in all environments including dry argon. For this material, the dry argon resulted in a $K_{th} \sim 30$ ksi$\sqrt{\text{inch}}$, the high humidity air threshold being $K_{th} = 24\sqrt{\text{ksi inch}}$ as compared to a value of $K_{th} = 22$ ksi$\sqrt{\text{inch}}$ for the 3 1/2% NaCl solution. Examination of the fracture surface showed similar equiaxed dimples with isolated areas of cleavage for specimens tested in all three environments.

In summary, the following conclusions seem appropriate:

1. The internal hydrogen level of a titanium alloy may increase the sustained load cracking behavior of the material.
2. The extent of this degradation is dependent upon the microstructure, environment and, possibly, short range order. Other submicrostructured features may also be involved.
3. Materials with an $\alpha + \beta$ microstructure seem to show a greater susceptibility to sustained load cracking and sensitivity to hydrogen level than do the β processed materials.

4. As the thickness and associated triaxial constraint decrease, the tendency to exhibit sustained load cracking in high humidity air and dry argon decrease for Ti-6Al-4V(RA) with a high hydrogen content.
5. Crystallographic texture in Ti-6Al-4V(RA) does not appear to exhibit a major influence on sustained load cracking in high humidity air or dry argon but does exhibit a major effect in 3 1/2% NaCl solution.

6. Great care must be exercised in assessing sustained load cracking behavior of Ti alloys since crack tip branching can result in crack arrest at a level much above that level where extensive sustained load cracking occurs. The occurance of crack arrest is dependent on the relative $\frac{dK}{da}$ gradient of the specimen geometry as well as the material and specimen thickness.

7. No single model for sustained load cracking appears to predict all of the observed sustained load cracking behavior. Rather it appears to involve a combination of effects involving internal hydrogen, creep, and environmental parameters which may not always be of a detrimental nature. In particular, the role of oxide formation at the crack tip needs to be further evaluated.

REFERENCES

1. Burte, H. M., Erbin, E. F., Hahn, G. T., Katfile, R. J., Seeger, J. W., and Wruck, D. A., "Hydrogen Embrittlement of Titanium Alloys," Metal Progress, Vol. 67, May 1955, pp. 115-120.

2. Williams, D. N., "Hydrogen in Titanium and Titanium Alloys," TML Report No. 100, Battell Memorial Institute, May 1968.

3. Daniels, R. D., Quigg, R. J., and Troiano, A. R., Transactions of the American Society for Metals, Vol. 51, 1959, pp. 843-861.

4. Yoder, G. R., Griffis, C. A., and Crocker, T. W., "The Cracking of Ti-6Al-4V Alloys Under Sustained Load in Ambient Air," Transactions of the ASME, J. of Engineering Materials and Technology, Vol. 96, Series H, October 1974, pp. 268-274.

5. Kraft, J. M., "An Interpretation of the Yoder-Griffis-Crooker Observations of Sustained Load Cracking in Ti-6Al-4V," Transactions of the ASME, J. of Engineering Materials and Technology, Vol. 96, Series H, October 1974, pp. 275-282.

6. Meyn, D. A., "A Procedure for Investigating the Effect of Hydrogen Content on Toughness and Sustained Load Cracking Resistance of Titanium Alloys," NRL Memorandum Report 2461, June 1972.

7. Beacham, D. C., and Meyn, D. A., "The Effect of Thickness Upon Sustained Load Crack Propagation," NRL Report 7449, August 1972.

8. Meyn, D. A., "Effect of Hydrogen in Fracture and Inert-Environment Sustained Load Cracking Resistance of α - β Titanium Alloys," Metallurgical Transactions, Vol. 5, November 1974, pp. 2405-2414.

9. Sandoz, G., "Subcritical Crack Propagation in Ti-8Al-1Mo-1V Alloy in Organic Environments, Salt, Water, and Inert-Environments," Proceedings of Conference on Fundamental Aspects of Stress Corrosion Cracking," Staehle, R. W., et al, editors, NACE, Houston, Texas, 1969, pp.684-690.

REFERENCES (Continued)

10. Chu, H. P., "Fracture Characteristics of Titanium Alloys in Air and Seawater Environment," Engineering Fracture Mechanics, Vol. 4, 1972, pp. 107-117.

11. Williams, D. N., "Subcritical Crack Growth Under Sustained Load," Metallurgical Transactions, Vol. 5, November 1974, pp. 2351-2358.

12. Williams, D. N., "Effect of Specimen Thickness on Subcritical Crack Growth Under Sustained Load," Materials Services and Engineering, Vol. 18, 1975, pp. 149-155.

13. Pettit, D. E., Krupp, W. E., Ryder, J. T., Hoeppner, D. W., "Investigation of the Effects of Stress and Chemical Environments of the Prediction of Fracture in Aircraft Structural Materials," AFML-TR-74-183, Vol. 1, December 1974.

14. Lane, Jr., I. R., Cavallaro, J. L., Morton, A. G. S., "Seawater Embrittlement of Titanium," Stress Corrosion Cracking of Titanium, ASTM, STP 397, ASM, 1966, pp. 246-259.

15. Crossley, F. A., and Carew, W. F., "Embrittlement of Ti-Alloys in the 6 to 10 Percent. Al Range," J. of Metals, Vol. 209, January 1957, pp. 1143-1146.

16. Murphy, T., and Feige, N. G., "Preliminary Evaluation of Degradation of Titanium Crack Resistance in Seawater Environment," TMCA Project Report No. BM-03-1, Titanium Metals Corp., Henderson, Nevada, May 1965.

17. Cowgill, D. S., Krupp, W. E., Fritzen, J. S., Krystakowiak, S., and Weber, K. E., "Crack Morphology Studies in the Ti-8Al-1V-1Mo Alloy," Paper presented at ASTM/ARPA Symposium on Stress Corrosion and Corrosion Principles, Atlanta, Georgia, 1968.

18. Williams, D., "A Review of Subcritical Crack Growth Under Sustained Load," AIAA Paper No. 75-804, 16th Structure, Structural Dynamics and Materials Conference, Denver, Colorado, May 1975.

REFERENCES (Continued)

19. Piper, D. E., Smith, S., and Carter, G. C., "Corrosion Fatigue and Stress Corrosion Cracking in Aqueous Environments," Metals Engineering Quality, Volume 8, No. 3, August 1968, p. 50.

20. Curtis, R. E., "Stress Corrosion Cracking of Titanium Alloys," paper presented at Annual Review of ARPA Stress Corrosion Program, Pittsburgh, Pennsylvania, May 1967.

21. Seagle, S. R., Seeley, R. R., and Hall, G. S., "The Influence of Composition in Heat Treatment on the Aqueous-Stress Corrosion of Titanium," Applications Related Phenomena in Titanium Alloys, ASTM STP 432, 1968, pp. 170-188.

22. Truax, D. J., McMahan, C. J., Jr., "Plastic Properties and Fracture of Titanium-Aluminum Alloys," University of Pennsylavnia, Philadelphia, Pennsylvania, August 1970.

23. Lane, I. R., Cavallaro, J. L., "Metallurgical and Mechanical Aspects of the Sea-Water Stress Corrosion of Titanium," Application Related Phenomena in Titanium Alloys, ASTM STP 432, 1968, pp. 147-169.

24. Shambler, C. E., Redder, T. K., "Air Contamination and Embrittlement of Titanium Alloys," The Science, Technology, and Application of Titanium, Penganom Press, New York, 1968, pp. 199-208.

25. Boyd, W. K., "Deformation Assisted Nucleation of Titanium Hydride in an Alpha-Beta Titanium Alloy," ibid, pp. 545-556.

26. Curtis, R. E., Spurr, W. F., "Effect of Microstructure on the Fracture Properties of Titanium Alloys in Air and Salt Solution," Transactions of the ASM, Volume 61, 1968, pp. 115-127.

27. Wood, R. A., Boyd, J. D., and Jaffe, R. I., "The Effects of Alloy Composition in the Salt-Water Stress Corrosion Susceptibility of Titanium-Aluminum-Base Alloys," Titanium Science and Technology, Volume 4, pp. 2639-2654, Plenum Press, New York, 1973.

REFERENCES (Continued)

28. Partridge, J. M., "Fracture Toughness Properties of Ti-6Al-4V," paper presented at ASM 1971 WESTEC, Los Angeles, California.

29. Sanders, G., Scully, J. C., "Some Observations on the Stress-Corrosion Cracking of Titanium Alloys," Proceedings, Conference on Environmental Sensitive Mechanical Behavior, Baltimore, Maryland, 1965.

30. Powell, D. T., Scully, J. C., "The Stress Corrosion Cracking of α-Titanium Alloys at Room Temperature," The Science, Technology and Application of Titanium, Perganom Press, New York, 1968, pp. 247-258.

31. Howe, D. G., Goode, R. J., "Effects of Heat Treating Environmental Conditions on the Stress-Corrosion Cracking Resistance of Several Titanium Alloys," Application Related Phenomena in Titanium Alloys, ASTM STP 432, 1968, pp. 189-204.

32. Sedricks, A. J., Green, J. A. S., Slattlery, P. W., "Stress Corrosion Cracking of Titanium and Ti-Al Alloys in Methonal-Iodine Solutions," The Science, Technology, and Application of Titanium, Perganom-Press, New York, 1968, pp. 283-292.

33. Kamber, K., Kendell, E. G., Raymond, L., "Effects of Halogen Containing Hydrocarbon Upon Stressed Ti-6Al-4V Alloy," ibid, pp. 293-298.

34. Fager, D. N. Spurr, W. F., "Some Characteristics of Aqueous Stress Corrosion in Titanium Alloys (Summary)," ibid, pp. 259-262.

35. Telephone discussion with Mr. W. Love of RMI, Los Angeles Office, 9-24-76.

36. E8-69, "Standard Methods of Tension Testing of Metallic Materials," ASTM 1975 Annual Book of Standards, Part 10, November, 1975.

37. "Aircraft Designer's Handbook for Titanium and Titanium Alloy," AFML-TR-67-142, March 1967.

38. Rockwell International Specification ST0170LB-0032.

REFERENCES (Continued)

39. Hudak, S. J., Jr., Saxena, A., and Bucci, R. J., "Development of Standard Methods of Testing and Analyzing Fatigue Crack Growth Rate Data," 2nd Semi-Annual Report, A.F. Contract F33615-75-C-5064, September 24, 1976.

40. "Standard Method of Test for Plane-Strain Fracture Toughness of Metallic Materials," ASTM 1974 Annual Book of Standards, Part 10, November, 1974, pp. 432-451.

41. "Damage Tolerant Design Handbook, Part 2," MCIC-MB-01, Metals and Ceramics Information Center, Batelle Memorial Institute, Columbus, Ohio.

42. Newman, J. C., Jr., "Crack Opening Displacements in Center-Crack, Compact, and Crack-Line Wedge-Loaded Specimens," NASA TND-8268, July, 1976.

43. Novak, S. R., and Rolfe, S. T., "Modified WOL Specimen for K_{Iscc} Environmental Testing," Journal of Materials, Volume 4, p. 701, September, 1969.

44. Wessel, E. T., "State-of-the-Art of the WOL Specimen for K_{Ic} Fracture Toughness Testing," Presented at the First International Symposium on Fracture Mechanics, June, 19-21, 1967.

45. Sommer, A. W. and Creager, M.; "Research Toward Developing an Understanding of Crystallographic Texture on Mechanical Properties of Titanium Alloys; AFML-TR-76-222, Jan., 1977.

☆U.S.Government Printing Office: 1978 — 757-080/480